THE ABSORPTION OF RADIATION IN THE VISIBLE SPECTRUM BY AN ARGON PLASMA

By

JARRETT CHARLES HESTER

Bachelor of Science
Arlington State College
Arlington, Texas
1962

Master of Science
Oklahoma State University
Stillwater, Oklahoma
1964

Submitted to the Faculty of the Graduate College
of the Oklahoma State University
in partial fulfillment of the requirements
for the degree of
DOCTOR OF PHILOSOPHY
May, 1966

THE ABSORPTION OF RADIATION IN THE VISIBLE SPECTRUM BY AN ARGON PLASMA

Thesis Approved:

D. R. Haworth
Thesis Adviser

J. A. Wiebelt

Ladislaus J. Fila

Dean of the Graduate College

ACKNOWLEDGMENTS

The author wishes to express his sincere gratitude to the many persons who have given him their support during the conduct of this thesis work.

The general guidance and direction of Dr. D. R. Haworth was greatly appreciated. The encouragement extended by Dr. Haworth during the various trial-and-error phases of the work was particularly helpful. To Dr. J. A. Wiebelt, for his invaluable assistance in the instrumentation problems, the author is greatly indebted. To the Mechanical Engineering faculty and staff, the author extends special thanks for the day-to-day assistance which helped to make the thesis work a more pleasant experience.

To my wife, Phyllis, I give thanks for the way she has maintained a home and raised our family during the years of graduate study.

TABLE OF CONTENTS

LIST OF TABLES

LIST OF FIGURES

CHAPTER I

INTRODUCTION

Hypervelocity flight, magnetofluidmechanics, electrothermal propulsion devices, and other high temperature research activities repeatedly confront the practicing engineer with the problem of ascertaining the state properties of various gases. When energy from such processes is added to the gas, it is distributed into various modes. At normal temperatures, most of the energy is contained in the translational velocities with some energy contained in the rotational mode and little energy in the remaining vibrational and electronic energy levels. As the energy is increased, the energy in the translational and rotational modes is increased and the vibrational mode becomes excited. As further energy is added to the gas some of the molecular bonds are broken and dissociation results. With the addition of more energy, the electrons in the orbits around the atomic nucleus become excited to energy levels above the ground state. As the process continues, some of the electrons attain sufficient energy to leave their orbits, and the gas becomes ionized. This resulting mixture which may be composed of free electrons, ions, atoms, and molecules is collectively identified as "plasma."

The problems associated with this plasma are varied and complex. One fundamental problem common to many fields of high energy gas phenomena, the calculation of heat transfer rates, is greatly complicated

by several factors. Contributing to this problem is the absence of a convenient method for measuring accurately the distribution of energy among various levels in the gas. Since the energy content under consideration may be quite high, an indirect method must be used for the determination of particle densities in a particular energy level. Any measuring device which might be placed in the plasma to obtain these distributions directly would not only be subjected to extreme heating rates but would also perturb the existing plasma region since the ionized and dissociated particles would recombine near the measuring surface and create a concentration gradient or "sheath" around the measuring device. This would require additional investigation to determine the effect of this sheath of cooler gas on the measured values.

Remote methods of obtaining energy level distributions have been developed using the emission of electromagnetic radiation from the plasma which may then be related to the state of the gas if certain characteristics of the plasma are known.

Other problems result when electromagnetic radiation propagates through this plasma which is electrically conductive, due to the presence of the free electrons and positively charged ions, even though the net charge of the mixture may be zero. This problem has been dramatically illustrated by the radio "blackout" experienced by the various space probes which, upon re-entering the earth's atmosphere, were immersed in a plasma field generated by conversion of kinetic energy into thermal energy.

A program is now under investigation by various research agencies to attempt to avoid this communication problem by changing the

information carrying frequencies. The visible spectrum is being considered as a possible alternative, but little data is present in the literature concerning the absorption characteristics of the gas in the visible spectrum. It is essential that these values be known if an amplitude modulated system is to be considered since any unknown attenuation of the signal by the plasma would negate the value of this method.

It was the purpose of this research program to provide the basic information describing the absorption characteristics of a high temperature gas. Particular emphasis was placed on a study of self-absorption by the gas. This absorption process occurs when the reaction energies associated with the various changes in state of the plasma particles are emitted as electromagnetic radiation and are then absorbed by surrounding particles. The self-absorption process then affects any measurements which are based on emission phenomena.

The study which is presented in this thesis deals specifically with the absorption characteristics of high temperature argon, a gas commonly used in many laboratory plasma generators. Absorption of energy in the wavelength region between 3500 and 6000 Angstroms is studied since this region encompasses most of the high intensity spectral lines emitted by the argon plasma. Of primary concern is information related to plasmas which have energy levels corresponding to equilibrium temperatures between 4,000 and 10,000 °K and absolute pressures of ten to seventy-five millimeters of mercury.

CHAPTER II

DETERMINATION OF THE PLASMA STATE

When energy is added to a gas, an increase in the number of particles in the higher translational, vibrational, rotational, and electronic energy levels is observed. In the case of argon, a monatomic gas, the vibrational and rotational modes do not exist and only the increases in translational and electron excitation energies need be considered. As the energy contained in the gas is increased, some of the electrons which surround the argon atom are raised to higher and higher energy levels until they possess sufficient energy to escape from their orbits about the nucleus. This energy may be added to the gas in a variety of ways, but one of the most common methods for producing this phenomenon in the laboratory is by means of resistance heating. In this method, high velocity electrons are forced to pass through a space filled with argon atoms. As the high velocity electrons encounter and interact with the electrons of the argon particles, there occurs an energy exchange in which the electronic energy level of the argon atom is increased as is the kinetic energy of the atom. By a series of several interactions the argon atom may acquire sufficient energy to become ionized. When this occurs, the free electron which has been produced is now available to collide with neighboring atoms thus raising them to even higher energy levels.

It is by this method that the plasma to be considered in the remainder of this thesis is produced.

After experiencing an increase in the various energy levels, the plasma is accelerated by a pressure gradient into a low pressure test section. In the test section the gas emits electromagnetic radiation to the surroundings. This radiation results from the acceleration of the charged particles, the recombination of ions and electrons, and the transition of an electron from a high electronic level to one of lower value. This emitted radiation may then be used to deduce the state of the plasma.

Spectral Line Emission

Electromagnetic radiation of wavelength λ is emitted from a plasma when the electrons which are still bound to the nucleus, but in an excited energy state, undergo a transition to a lower energy level. This emission may occur at selected points in the spectrum only since the electron energy is restricted to a number of discrete levels. If E_1 is the energy level from which the transition begins and E_2 is the final energy which the electron possesses, one obtains

$$E_1 - E_2 = h\nu,$$

but since $\nu = \frac{c}{\lambda}$, the wavelength of the emitted radiation is given by

$$\lambda = \frac{hc}{E_1 - E_2},$$

where h = Planck's constant,

ν = frequency of the emitted radiation,

λ = wavelength of the emitted radiation, and

c = speed of light.

Radiation is also emitted when the charged particles undergo an acceleration or when these particles recombine to form neutral argon atoms. This radiation is emitted in a continuous spectrum and will not be considered directly in the methods presented in the following sections.

In order to use this emitted radiation to determine the energy distribution at some cross section of the plasma column it is necessary to observe the intensity of selected spectral lines. This is done by dispersing the emitted energy into appropriate wavelengths through the use of a spectrograph. The observed intensities at different wavelengths are then used to obtain radial intensity distributions by a method summarized by Haworth (1)*. The development of the measured intensity values I_x as a function of the radial intensity distribution is described in Appendix A.

The evaluation of the radial intensity distribution which is used in deducing the energy distribution is based upon the solution of the particular form of Abel's integral equation,

$$I_x = \int_{r=x}^{r=r_o} \frac{r \cdot I(r)\, dr}{[r^2 - x^2]^{1/2}}, \qquad (1)$$

*Numbers in parentheses indicate references in the bibliography.

where I_x = measured intensity values,

$I(r)$ = the radial intensity values,

r = radius, and

x = vertical distance from centerline.

The I(r) values of equation 1, which generally cannot be expressed in closed analytical form, may be obtained numerically by a method presented by W. J. Pearce (2). The method consists of subdividing the plasma column into a number of annular regions (Figure 1) within which it is assumed that the I(r) maintains a constant value. The recorded intensity I_x, at any vertical position, is proportional to the area weighted I(r)'s in that horizontal column (Figure 2). The weighted area coefficients $\Delta A_{j,k}$ are given in Table I. These coefficients are used in the following set of simultaneous linear equations:

$$
\begin{aligned}
I_{x(j)} &= I(r)_k \cdot \Delta A_{j,k} \\
I_{x(j-1)} &= I(r)_k \cdot \Delta A_{j-1,k} + I(r)_{k-1} \Delta A_{j-1,k-1} \\
I_{x(j-2)} &= I(r)_k \cdot \Delta A_{j-2,k} + I(r)_{k-1} \Delta A_{j-2,k-1} + \\
&\qquad I(r)_{k-2} \cdot \Delta A_{j-2,k-2} \\
&\;\;\vdots \\
I_{x_{(1)}} &= I(r)_k \cdot \Delta A_{1,k} + \cdots + I(r)_1 \Delta A_{j,1} \quad ,
\end{aligned}
\tag{2}
$$

where the observed $I_{x,j}$'s proceed from the outer boundary toward the centerline. It may be seen (Figure 2) that the number of vertical

TABLE I

WEIGHTED AREA COEFFICIENTS $\Delta A_{j,k}$

k

j	1	2	3	4	5	6	7	8	9	10	11	12	13	14	15	16	17	18	19	20	21	22	23	24	25	j
1	1.57080	2.25565	2.06051	2.02891	2.01706	2.01128	2.00802	2.00600	2.00466	2.00372	2.00304	2.00253	2.00214	2.00184	2.00159	2.00139	2.00123	2.00109	2.00098	2.00088	2.00079	2.00072	2.00066	2.00060	2.00056	1
2		2.45674	2.69599	2.23719	2.13023	2.08348	2.05838	2.04323	2.03334	2.02652	2.02161	2.01795	2.01515	2.01296	2.01122	2.00980	2.00864	2.00768	2.00686	2.00617	2.00558	2.00507	2.00463	2.00424	2.00390	2
3			3.09748	3.10898	2.43399	2.25572	2.17189	2.12445	2.09465	2.07457	2.06035	2.04989	2.04195	2.03579	2.03090	2.02695	2.02372	2.02104	2.01879	2.01689	2.01526	2.01386	2.01264	2.01158	2.01064	3
4				3.62649	3.46836	2.62587	2.38525	2.26717	2.19813	2.15358	2.12291	2.10078	2.08425	2.07153	2.06154	2.05352	2.04699	2.04160	2.03710	2.03329	2.03005	2.02726	2.02484	2.02274	2.02089	4
5					4.08753	3.80085	2.80879	2.51312	2.36390	2.27468	2.21602	2.17499	2.14498	2.12228	2.10464	2.09064	2.07932	2.07002	2.06230	2.05580	2.05028	2.04505	2.04146	2.03790	2.03479	5
6						4.50156	4.10745	2.98257	2.63750	2.45988	2.35192	2.27995	2.22899	2.19131	2.16254	2.14000	2.12196	2.10728	2.09516	2.08502	2.07644	2.06962	2.06282	2.05736	2.05258	6
7							4.88057	4.39322	3.14795	2.75790	2.55405	2.42875	2.34425	2.28384	2.23880	2.20414	2.17679	2.15477	2.13674	2.12178	2.10920	2.09852	2.08936	2.08145	2.07456	7
8								5.23219	4.66179	3.30579	2.87429	2.64631	2.50461	2.40830	2.33892	2.28682	2.24648	2.21446	2.18855	2.16724	2.14946	2.13446	2.12166	2.11066	2.10112	8
9									5.56162	4.91590	3.45690	2.98685	2.73622	2.57923	2.47176	2.39384	2.33500	2.28921	2.25266	2.22296	2.19842	2.17788	2.16048	2.14560	2.13275	9
10										5.87259	5.15763	3.60200	3.09580	2.82389	2.65246	2.53441	2.44836	2.38307	2.33200	2.29111	2.25773	2.23006	2.20682	2.18707	2.17012	10
11											6.16790	5.38861	3.74171	3.20140	2.90938	2.72425	2.59625	2.50234	2.43086	2.37473	2.32963	2.29269	2.26197	2.23609	2.21404	11
12												6.44971	5.61016	3.87655	3.30389	2.99277	2.79479	2.65662	2.55568	2.47826	2.41727	2.36809	2.32771	2.29402	2.26557	12
13													6.71970	5.82332	4.00699	3.40349	3.07415	2.86357	2.71667	2.60833	2.52520	2.45951	2.40641	2.36268	2.32612	13
14														6.97925	6.02899	4.13340	3.50043	3.15365	2.93115	2.77545	2.66025	2.57163	2.50141	2.44451	2.39753	14
15															7.22950	6.22790	4.25614	3.59486	3.23137	2.99741	2.83324	2.71145	2.61752	2.54293	2.48234	15
16																7.47136	6.42087	4.37550	3.68698	3.30740	3.06241	2.89006	2.76192	2.66286	2.58403	16
17																	7.70564	6.60783	4.49174	3.77693	3.38182	3.12619	2.94596	2.81166	2.70764	17
18																		7.93300	6.78985	4.60509	3.86486	3.45473	3.18882	3.00095	2.86069	18
19																			8.15402	6.96713	4.71574	3.95089	3.52621	3.25033	3.05506	19
20																				8.36921	7.14002	4.82389	4.03513	3.59634	3.31078	20
21																					8.57900	7.30882	4.92967	4.11768	3.65518	21
22																						8.78378	7.47383	5.03327	4.19865	22
23																							8.98390	7.63527	5.13479	23
24																								9.17965	7.79337	24
25																									9.37132	25

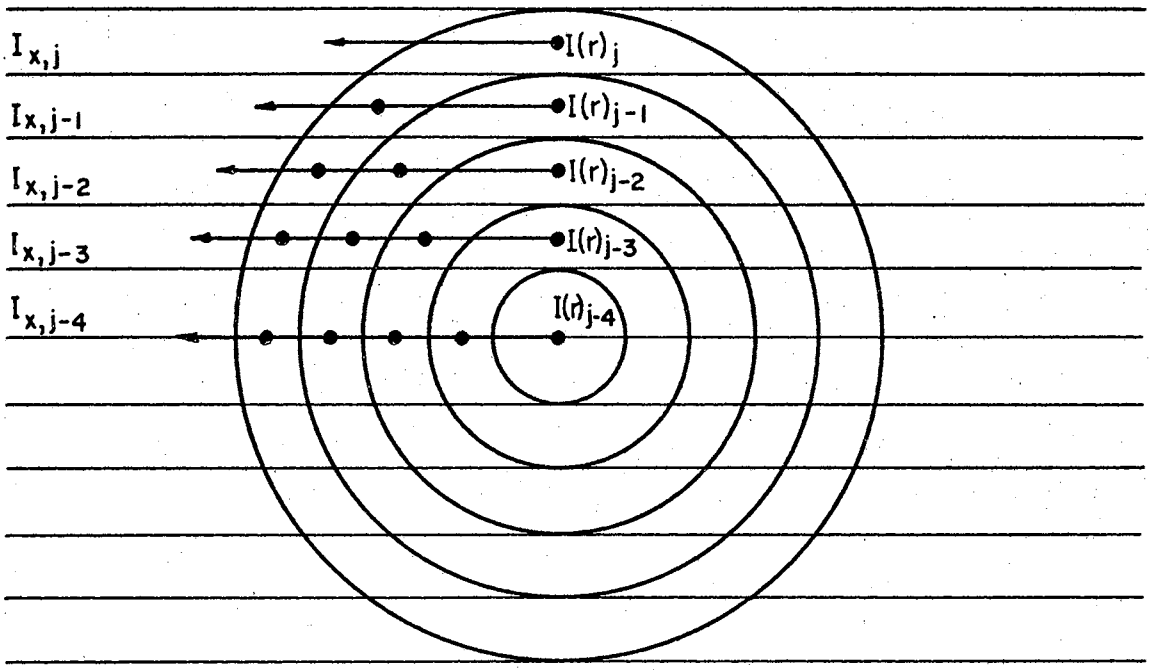

Figure 1. Observed Emission From Concentric Layers.

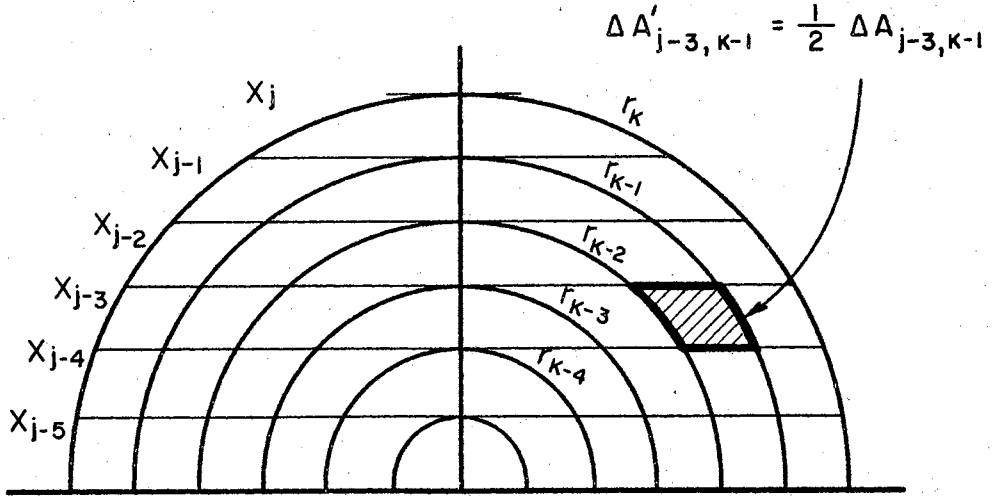

Figure 2. Definition of the Weighted Area Coefficient $\Delta A_{j,k}$.

sections above the centerline of the jet must equal the number of annular regions selected. The tabulated values of the weighted area coefficients which were presented in Table I are used in conjunction with the set of simultaneous equations previously presented to obtain a radial intensity distribution I(r) from an intensity distribution I_x observed perpendicular to the direction of flow.

Before entering into a discussion of various methods that may be used for obtaining temperature distributions from the radial intensity values, it is beneficial to enumerate the more restrictive assumptions which are involved in the derivation of these intensity values. The following assumptions were involved in this derivation: (1) the plasma column is axisymmetric, (2) local temperature equilibrium exists within each of the annular regions, and (3) the amount of absorption of radiation within the plasma is negligible.

The first of these assumptions, the condition of axisymmetric flow, is easily verified by obtaining intensity readings at various vertical positions at a fixed axial position in the plasma column.

The second and third of these assumptions require considerably more investigation. A great many investigations have been made concerning the thermal equilibrium assumption. A summary of the results of these investigations is presented by Cambel (3). The general concensus is that local thermodynamic equilibrium (LTE) exists for the condition

$$\frac{m_H}{8m_e}\left[\frac{eEd}{\frac{3}{2}kT_e}\right]^2 << 1,$$

where m_H = mass of heavy particles (atoms and ions),

m_e = mass of electron,

e = charge of electron,

d = electron mean free path,

T_e = electron temperature, and

k = Boltzmann's constant.

Sherman, Jacobs, and Grey (4) have studied electron temperatures and equilibrium in argon plasma jets and shown that for the case of slow mixing with cooler gases, the departure between electron and heavy particle temperatures is quite small.

The third of these assumptions, that of negligible self-absorption, has been investigated only slightly. The results of these investigations are presented in Chapter V. Spectral lines in various plasmas have been shown to be appreciably absorbed, a condition contradictory to assumption three. If this condition is present in plasma to which the "unfolding" process of the previous section is applied, erroneous state properties will be obtained, and an alternate method for obtaining properties must be devised. The evaluation of the absorption characteristics for an argon plasma is the central problem of this thesis.

Single Line Intensity - Temperature Correlation

In 1923, Fowler and Milne (5) published a method for relating the intensity of electromagnetic radiation at some wavelength λ to the temperature of the emitting gas. Additional contributions have been made by Larenz (6). The resulting method is outlined briefly in the following section.

The intensity I of an emitted spectral line which occurs with the transition of an electron from an excited energy state to one of lower energy is given by

$$I = n_u A^u_\ell h \nu_{u_\ell} \tag{3}$$

where ν_{u_ℓ} = radiation frequency equal to c/λ,

h = Planck's constant,

n_u = number of atoms per unit volume in the upper energy level, and

A^u_ℓ = Einstein transition probability describing the probable number of transitions per unit time.

The number of atoms per unit volume in the excited state is given by the Boltzmann distribution as

$$n_u = n_o \frac{g_u}{Z_o} e^{-E_u/kT}$$

where n_o = the number of atoms per unit volume,

g_u = the statistical weight of the upper state,

E_u = the energy of the upper state, and

Z_o = the partition function for the basic particle.

Using this expression for n_u, one obtains the following intensity equation:

$$I = n_o \frac{g_u}{Z_o} e^{-E_u/kT} A^u_\ell h \nu_{u_\ell} ,$$

or

$$I = n_o \frac{g_u}{Z_o} e^{-E_u/kT} A^u_\ell \frac{hc}{\lambda} \quad . \tag{4}$$

The transition probabilities are not well known for most elements, but considerable experimental work has been done in obtaining a number of these values for several lines emitted by the argon atom and argon ion. The latest data available to this investigation are listed in Table II (7,8). It should be pointed out that errors exceeding fifteen to twenty per cent are common in such calculations, and much work remains to be done in this area.

For a fixed pressure, each of the variables contained in equation 4 is a function of temperature only, and as such the intensity is a function of temperature only. Since the intensity versus temperature curve has a maximum (Figure 3), the detector may be calibrated in terms of the observed intensity which corresponds to the known temperature T_{REF}.

The resulting intensity-temperature correlation is

$$\frac{I}{I_{REF}} = \frac{n_o(T)Z_o(T_{REF})}{n_o(T_{REF})Z_o(T)} e^{-\frac{E_u}{k}\left(\frac{1}{T} - \frac{1}{T_{REF}}\right)} \quad . \tag{5}$$

where the quantities n_o and Z_o may be evaluated by a method presented by Haworth (1). This intensity-temperature correlation, though void of errors caused by uncertainties in A^u_ℓ, has certain disadvantages associated with it. The value of T_{REF} is often extremely high and may

TABLE II

TRANSITION PROBABILITIES OF NEUTRAL ARGON SPECTRA

λ (Å)	E_u (cm^{-1})	A^u_ℓ ($\times 10^{-5}$)		
		Olsen	Gericke (P)*	Gericke (PE)**
4158.6	117183.7	6.6	11.0	12.0
4164.2	117151.4		2.0	1.9
4181.9	118459.7		3.8	4.3
4198.3	117563.0		26.0	23.0
4200.7	116942.8		7.6	7.7
4251.2	116660.0		0.79	0.71
4259.4	118870.9	24.6	36.0	29.0
4266.3	117183.7		2.8	2.4
4272.2	117151.4	3.7	7.1	6.7
4300.1	116999.4		3.4	3.1
4333.6	118469.1		4.9	4.6
4335.4	118459.7		4.0	3.3
4345.2	118407.5		2.8	2.5
5558.7	122086.9		8.3	
5572.6	123557.5		3.9	
5606.7	121932.9		15.0	
5650.7	121794.2		19.0	

*Obtained Photographically

**Obtained Photoelectrically

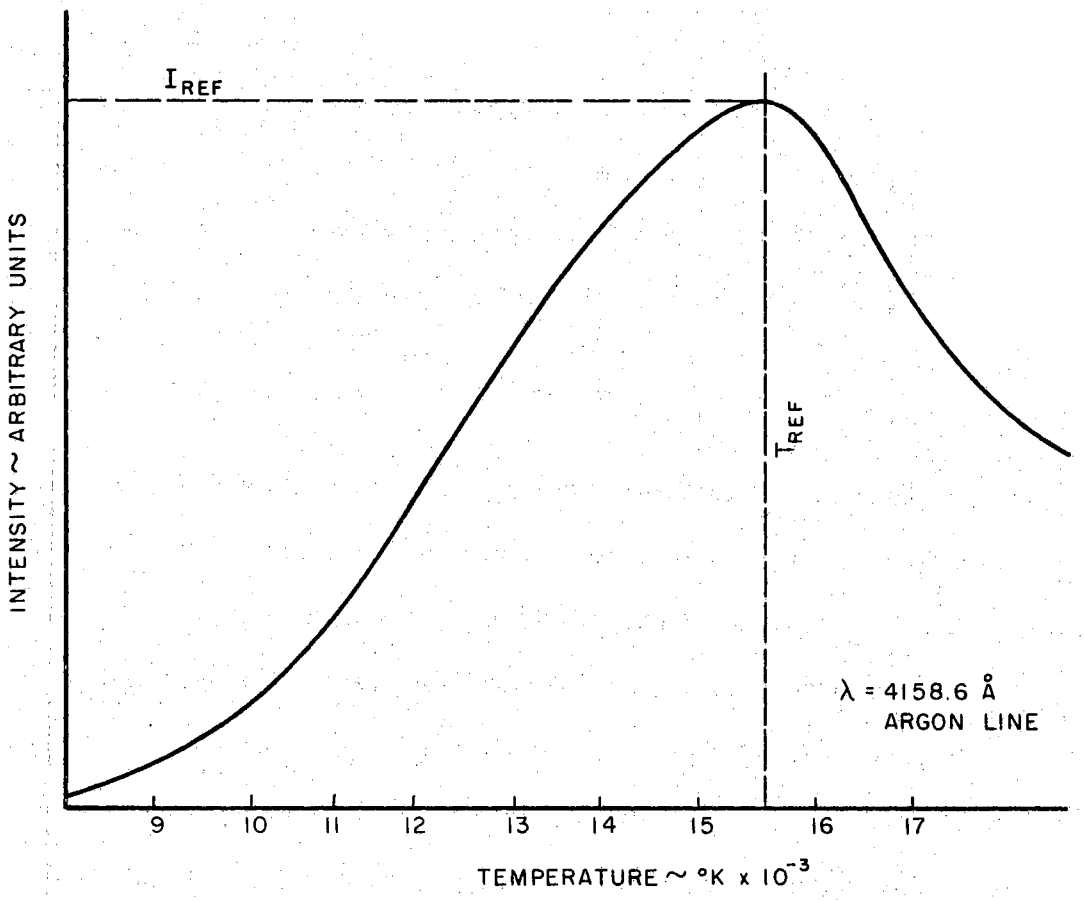

Figure 3. Intensity Variation as a Function of Temperature at Fixed Pressure for the 4158.6 Å Argon Line.

not be attainable in many plasma devices. In addition, the intensity I_{REF} is altered by any geometric changes in the detection system. Thus rigid geometric restrictions must be maintained in order to prevent frequent recalibration.

However, if some method other than the peaking of the intensity curve could be found to establish the temperature at some point in the plasma column, this one-line method would provide an excellent means of establishing T(r) as a function of the known temperature.

Relative Intensity - Temperature Correlation

In order to avoid the aforementioned problems, a method similar to that above has been developed which employs the principle of relative intensity measurements of two lines in the emission spectrum which have different wavelengths. Reference 2 presents a more complete discussion of the method which is outlined in the following section.

One can apply equation 4 to two separate spectral lines which are emitted from the same region in the plasma and obtain the following expression:

$$\frac{I_1}{I_2} = \frac{n_{o_1} g_{u_1} Z_{o_2} {}^{1}A^{u}_{\ell} \lambda_2 \, e^{-E_{u_1}/kT}}{n_{o_2} g_{u_2} Z_{o_1} {}^{2}A^{u}_{\ell} \lambda_1 \, e^{-E_{u_2}/kT}} \tag{6}$$

where 1 and 2 apply to the separate transitions under consideration. If both lines under consideration originate from an excited particle of the same type, i.e., both lines from an argon atom or both lines from an argon ion, then the number density n_o and the partition function Z_o for both transitions are the same, and one obtains the

following expression,

$$\frac{I_1}{I_2} = \frac{g_{u_1} {}^{1}A^{u}_{\ell} \lambda_2}{g_{u_2} {}^{2}A^{u}_{\ell} \lambda_1} e^{\frac{-(E_{u_1} - E_{u_2})}{kT}} . \qquad (7)$$

If spectral lines which originate from different types of excited particles, i.e., one line from an argon atom transition and one line from an argon ion transition, are used then one must retain all the variables in equation 6 and the number densities of the ground state, n_o, and the partition functions, z_o, for both the argon atom and the argon ion must be calculated using the method presented in reference 1.

The intensity methods described by equations 5 and 7 were adopted for use in the experimental work which is described in later chapters. The advantages and disadvantages of both intensity methods are discussed in Chapter VI.

Other techniques exist which may be used for temperature determination, but most of those which do not alter the flow field are based upon an intensity measurement of emitted electromagnetic radiation. Complete discussions of these methods are presented by Griem (9). References 10-17 also presented discussions of these methods which were found to be of great value in selecting a temperature determining technique to be used in this study.

Since the methods which have been presented in the previous sections all relate the state of the gas at some region in the jet to the energy emitted at that point, it is essential that the observer know the correlation between the energy which is emitted at the point in

question and that which is received by the detector. The cause of difference in these two values will now be investigated in greater detail.

CHAPTER III

SELF-ABSORPTION PHENOMENA

In the intensity-temperature correlation methods presented in Chapter II, line intensities which have not been attenuated due to self-absorption are needed. Cowan and Dieke (18) performed detailed investigations on various lines in ordinary metal arcs and found that many lines may lose as much as 95 per cent of their original intensity by self-absorption while others experienced only slight self-absorption. Profiles of lines which have experienced various degrees of self-absorption are shown in Figure 4. It is seen that a spectral line which is moderately absorbed, profile (b), is in no way distinguishable from an unabosrbed line of lesser intensity. However, if the self-absorption becomes quite severe, as is the case with profile (d), then self-reversal is said to occur. This condition is easily recognized if high spectral resolution is obtained. Conditions which produce profile (d) are not present in the plasma under consideration, and further discussions of self-absorption will apply to lines similar to profiles (b) and (c).

Lines similar to profiles (b) and (c) may be produced when light is emitted from the interior of a plasma column and must travel through other sections of the plasma in order to reach the detector. During this passage it is subject to absorption because there are in its path

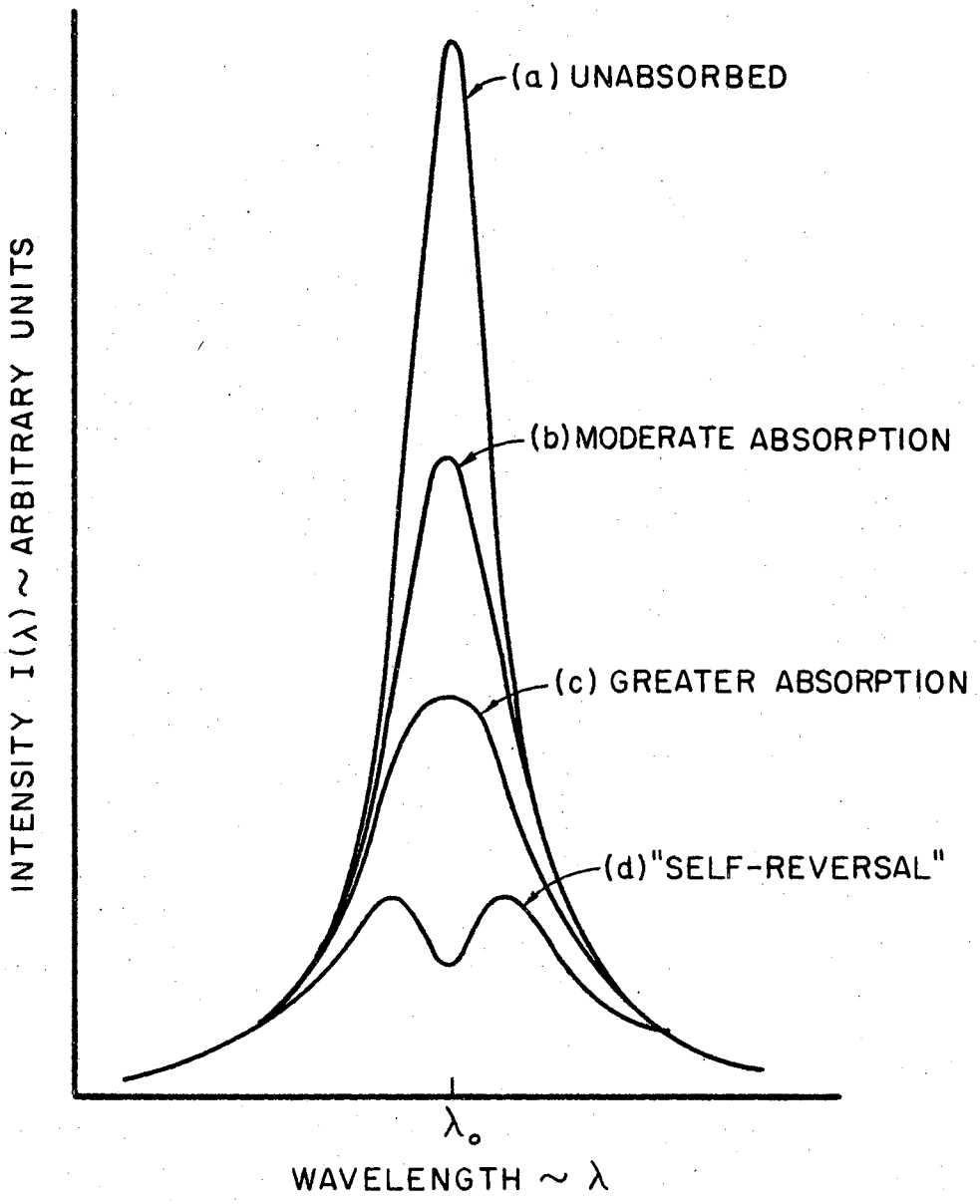

Figure 4. Typical Line Shapes for Various Degrees of Absorption.

atoms of the same kind that cause the emission. Thus a photon of energy hc/λ which was emitted from atom A (Figure 5) as a result of the transition of an electron from energy level E_2 to energy level E_1 may be absorbed by atom B thereby raising an electron of atom B from energy state E_1 to energy state E_2. At some later time (perhaps only 10^{-8} seconds later) a photon may be emitted by atom B, but in a direction different from that following by the first photon.

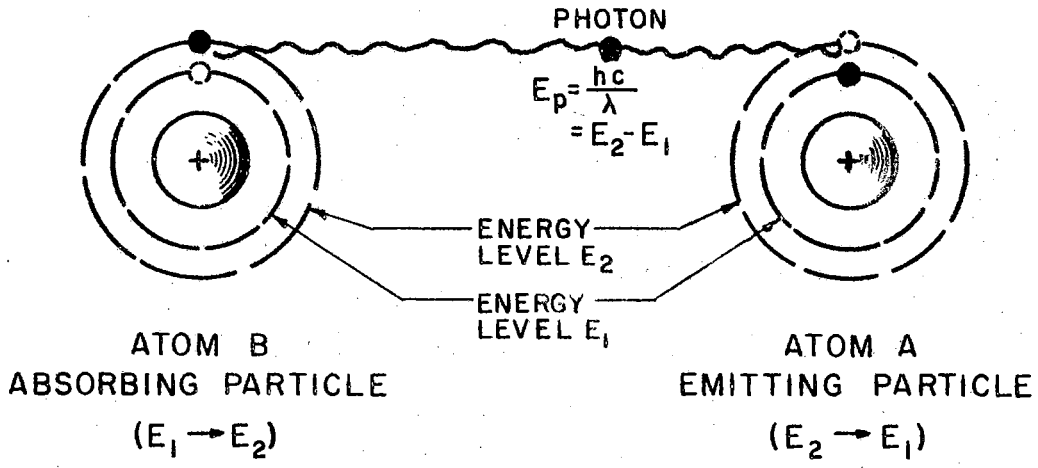

Figure 5. Photon Absorption by Electronic Excitation on a Microscopic Scale.

In addition to the electronic excitation process described in the previous paragraph, another absorption process is also possible. If the energy of the incident photon is large enough to produce the electronic transition $E_1 \rightarrow E_2$, then it may be large enough to cause an

electron in some of the higher energy levels to acquire sufficient energy to become free of the nucleus. This phenomenon is called the photoelectric effect, and is expressed by

$$\frac{1}{2} m_e v_e^2 = \frac{hc}{\lambda} - \left(E_{i.p.} - E_{e\ell} \right) ,$$

where $E_{i.p.}$ = the ionization potential,

$E_{e\ell}$ = the electronic energy level,

m_e = the mass of the ejected electron, and

v_e = the velocity of the electron after escape.

Thus either of these absorption processes may occur if a photon of sufficient energy encounters an atom or ion with the corresponding energy distribution.

On a somewhat larger scale, a volume of gas R_1 may emit photons of varying wavelengths in all directions since the region contains particles in many different energy states. Those photons which are emitted in the x-direction (Figure 6) may be used to determine the state of R_1 if region R_2, which lies between R_1 and the detector, has known absorption characteristics.

The controlling factor in the absorption process is the absorption coefficient which indicates the fractional decrease of intensity dI/I per unit path length. Lambert's Law states that the proportion of radiation absorbed by a substance is independent of the intensity of the incident radiation; or in an alternate form, that each successive layer of thickness dx of the medium absorbs the same fraction dI/I of

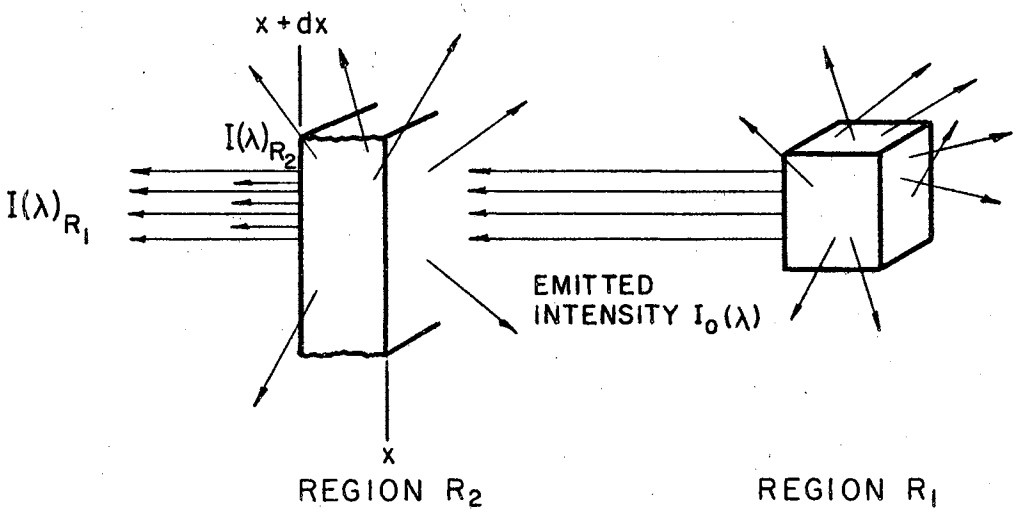

Figure 6. Photon Absorption and Scatter on a Macroscopic Scale.

of the radiation of intensity I incident upon it, i.e., $dI/I = -\mu dx$ where μ is the absorption coefficient (19).

It is important to note that Lambert's Law applies to monochromatic radiation only, and that μ is a function of wavelength λ. In the case of a plasma, it is necessary to restrict the application to radiation which was initially incident upon the absorbing region. This requires that the contribution to the emerging radiation from the absorbing region which may emit energy of the same wavelength must be eliminated. Thus, the correct mathematical statement of this law is

$$\frac{dI(\lambda)}{I(\lambda)} = -\mu(\lambda)dx \ ,$$

where $I(\lambda)$ indicates the intensity in the wavelength region λ to $\lambda + d\lambda$ which results from that radiation which crosses the x-plane (Figure 6) in the positive x-direction only. The fact that the absorbing volume spontaneously emits radiation of wavelength λ due to its state in no way influences the conventional definition of the absorption coefficient.

An integration of the preceding equation results in the following expression,

$$\frac{I(\lambda)}{I_o(\lambda)} = e^{-\int_o^x \mu(\lambda)dx} \ , \qquad (8)$$

where $I_o(\lambda)$ is the intensity of the radiation in the wavelength interval λ to $\lambda + d\lambda$ incident upon the x-plane in Figure 6. The absorption

coefficient varies with the state of the absorbing media as well as with wavelength. For the plasma column considered in this study the properties vary from centerline to outer radius and $\mu(\lambda)$ may not be considered constant across the absorbing layer. In view of the variation of $\mu(\lambda)$ it is advantageous to define an average absorption coefficient $\bar{\mu}$ as

$$\bar{\mu}(\lambda)x = \int_0^x \mu(\lambda)dx \quad .$$

The final expression relating the observed to initial intensity values is

$$\frac{I(\lambda)}{I_o(\lambda)} = e^{-\bar{\mu}(\lambda)x} \quad . \tag{9}$$

A modified form of the linear absorption coefficient $\bar{\mu}(\lambda)$ is the mass absorption coefficient $\mu_m(\lambda)$. This quantity which is equal to $\bar{\mu}(\lambda)/\rho$, where ρ is the mass density of the absorbing material, exhibits far less variation from material to material than does $\bar{\mu}(\lambda)$. In terms of this mass absorption coefficient equation 9 assumes the form

$$\frac{I(\lambda)}{I_o(\lambda)} = e^{-\bar{\mu}(\lambda)\frac{\rho x}{\rho}} = e^{-\mu_m(\lambda)\, m_a} \tag{10}$$

where m_a is the mass per unit area of the irradiated media.

It should be pointed out that the absorption coefficients defined above are independent of the mechanism of absorption. The coefficients are defined only in terms of observed intensities and no attempts will

be made to differentiate between energy lost by Compton scattering, photoelectric emission, electronic excitation or any other absorption phenomenon since the net result for all such processes is the same, namely a reduction in the amount of energy received, in a specified direction, from the region in question.

The attenuation process under consideration theoretically applies to radiation in a wavelength region λ to $\lambda + d\lambda$, but in any measurement of $\bar{\mu}(\lambda)$, the increment $d\lambda$ must be approximated by a finite $\Delta\lambda$. The absorption characteristics may vary with λ_i in $\Delta\lambda$ (Figure 7) therefore, it is necessary to define the wavelength region to which $\bar{\mu}(\lambda)$ applies, since an averaging process over the wavelength region $\Delta\lambda$ is implied.

If a large $\Delta\lambda$ is associated with $\bar{\mu}(\lambda)$, then the integrated or total intensity of the region in question may obliterate the effects of absorption in some smaller region $\Delta\lambda_i$. If in this observed region $\Delta\lambda$ the intensity distributions $I(\lambda)$ and $I_o(\lambda)$ have the form shown in Figure 7, then the value of $\bar{\mu}(\lambda)x$ would be very small since the ratio of the two areas or integrated intensities is very nearly one. Thus severe errors in the absorption coefficient associated with λ_i would be introduced.

The most desirable averaging process involves resolving the wavelength region in question into a number of segments for which $\Delta\lambda << 1$ Angstrom and evaluating $\bar{\mu}(\lambda)$ for each of these small sections. Unfortunately, an extremely high degree of resolution would be necessary in order to attain this result. The averaging technique associated with the $\bar{\mu}(\lambda)$ of this thesis is discussed in more detail in Chapter V.

In order to evaluate the amount of absorption experienced by the energy which was emitted from the center of the plasma column, one

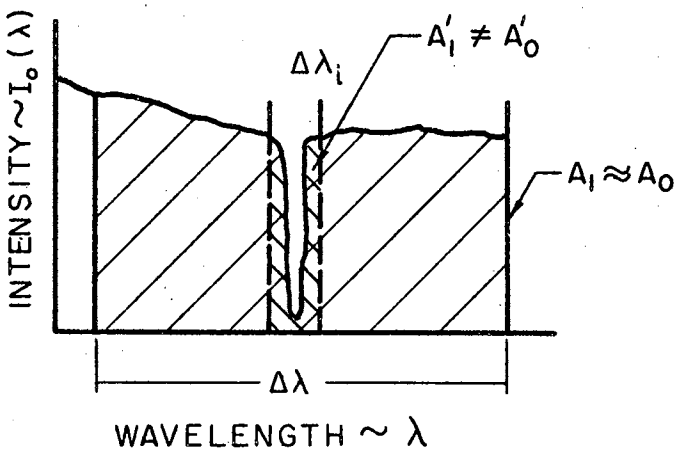

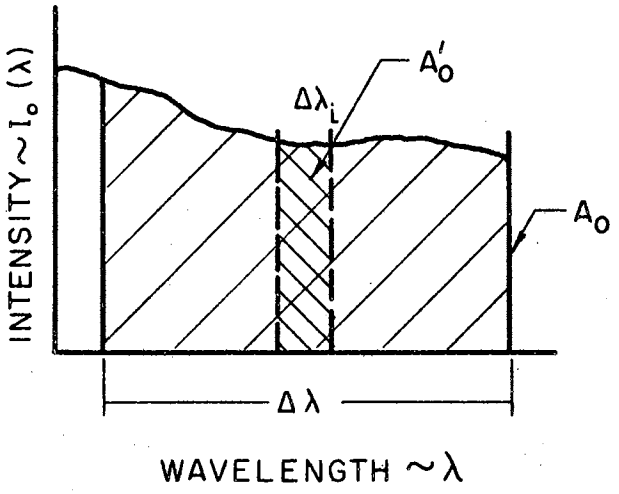

Figure 7. Dependence of Absorption Characteristics upon Wavelength Interval.

would have to observe its intensity both prior to and after passing through the rest of the plasma column. This is not possible since the only energy one may observe is that which has already passed through the possibly absorbing medium. Thus the self-absorption phenomenon must be simulated in such a way that one may observe the unattenuated intensity values.

If it may be assumed that the mechanism of absorption is dependent only upon the absorbing particle and the energy of the photon, and independent of the source of the photons; then a secondary source of photons may be used to obtain absorption data. In this way the unattenuated intensity values may be determined by merely removing the absorbing matter. A method of this type was used in this study and is described in detail in Chapter IV.

One then assumes that the absorption coefficient predicted by the intensity ratio of the attenuated and unattenuated signal from the secondary source is the same as that which is obtained from the absorption of energy produced by the plasma itself. Embodied in this assumption is the idea that the absorption of energy emitted by the plasma itself does not significantly affect the absorption of the energy from the secondary source.

Theoretical Absorption Coefficients

The theoretical approach to the calculation of the absorption coefficient is based on the interaction of an electromagnetic wave with an electric dipole. It should be pointed out that although the electric dipole moment of an argon atom is zero in the absence of an

electromagnetic field, the interaction energy associated with an atom in the proximity of a charged particle, the situation in a plasma column, induces a difference in center of positive charge and center of negative charge resulting in a non-zero electric dipole moment. For a detailed discussion of this interaction the reader is referred to Herzberg (20), Kuhn (21), or Penner (22). The following is a brief discussion of the development of the theoretical absorption coefficient.

In the following section N_ℓ is the number of atoms per unit volume in the lower energy state which is identified by the subscript ℓ, N_u is the number of atoms per unit volume in the upper energy state which is identified by the subscript u, and $B_{\ell\to u}$ is the Einstein coefficient for induced absorption, $B_{u\to\ell}$ is the Einstein coefficient for induced emission, and $A_{u\to\ell}$ is a modified form of the previously defined Einstein coefficient for spontaneous emission. The atoms are located in a radiation field of spectral density $\rho_{\nu_{\ell u}}$, the radiant energy per unit volume in a frequency interval $\nu_{\ell u}$ to $\nu_{\ell u} + d\nu_{\ell u}$.

The number of transitions in unit time per unit volume from energy state E_ℓ to energy state E_u is $N_\ell B_{\ell\to u}\rho_{\nu_{\ell u}}$, and the number of induced transitions in unit time per unit volume from energy state E_u to energy state E_ℓ equals $N_u B_{u\to\ell}\rho_{\nu_{\ell u}}$. Thus the net number of transitions N_{tr} from energy level E_ℓ to energy level E_u per unit time per unit volume induced by the radiation field is given by

$$N_{tr} = \left(N_\ell B_{\ell\to u} - N_u B_{u\to\ell} \right) \rho_{\nu_{\ell u}}$$

Since the absorption may occur at frequencies very near $\nu_{\ell u}$ due to the fine structure of the atom, all the photons whose energy falls in some small frequency interval $\Delta\nu_{\ell u}$ must be considered subject to absorption. Penner reports the number of photons N_p which are absorbed is given by

$$N_p = c \int_{\Delta\nu_{\ell u}} \rho_{\nu_{\ell u}} \mu_\nu \, d\nu/h\nu,$$

where μ_ν is the absorption coefficient at frequency ν. For small values of $\Delta\nu_{\ell u}$, the previous equation may be approximated by

$$N_p \cong \frac{1}{h\nu_{\ell u}} c \, \rho_{\nu_{\ell u}} \int_{\Delta\nu_{\ell u}} \mu_\nu d\nu \, .$$

Since the number of transitions N_{tr} must equal the number of photons absorbed, then

$$\left(N_\ell B_{\ell \to u} - N_u B_{u \to \ell} \right) \rho_{\nu_{\ell u}} = \frac{1}{h\nu_{u\ell}} c \, \rho_{\nu_{\ell u}} \int_{\Delta\nu_{\ell u}} \mu_\nu d\nu \, .$$

Thus the integrated absorption for the spectral line whose center frequency is $\nu_{u\ell}$ is obtained, i.e.

$$\int_{\Delta\nu_{\ell u}} \mu_\nu d\nu = \left(N_\ell B_{\ell \to u} - N_u B_{u \to \ell} \right) \frac{h\nu_{\ell u}}{c} \, .$$

Penner equates the total number of downward transitions per unit time per unit volume to the number of upward transitions and obtains the following;

$$A_{u\to\ell} = \frac{8\pi h\nu_{u\ell}^{3}}{c^{3}} B_{u\to\ell} ,$$

and

$$g_{\ell}B_{\ell\to u} = g_{u}B_{u\to\ell} ,$$

where g is the statistical weight of the energy state.

Substituting these expressions into the integrated absorption equation produces

$$\int_{\Delta\nu_{\ell u}} \mu_{\nu} d\nu = \frac{c^{2}}{8\pi\nu_{\ell u}^{2}} N_{\ell} A_{u\to\ell} \frac{g_{u}}{g_{\ell}} \left(1 - \frac{N_{u}}{N_{\ell}} \frac{g_{\ell}}{g_{u}} \right) .$$

As previously defined, the particle distribution is given by

$$\frac{N_{\ell}}{N_{u}} = \frac{g_{\ell}}{g_{u}} e^{+\frac{h\nu_{u\ell}}{kT}} .$$

Therefore the integrated absorption expression is given by

$$\int_{\Delta\nu_{\ell u}} \mu_{\nu} d\nu = \frac{c^{2}}{8\pi\nu_{\ell u}^{2}} N_{\ell} A_{u\to\ell} \frac{g_{u}}{g_{\ell}} \left[1 - e^{-\frac{h\nu_{u\ell}}{kT}} \right] .$$

An absorption coefficient $\mu^*(\lambda)$ is now defined such that $\mu^*(\lambda)\delta = \int_{\Delta\nu_{\ell u}} \mu(\lambda)d\lambda$ where δ is the width of the emission line when $I(\lambda)$ is equal to one-half the maximum intensity (Figure 8). The final expression for the theoretical absorption coefficient is

$$\mu^*(\lambda) = \frac{g_u A_{u\to\ell} c^2 N_\ell}{g_\ell \nu^2 \delta} \left[1 - e^{-\frac{hc}{\lambda_o kT}} \right] .$$

There exist two severe restrictions on the application of the preceeding equation to actual evaluation of $\mu^*(\lambda)$. Neither δ nor $A_{u\to\ell}$ is well known for many of the argon spectral lines. Approximations may be made for δ, but for those lines whose $A_{u\to\ell}$ values are unknown, experimentation currently offers the only means of obtaining absorption coefficients. However, this expression for $\mu^*(\lambda)$ does indicate the importance of various variables in the absorption process.

The method which has been presented above indicates that the absorption coefficient is a function of the number of particles in the lower energy level ℓ. Thus for some particular particle density n_i in state ℓ, it is anticipated that the probability of an atom interacting with a photon will be so small that the attenuation of the incident beam will be negligible; but as the particle density increases, a density of sufficient magnitude to attenuate appreciably the incident beam may be reached. Absorption coefficients corresponding to varying particle densities for selected wavelengths in the argon spectrum are presented in Chapter VI.

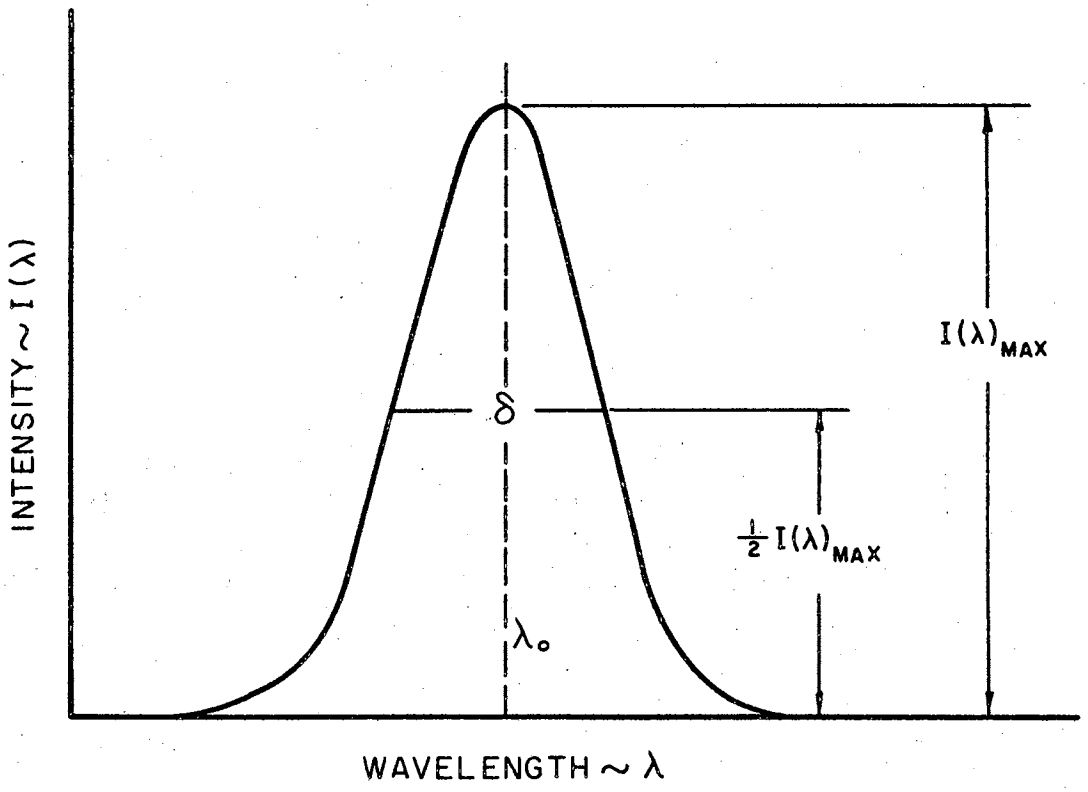

Figure 8. Intensity Profile of a Spectral Line of Wavelength λ_o.

CHAPTER IV

EXPERIMENTAL APPARATUS

A plan view of the Oklahoma State University Plasma Facility is given in Figure 9. The basic design of this facility is described in reference 1; however, modifications have been made for the study of absorption characteristics. These modifications will be described in the appropriate sections.

Generator - Expansion Assembly

The plasma generator or plasma head shown in Figure 10 was composed of three separate items: the rear electrode, the copper anode or nozzle, and a low pressure chamber. The details of the generator are shown in Figure 11.

The rear electrode consisted of two concentric copper tubes to the end of which was silver soldered a two per cent thoriated tungsten rod which was ground to approximately a ninety degree angle with a rounded tip. Several tip configurations were investigated and the one described here resulted in maximum stability for the operating conditions selected. The rear electrode was water-cooled and served as the cathode in the power circuit. Power leads from the DC power supply were attached to the rear electrode and to the copper nozzle to complete the power circuit for the generator. The DC power supply consisted of

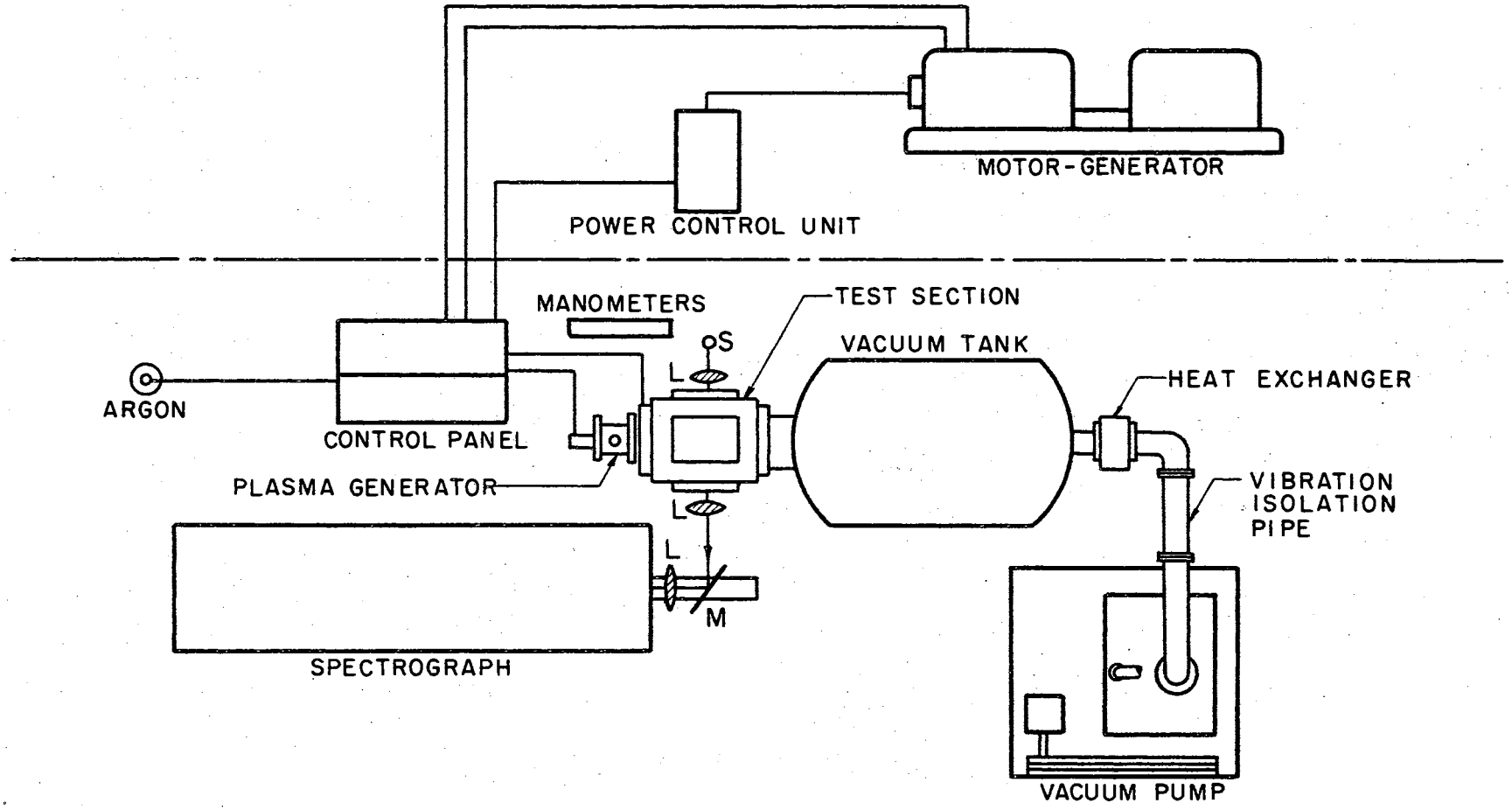

Figure 9. Plan View of the OSU Plasma Facility.

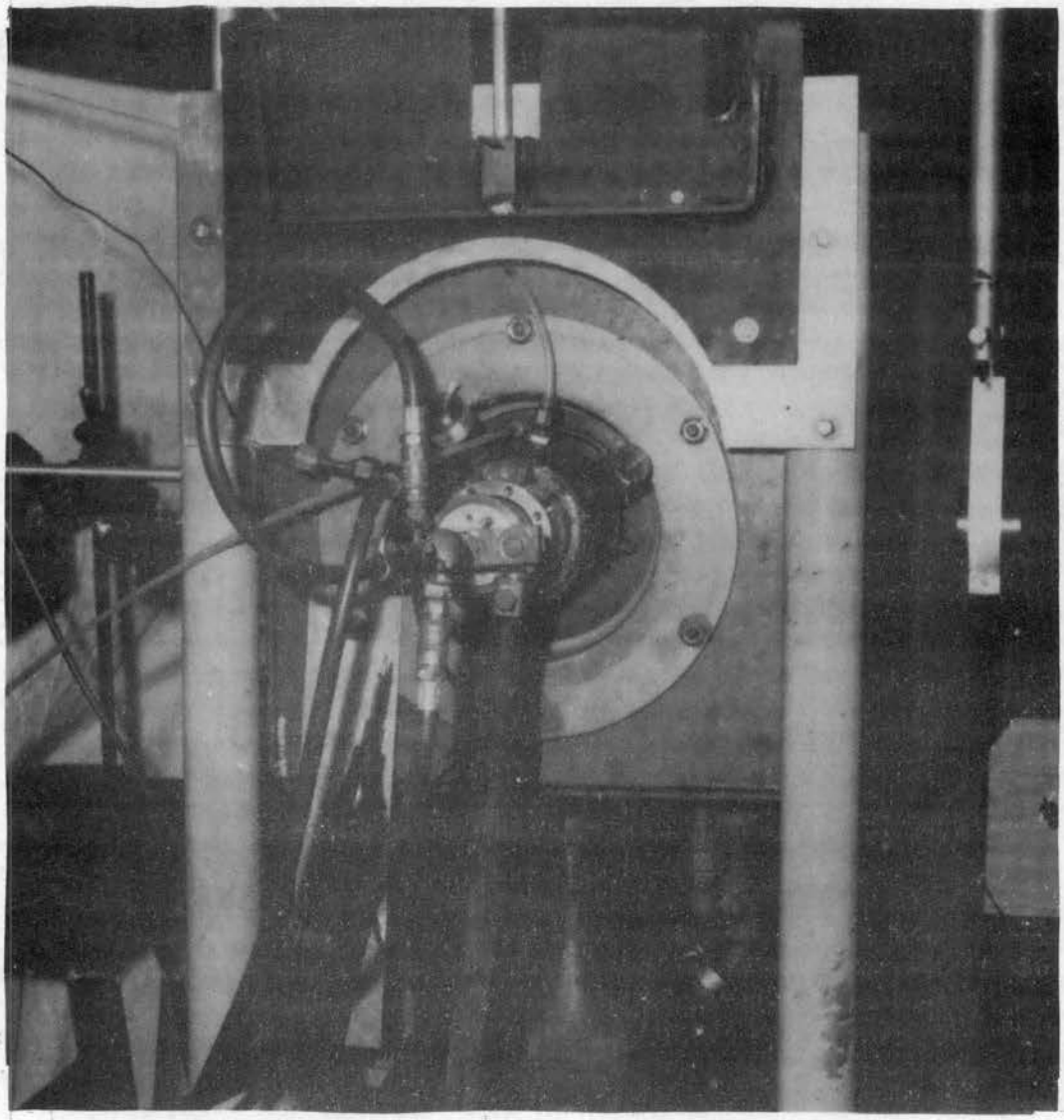

Figure 10. Plasma Generator.

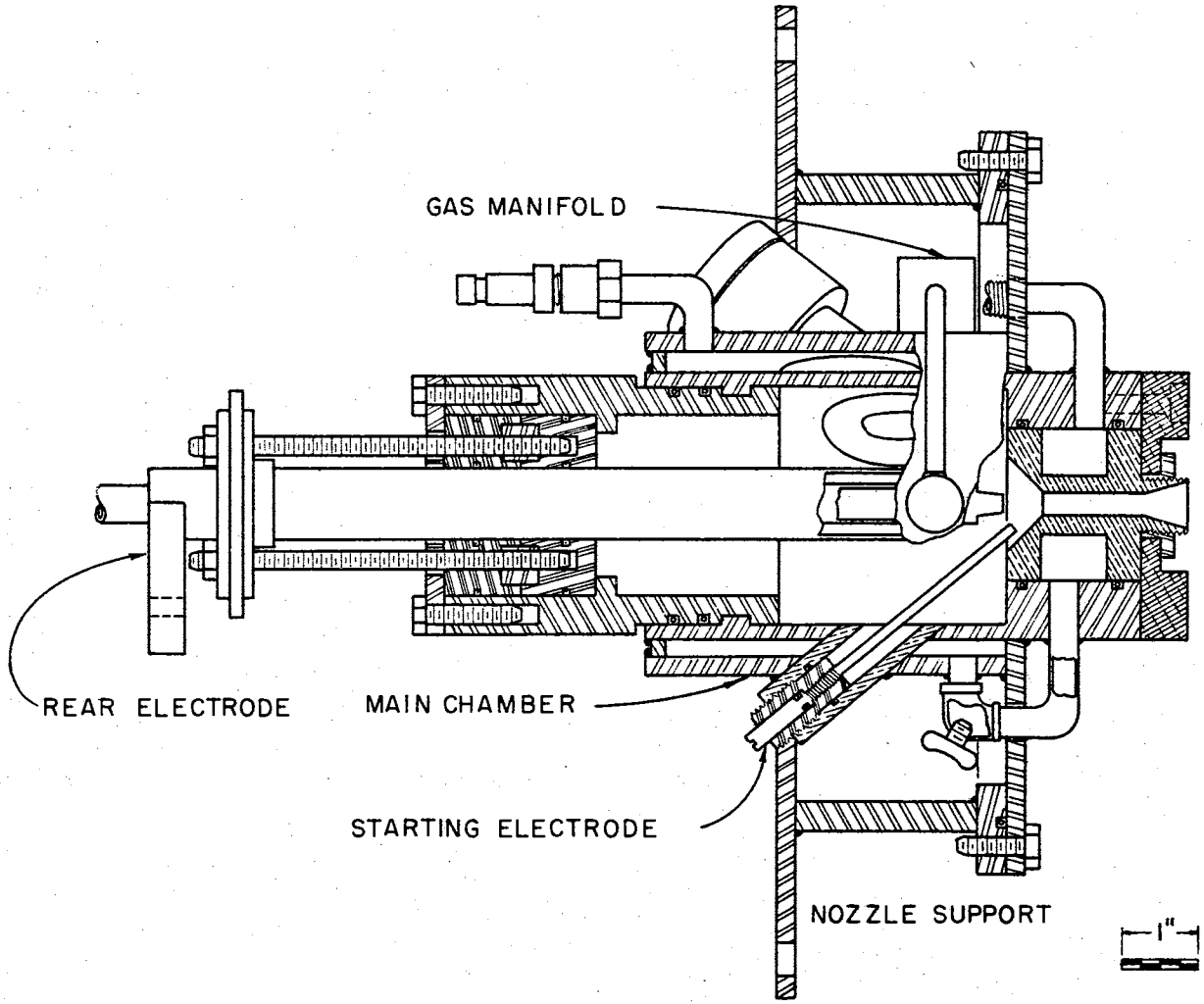

Figure 11. Plasma Generator Details.

a DC generator driven by an AC motor and was capable of supplying up to 700 amperes at whatever voltage resulted across the arc. However, the power leads to the rear electrode and nozzle were unable to carry this current and a maximum of 450 amperes for prolonged periods of time was established.

The copper nozzle shown in Figure 12 (a) was also water-cooled since it served as the anode of the power circuit and as such received the energy released upon impact by the high velocity electrons. This particular design for the nozzle was chosen after unstable operation of the jet resulted when nozzles (b) and (c) were used. After a series of trial-and-error adjustments, it was decided that a part of the unstable operation of the jet could be contributed to the fact that pressures of 150 to 250 mm of mercury were occurring in the main chamber. It was believed that these pressures were too low to stabilize the arc, and that the normal perturbations associated with a system of this type were causing the arc to oscillate within the chamber. Thus a longer straight section was included in a new nozzle design and a divergent section added to the end to produce a jet with a maximum diameter. A thicker boundary layer was produced in this longer straight section and a smaller effective flow area resulted. Thus for a fixed mass flow rate, at a choked condition, the pressure in the arc chamber was higher than those at comparable conditions for nozzles (b) and (c). The increased pressures attained with the use of nozzle (a) did in fact result in more stable operation.

The main chamber which was also water-cooled, was designed to hold the rear electrode, expansion nozzle and starter system as shown in

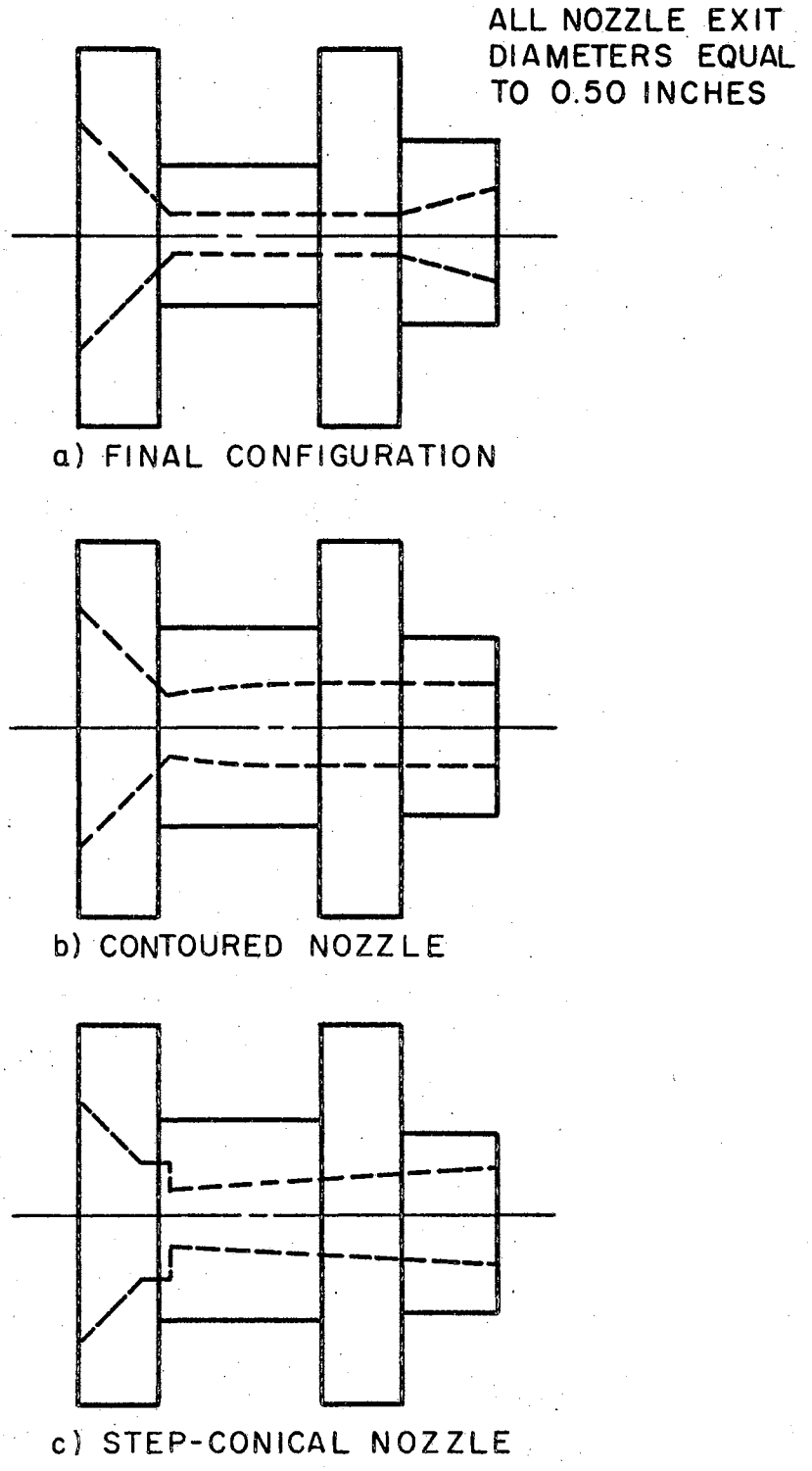

Figure 12. Water Cooled Expansion Nozzles.

Figure 11. Gas inlets were located in the main chamber as was a pressure top for monitoring arc pressures. During this study several new starter systems were designed after the previous system either began leaking or overheating due to its close proximity to the arc. It was essential that both these effects be avoided since either would introduce foreign elements into the flow which might affect the absorption characteristics. When the final chamber design was complete, the facility was run continuously for durations up to one hour and no visible deterioration in nozzle, rear electrode or starter assembly was observed.

Optical Systems

The optical system which was used in this study had to satisfy three distinct requirements. This system was required to: (1) produce a steady and reproducible supply of radiation in the 3500 to 6000 Angstrom wavelength region, (2) direct this radiation so that it passed at right angles through the plasma column, and (3) direct the radiation which was transmitted through, and emitted by, the plasma column to the detector for analysis.

Four different systems were designed, assembled and evaluated in an attempt to satisfy these requirements.

The first system (Figure 13) that was investigated used the emission of the plasma jet itself as the source of radiation. In this way, the spectrum resulting from this source was composed of the very lines in the argon spectrum for which the absorption coefficients were most desired. The remainder of this system consisted of two 2 1/4 inch

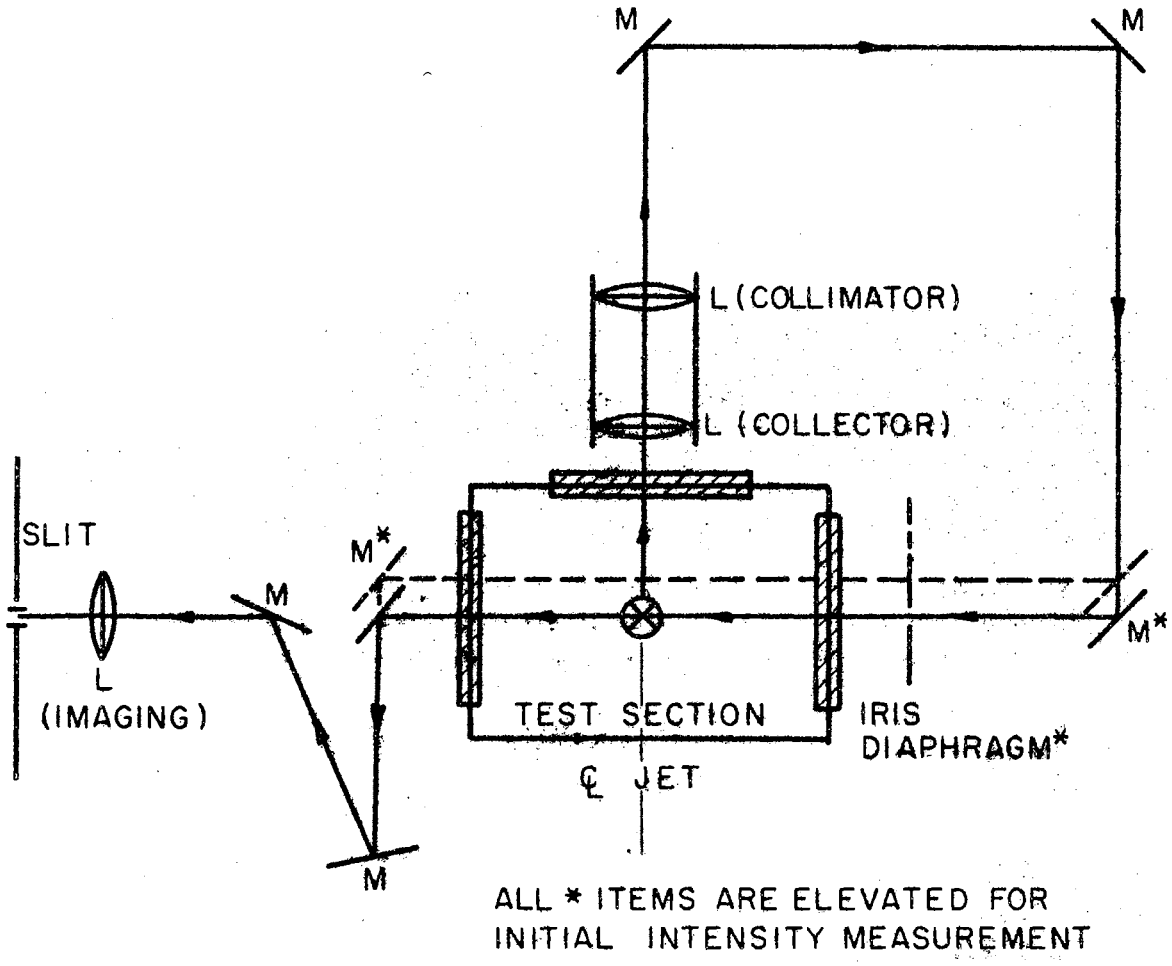

Figure 13. Argon Plasma Emission as Secondary Source.

diameter, 4 1/2 inch focal length achromatic lens for focusing the beam on the spectrograph slit.

This system would collect and collimate the emission through the top viewing panel of the test section. The beam was then directed, using a series of front surfaced mirrors, through the side viewing panel and passed horizontally through the center line of the jet. The mounting system was then elevated so that the beam no longer passed through the jet, but passed above it so that comparative measurements might be made. This system was abandoned when it was found that low intensity values were obtained after completing the long optical path. The resultant intensities produced a detector signal of measurable magnitude, but it was of such a level that the resultant output signal to electronic noise ratio was of such a low value as to make quantitative measurements of these low intensities of dubious value.

The second system (Figure 14a) investigated consisted of a Pryometric Molarc Lamp as the radiation source; an 8 1/2 inch focal length achromatic collimator lens; two front surface aluminum mirrors; one iris diaphragm; and the 4 1/2 inch focal length focusing lens. The source used with this system produces a high intensity, continuous spectrum throughout the 3000 to 42,000 Angstrom range. This source, a carbon arc whose spectral distribution is similar to that of a 3800 °K black body, provided the desired intensity and reproducibility, but lacked stability. Movement of the cathode spot on the carbon electrode, on which the collector lens was focused, caused intensity fluctuations of such a magnitude as to make this source undesirable. This type of source, i.e., emission by a source other than the jet, has advantages

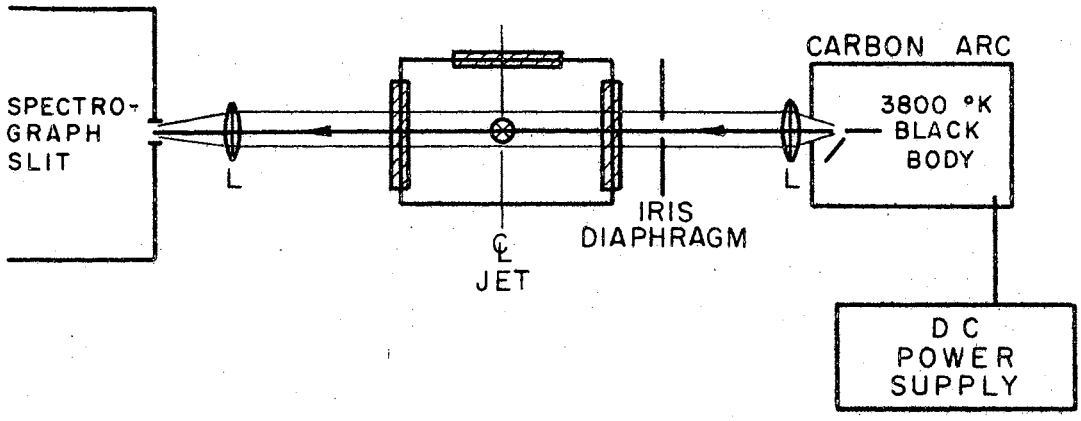

Figure 14a. Carbon Arc (3800 °K Black Body) Emission as Secondary Source.

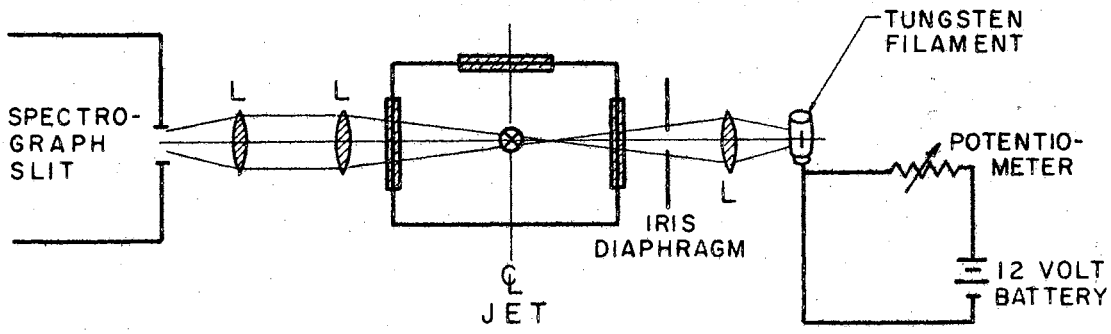

Figure 14b. Tungsten Filament Emission as Variable Intensity Secondary Source.

in that reproducibility and steadiness of operation may be easily verified and provides a greater flexibility in selecting initial intensity values so that the intensity to noise ratio may be kept high. However, there are certain disadvantages associated with a continuous spectrum. It becomes increasingly important in a system of this type that the problem of integrated intensities be monitored closely and that a $\Delta\lambda$ be observed which does not obliterate any absorption effects.

System 2 was discarded due to fluctuations of approximately twenty per cent in spectral intensities, but the continuous spectrum approach was maintained throughout the third and fourth systems, as was the optical arrangement of System 2.

The third and fourth designs were very similar in many respects, but their slight differences proved to be quite significant. After failure of System 2, the next logical step was to attempt to produce a similar spectrum, though not necessarily as intense, in a more stable manner. Having decided on the continuous spectrum approach, a common tungsten filament appeared to exhibit the desired reproducibility and steadiness. Also, the intensity level was adequate in the shorter wavelength region if the filament was operated at voltages higher than design level. However, since an image of the original source is eventually produced on the spectrograph slit, the coiled filament was unacceptable due to large intensity variations that occurred from the spacing between the coils. With these variations, a very slight movement of the source or detector might cause a different section of the coil to be observed with a resulting large variation in intensity. In an attempt to avoid these intensity variations in the image on the

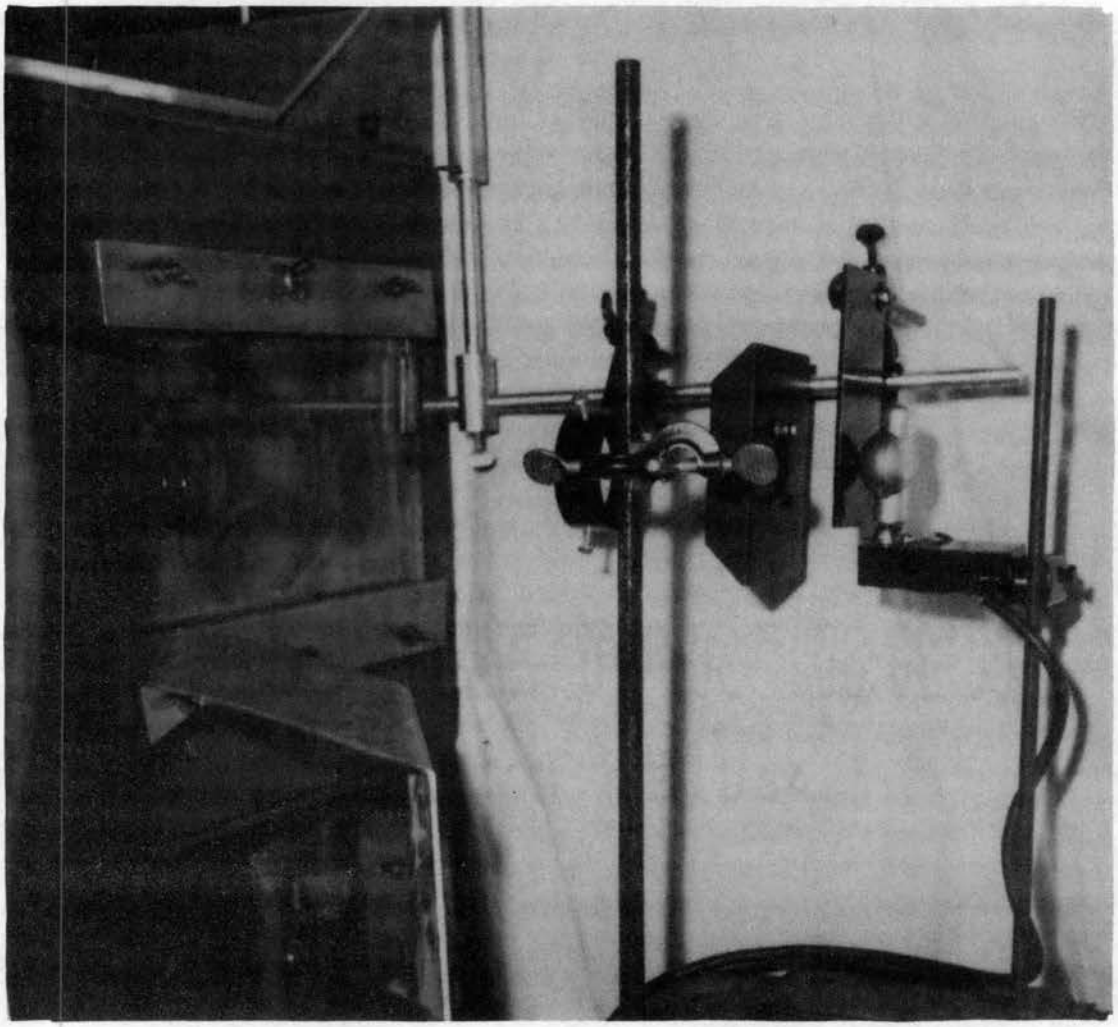

Figure 15. Secondary Radiation Source.

spectrograph slit, a wide ribbon type tungsten filament source was obtained. Since the image of the ribbon filament on the spectrograph slit was wider than the slit, slight movements of the optical system did not alter the intensity readings. Unfortunately, it was necessary to overheat this filament in order to obtain the desired intensities in the 3500 Angstrom region, and without the added strength supplied by the coils of a typical tungsten filament, the ribbon filament was unable to support its own weight and failed.

Figure 15 shows the final design for the secondary radiation source. This source was a fifty watt "Kondo" projector lamp with aluminized bulb. The emission from the coiled tungsten filament eventually left the bulb from a 3/4 inch diameter non-aluminized area. This emission was directed onto a blackened aluminum plate in which a small hole (approximately .04 inch diameter) had been drilled. The energy reflected from the aluminum bulb and that emitted directly toward the hole produced essentially a uniform distribution over this small area. In this way the hole very nearly approximated a small point source of continuous radiation. The remaining optics were adjusted so that the hole served as the object which was eventually imaged on the centerline of the plasma jet and then again on the spectrograph slit. Lens 2 (Figure 16) was adjusted to produce an image of the illuminated hole at the centerline of the plasma jet, and the remaining components were adjusted to image the jet and this centerline image of the hole on the spectrograph slit.

The imaging distance for the illuminated hole was adjusted by varying the object distance until the incident beam converged to an image

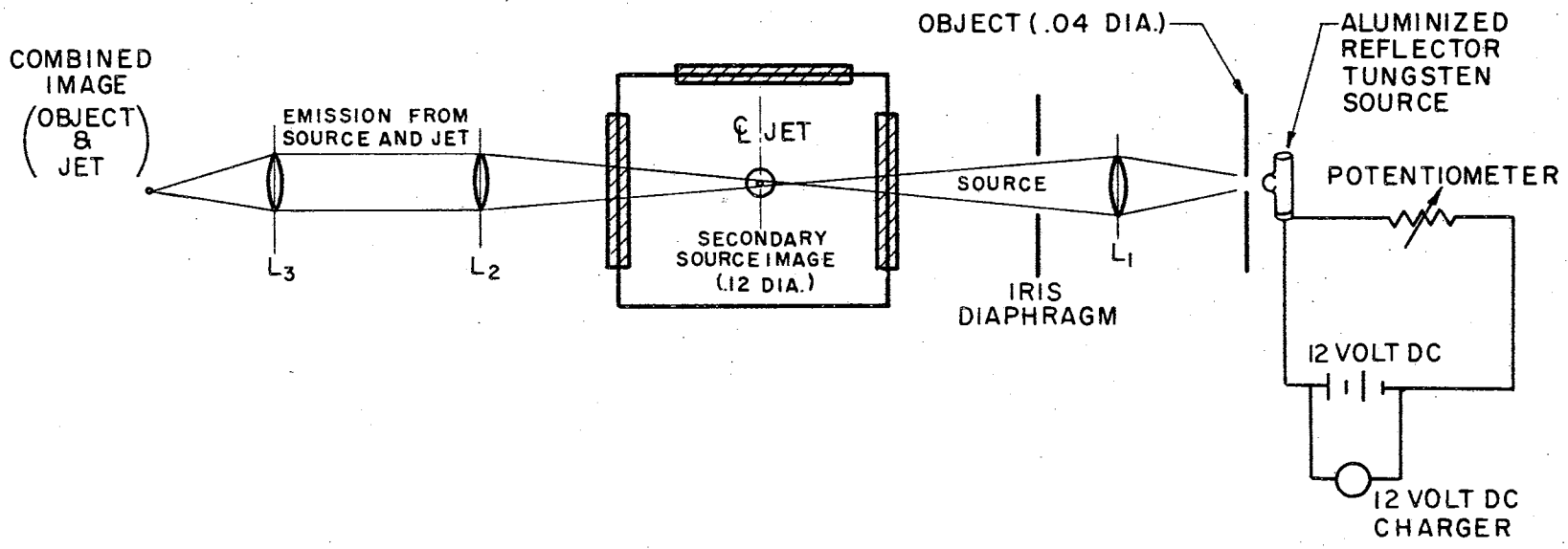

Figure 16. Final Secondary Source--Optical Arrangement.

at a distance of 19 inches from the lens. With this arrangement, the radiation from the hole converged slowly to the image at the centerline, but closely approximated a parallel beam of radiation whose energy per unit area varied slightly across the jet. The diameter of the secondary beam at the outer radius of the plasma column was .18 inches while the minimum diameter of .12 inches occurred at the jet centerline.

In order to insure the stability of the secondary source, a twelve volt storage battery was used as a power supply, and a battery charger included in the circuit to maintain the supply voltage. A variable potentiometer was placed in series with the power supply and source in order to provide flexibility in selection of the intensity of the incident radiation.

Thus a stable, reproducible, variable intensity source of electromagnetic radiation in the 3000 to 8000 Angstrom wavelength region was obtained.

Detection System

In order to accomplish the objectives of the absorption research program, certain modifications had to be made to the existing radiation detection system. The 3.4 meter Ebert spectrograph was modified to incorporate an indicating system more sensitive than the photographic plates which had been used previously. This modification was the subject of a Master's report by Mr. H. Smith (23). A summary of his report is given below.

An American Instrument Company Photomultiplier-Microphotometer Assembly, Model No. 10-211 (Figure 17) was selected as the indicating

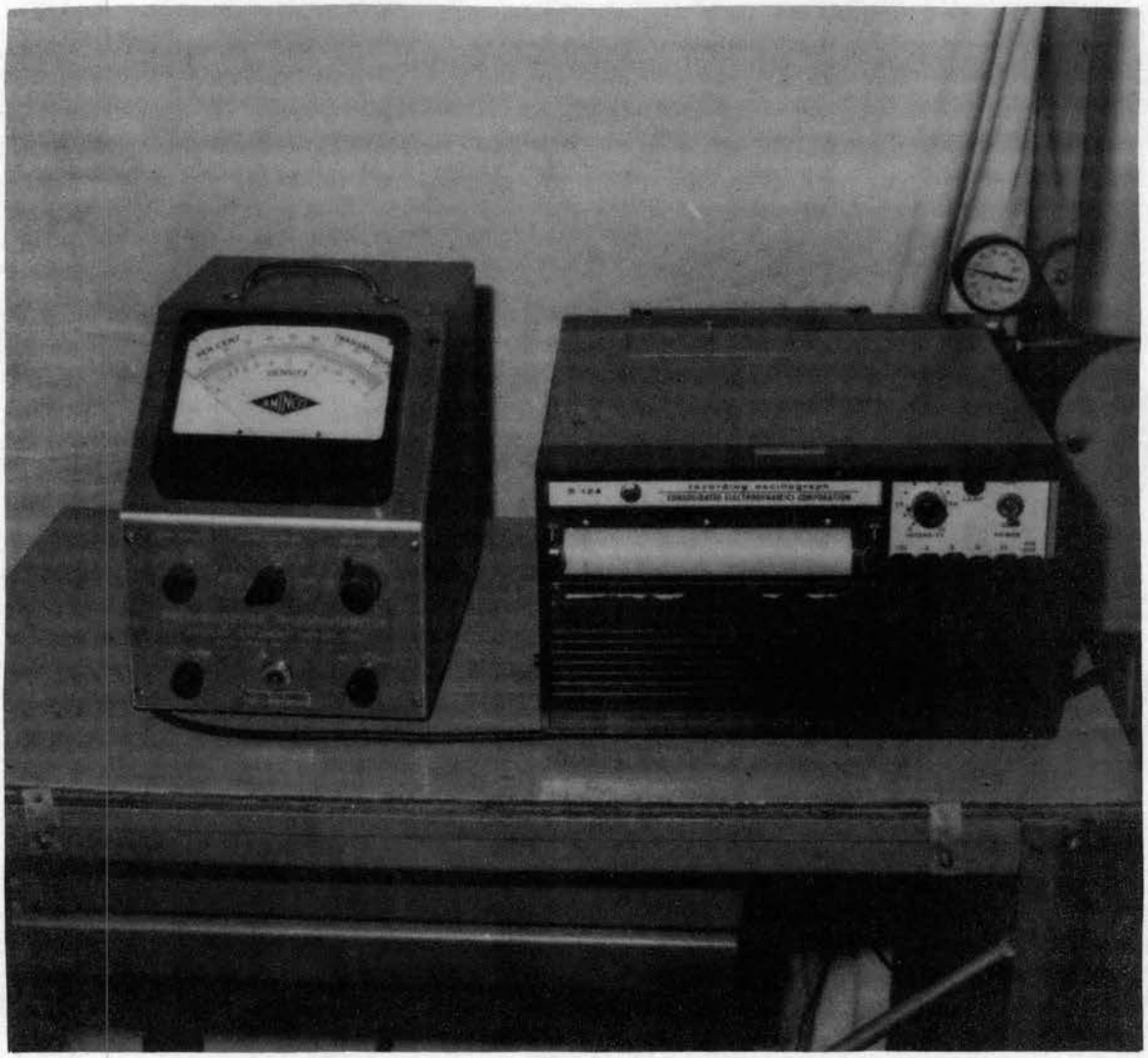

Figure 17. Detection-Recording System.

instrument for measuring the intensity of radiation incident on the entrance slit of the spectrograph. The assembly consisted of a photomultiplier tube and the associated electronic equipment for its operation and for amplification of the output signal. The amplified signal was indicated on a meter provided with the assembly; and in addition, output terminals were available in order that the phototube indication could be recorded on either an oscilloscope or recorder.

Two different types of phototubes were obtained and evaluated. Both types listed applicability for a wavelength range from 3000 to 7000 Angstroms, and exhibited a response curve typified by Figure 18. This figure should not be considered exact when attempting to evaluate the performance of a particular phototube since the manufacturer predicts slight variations from tube to tube, but it may be considered representative of the response from a tube of this type.

The two detectors investigated were the 931A and 1P21 phototubes. The 931A is the more economical of the two and has a lower noise level, but also has a lower sensitivity. Since some of the argon lines are of relatively low intensity, the 1P21 was selected for use in the actual measurements.

The photomultiplier tube was mounted in a completely dark enclosure and was located such that a detector slit placed in front of the tube was positioned exactly at the image plane of the spectrograph. By varying the slit width at the image plane, the wavelength range $\Delta\lambda$ which would fall on the photomultiplier tube was selected. The dispersion of the spectrum at this image plane was 5 Angstroms per millimeter in the first order. Thus by selecting a one millimeter detector slit, all

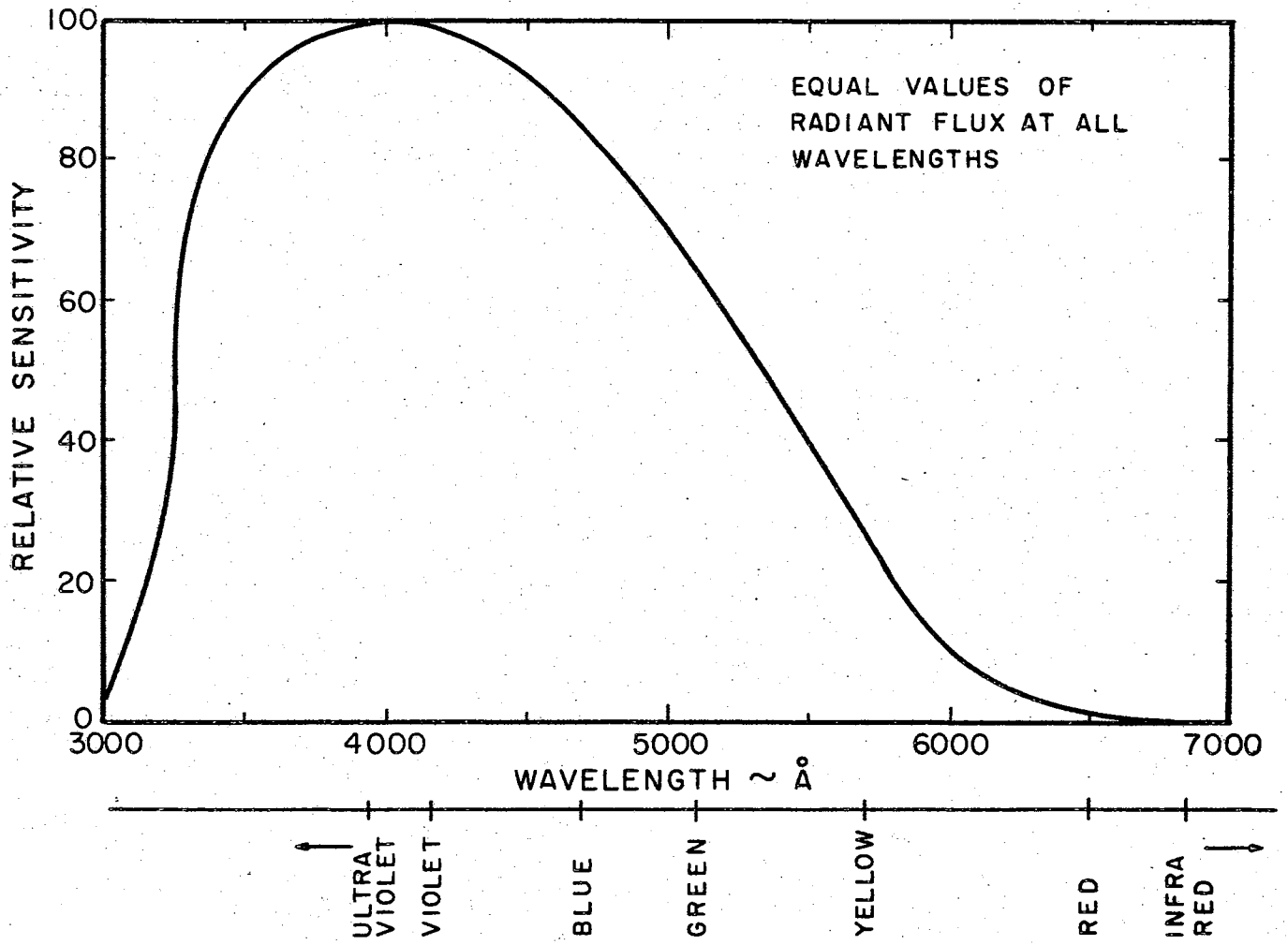

Figure 18. Typical Spectral Response Characteristics of a 1P21 or 931A Phototube.

radiation emitted over a 5 Angstrom region would be received and an integrated intensity for this region displayed on the meter. The selection of the slit width is based on criteria previously presented where it was pointed out that $\Delta\lambda << 1$ Angstrom was desired. However, as the $\Delta\lambda$ becomes very small, the intensities obtained become small and at some lower value of $\Delta\lambda$ a point is reached where the signal to noise ratio becomes very nearly one. It was found that a 50 micron detector slit width which was used in these measurements produced high signal to noise ratios for the argon lines under consideration, and still restricted $\Delta\lambda$ to .25 Angstroms.

Since intensity readings were to be taken at various vertical positions in the plasma column in order to determine the temperature profile, it was necessary to restrict the vertical height of the detector slit. In order to obtain true local intensities the vertical height should be as small as possible, again keeping the signal to noise ratio high. Since the luminous jet produced an image approximately 5 millimeters high on the spectrograph slit from a .5 inch diameter jet, then the correspondence between slit height and physical height was known. A slit height of .1 millimeter, which corresponds to a column of plasma whose height is .01 inches, was selected. This satisfied both the local emission and the high signal to noise ratio requirements.

In order to scan over a given wavelength range, the photomultiplier tube was moved horizontally parallel to the image plane at constant velocity by a pneumatic-hydraulic actuating system (Figure 19). Variable scanning rates were made available by opening or closing a needle valve in the hydraulic system. The length of movement of the photomultiplier tube was found to correspond to a 420 Angstrom wavelength region.

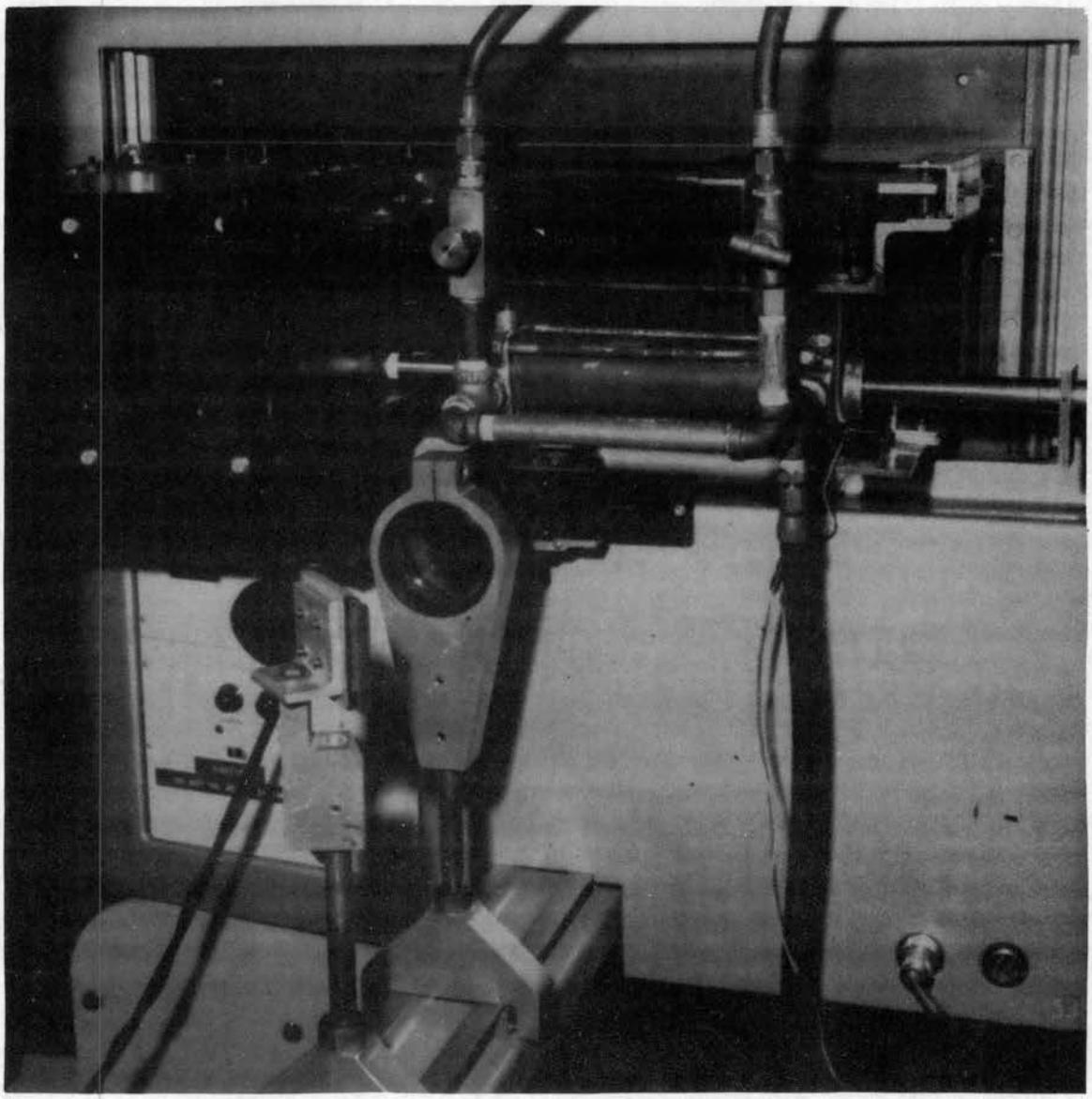

Figure 19. Pneumatic-Hydraulic Scanning System.

By independently setting the grating angle, a particular part of the spectrum could be investigated; and by changing the setting, a different region was covered by the 420 Angstrom scan.

Data Display System

The data obtained in this study was classified as state data or absorption data. The parameters which fix the state of the plasma such as mass flow rate, arc voltage, arc current, water flow rates and temperatures, observed vertical intensity distributions, and system pressures fall into the first category. The second group is made up of the centerline intensity values at various wavelengths for the simultaneous emission by the jet and source, emission by the jet alone, and emission by the source alone.

Many of the parameters listed in the first group were easily controlled and not subject to variation during a test, and as such were monitored visually.

The system temperatures, the arc voltage, the duration of the scan over the 420 Angstrom region, and the output of the phototube were continuously recorded.

The entering gas and water temperatures, and the temperature of the cooling water leaving the head were recorded by a Brown Electronic Multipoint Recorder. The arc voltage and current, the duration of the scan and the output of the photocell were recorded by a Consolidated Electrodynamics Corporation 18-Channel Optical Oscillograph. This system was chosen for the low inertia effects associated with its optical galvanometers. A model 7-315 galvanometer with natural frequency of

100 cycles per second and a damping resistance of 350 ohms was selected for the phototube output circuit. The schematic diagram for this circuit is presented in Figure 20.

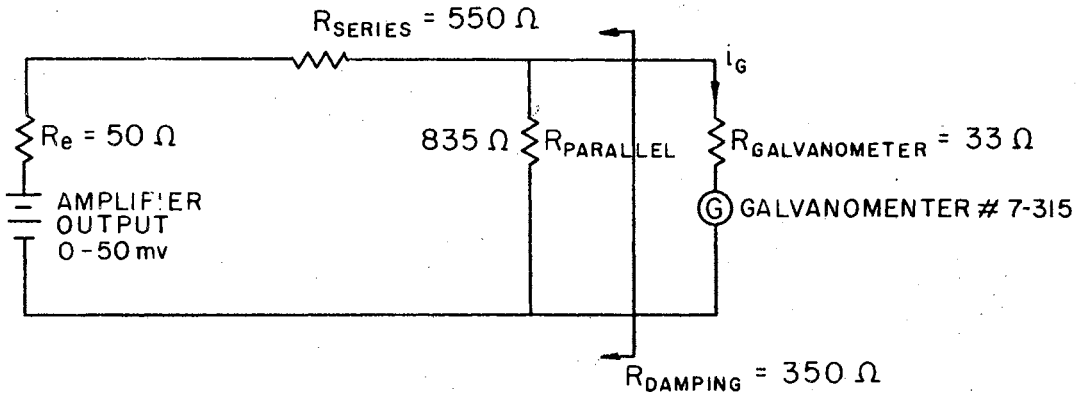

Figure 20. Schematic Diagram of Galvanometer Circuit.

The schematic diagrams for the voltage and current systems are essentially the same as that for the phototube except that the supply voltage was different and as such the circuit resistances were different.

In order that a wavelength position could be established for the continuous spectrum, an indicating system was designed so that precise limits could be established for the beginning and ending of the scanning movement. A microswitch was placed in series with the electrically actuated hydraulic valve and a relay placed in parallel with the valve. The schematic diagram for this circuit is shown in Figure 21. The microswitch was normally closed, but when the phototube reached a predetermined position, the switch was opened causing the hydraulic valve to close and stopping the current to the galvonometer. Having previously established the uniformity of the scanning velocity, any λ_i could be

determined once the final λ in the scan had been established. This method will be discussed in more detail in Chapter V. In this way, very well defined limits were placed on the beginning and ending of the observed spectrum.

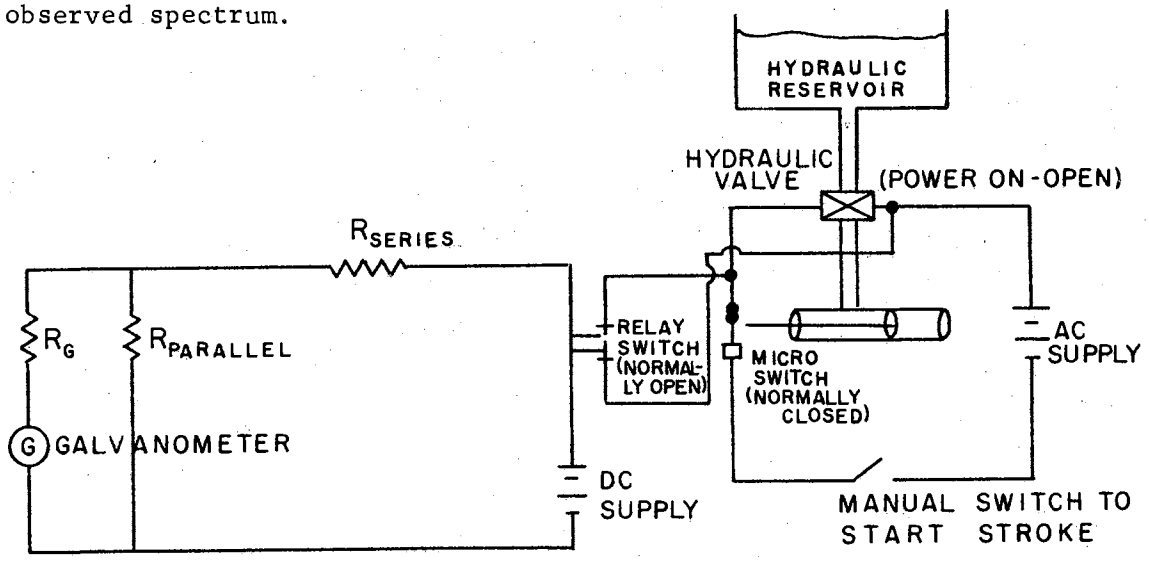

Figure 21. Schematic Diagram of Scanning Indicator Galvanometer.

The previous sections have presented the general descriptions of the apparatus involved in this study which were added to the basic plasma facility described in reference 1. Figure 22 shows the general arrangement and appearance of this apparatus.

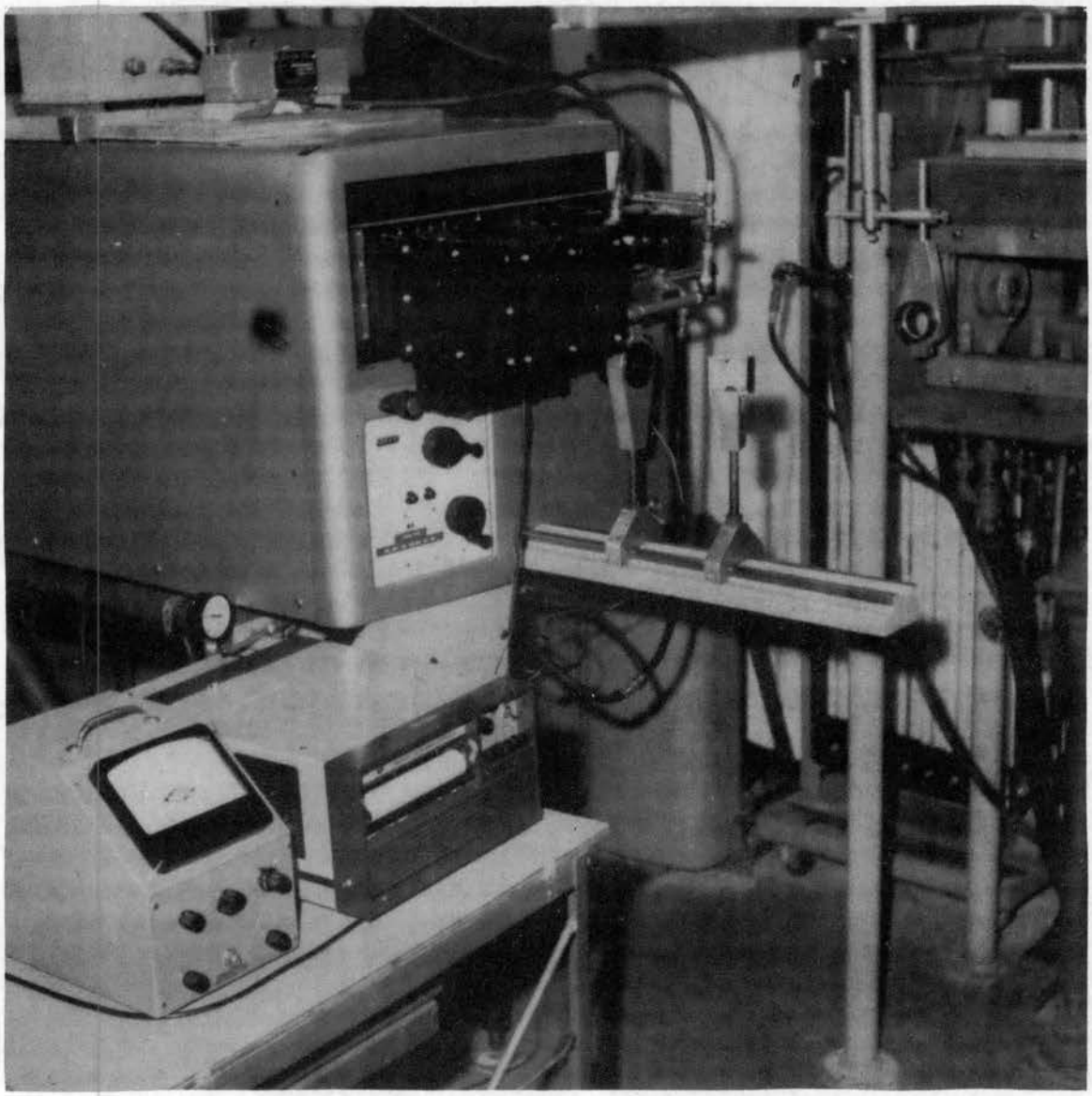

Figure 22. General Arrangement of Absorption Apparatus.

CHAPTER V

EXPERIMENTAL PROCEDURES

Previous Experimental Investigations

Olsen (24) previously reported significant amounts of absorption for the strong red lines in the argon atomic spectrum by an argon plasma. Unfortunately, only one operating condition was reported and the specifications of the plasma state were not complete at this one point. Since the primary purpose of Olsen's paper was the evaluation of transition probabilities, no values of the absorption coefficient were reported, and the lines which exhibited absorption were merely omitted from his study. As such, no efforts were made to show the dependence of this absorption on the state of the gas.

Knopp (25) used what is known as the mirror method to attempt to evaluate the amount of absorption by an argon plasma. In this method a parabolic mirror is placed behind the plasma and a reflected image of the plasma jet is focused upon the original plasma column. This method produced intensities approximately ninety-five per cent greater than the intensity of the plasma alone. However, no indication was given as to the wavelength considered or to the state of the plasma when these readings were taken. Tourin et al. (26) reported in a study of absorption in the infrared spectrum that this method presented several difficulties. The method was found to be useful mainly for large homogeneous

flames where the difficulties associated with making the optical path through the flame the same for both the emission and the absorption measurements were minimized. This mirror or "two-path" method is also inconvenient since it requires an accurate determination of $\rho(\lambda)$, the reflectance of the mirror for all wavelengths being considered.

Ryan, Babrov, and Tourin (27) reported that an argon plasma exhibited no absorption in the .37 to .65 micron wavelength region for a single operating condition. The method used by Ryan et al. was based on passing a continuous spectrum through a plasma column and observing intensities in selected wavelength regions $\Delta\lambda$. No data were reported as to the $\Delta\lambda$ considered, but resolution on the order of 50 to 150 Angstroms per millimeter with the type monochrometer used in these experiments would be considered representative. As previously mentioned, large values of $\Delta\lambda$ may tend to obliterate moderate absorption effects.

Thus it may be seen that a shortage of absorption data exists for a plasma whose composition is known and varied through a series of typical states.

Experimental Method

The absorption coefficient $\bar{\mu}(\lambda)$ varies with wavelength and the state of the absorbing medium. In this study an average coefficient $\bar{\mu}(\lambda)$ was obtained, and expressed by

$$\frac{I_1(\lambda)}{I_o(\lambda)} \equiv e^{-\bar{\mu}(\lambda)x} ,$$

where I_1 = the intensity of the emerging beam due to I_o only,

I_o = the intensity of the incident beam, and

x = the total distance traveled by the beam while in the media.

The average absorption coefficients were obtained by observing the incident and emergent intensities of radiation which was attenuated by a cylindrical column of argon plasma. Since the plasma was emitting radiation at the same wavelengths for which the absorption coefficients were sought, it was necessary to account for the contribution to the observed intensity from this emission. In order to compensate for the jet emission, three intensity measurements were required. Intensity values were obtained at selected wavelengths under the following conditions: (1) with the plasma jet only emitting, $I(\lambda)_{M_1}$, (2) with both the secondary radiation source and the jet emitting simultaneously $I(\lambda)_{M_2}$, and (3) with the secondary source only emitting, $I(\lambda)_{M_3}$. After assuming steady state operation of both the jet and the source, the contribution to the observed intensity from the jet was established. The last measurement produced the intensity values for the radiation incident upon the jet, I_o. The difference in measurements one and two was identified as the intensity of the emergent radiation, I_1. Thus the average absorption coefficient $\bar{\mu}(\lambda)$ is obtained from

$$-\bar{\mu}(\lambda) = \frac{1}{d} \ell n \left[\frac{I(\lambda)_{M_2} - I(\lambda)_{M_1}}{I(\lambda)_{M_3}} \right] . \qquad (11)$$

A method was considered to eliminate the effects of the plasma emission by modulating the source emission at some prescribed frequency and using a detection device which would respond to this modulated

frequency. Hamberger (28) found this to be necessary when using a method similar to the one described in this study to evaluate the number densities of particles in certain energy states by a radiation absorption technique. Since the intensity of his probing beam was much less than the intensity at the same wavelength emitted by the plasma, a much more elaborate electrical system was required. However, with the optical system described in Chapter IV, high intensity values were easily attainable and the modulation technique was rejected in favor of the simpler compensation technique described above.

In order to insure the steady state operation of both the secondary radiation source and the plasma jet, each of the intensity readings obtained in determining the absorption characteristics were obtained twice. If a discrepancy of greater than one per cent occurred from one reading to the next, the data were rejected. The following data scheme was used to obtain the intensity values in a scan over a 420 Angstrom region. (1) Intensity versus wavelength measurements were made at five vertical positions below the jet centerline as the detector position was changed in one-half millimeter steps. (2) The final intensity versus wavelength vertical measurement was taken at the previously determined jet centerline, and then repeated to determine the steadiness of the jet emission. (3) The diaphragm which had been preventing the introduction of the probing beam was opened, and two intensity versus wavelength measurements taken which were made up of the simultaneous emission from the secondary source and the jet. (4) The jet was extinguished, and two intensity versus wavelength measurements taken to establish the emission of the secondary source.

Extreme care was exercised to insure the constancy of the geometric arrangement between source and detector during steps (2), (3), and (4). If during steps (1), (2), and (3), any fluctuations were observed in the arc voltage, current, or position, all the data were rejected and the sequence repeated.

System Evaluation

In order to insure the validity of the obtained data, many conditions must be satisfied in addition to the reproducibility of the intensity versus wavelength measurements.

As mentioned previously, an exit slit width corresponding to a $\Delta\lambda$ of .25 Angstroms was selected. The signal which was displayed on the oscillograph was proportional to the average intensity across the slit. Since the emission profile for an argon line is on the order of 1 Å wide and the maximum absorption should occur at the center of the profile, then the intensity measurement over this .25 Angstrom region should exhibit the true absorption characteristics of an isolated spectral line (9).

The location on the output data of the wavelength region whose intensity value was sought was established by the procedure which is described in the following section.

The data from the intensity versus wavelength measurements (1), (2), and (3) were similar to that shown in Figure 23 a), b), and c) respectively. Measurements (1) and (2) produced intensity peaks which corresponded to certain known wavelengths. The maximum value of each of these peaks represented the average intensity over the .25 Angstrom

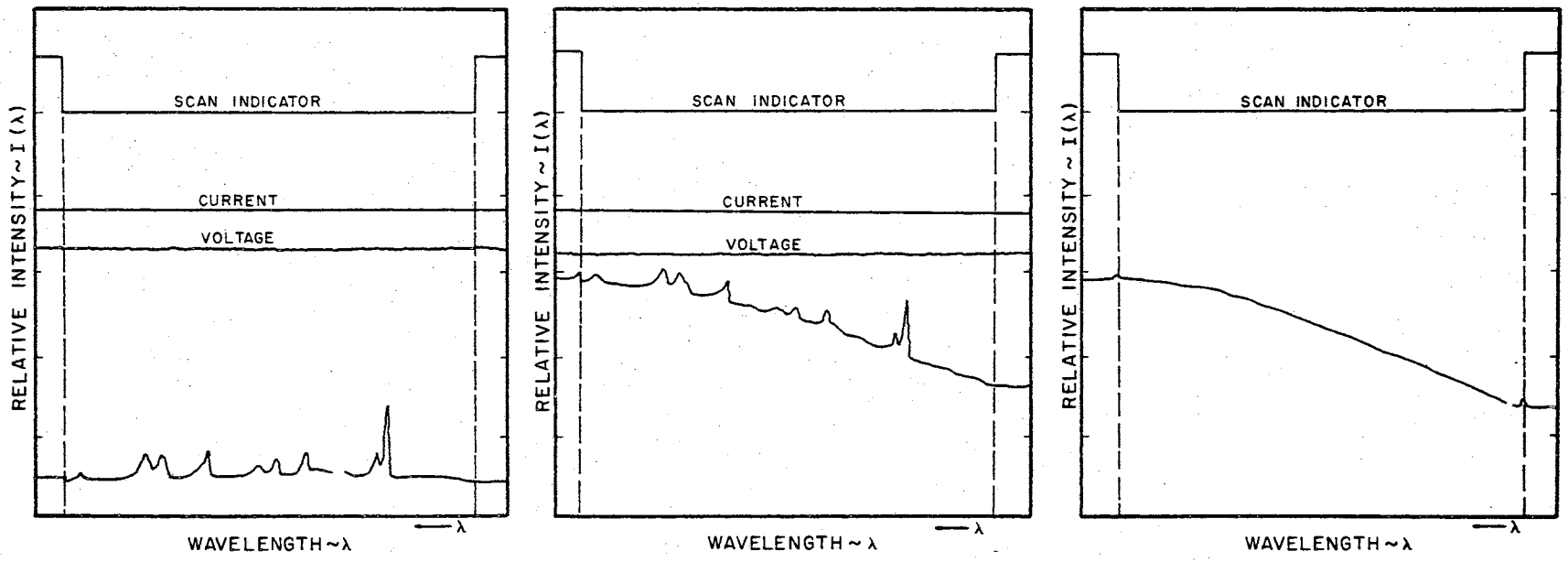

a) Jet Emission Only. b) Jet and Source Emission. c) Source Emission Only

Figure 23. Intensity Versus Wavelength Measurements.

wavelength region centered at λ_o, and the location of the maximum value established a reference wavelength position corresponding to λ_o on the output data. By establishing two such reference points, the wavelength value corresponding to any position was known, if the scanning rate was known to be uniform. The uniformity of the scanning rate was the subject of a special report done by Day, Cobb, and Smith (29). The results of this study showed the scanning rate to be uniform after a short initial surge for a pneumatic pressure between 15 and 40 psig and a scanning time between 15 and 60 seconds.

Since no identifying intensity lines were produced by the final measurement of the secondary source intensity, a reference point was needed to establish the position of the wavelength region for which the intensity values were sought. The final wavelength reading λ_f was selected as the reference value. This point was selected and circuitry designed to insure the repeatability of λ_f through the use of the microswitch, hydraulic valve, galvanometer deflection arrangement given previously in Figure 21 of Chapter IV. In this way, the distance from λ_f to the desired wavelength region was measured on the intensity output data from the jet alone, checked by a measurement on the data for the combined emission, and then used to establish λ on the data from the secondary source alone.

The scanning rate was adjusted until the elapsed time for each scanning stroke was approximately fifteen seconds. For times shorter than about six seconds, the response rate of the intensity indicator galvanometer was too slow to produce good resolution of lines separated in wavelength by less than 1.5 Angstrom. For scanning times of

approximately ten seconds, good resolution was obtained at oscillograph chart speeds to two inches per second or larger. A chart speed of one-half inch per second was found to produce good resolution for the fifteen second scanning time used in this study.

The response characteristics of the radiation detection system were also investigated completely. The basic detection device was an RCA 1P21 photomultiplier tube. This tube is actually a combined photoemissive cell and DC amplifier in a single envelope. The basic principle embodied in this tube is the principle of secondary electron emission from a treated metal under bombardment by primary electrons. In this device electrons are emitted from a surface as a result of radiation impinging upon this surface. These electrons are then accelerated by an electrical potential to a second surface. Each of these accelerated electrons impinge on this second surface with sufficicient velocity to eject several secondary electrons. The newly released secondary electrons are then accelerated to another surface where several electrons are ejected for each impinging electron. This process continues through nine separate stages during which time an amplification of approximately one million to one occurs. The final surface collects the electrons and conducts them away as a photocurrent. Since electrons may also be ejected from the initial surface by thermionic emission, low light intensity measurements may be subject to large errors. The detection device used in this study was equipped to compensate for the contribution to an intensity reading from this "dark current," but this does not alleviate the problem which exists when the number of photo-emissions is only slightly greater than the number of thermal-emissions. It was

observed that the "dark current" was much larger after the phototube had been handled, and that the current decreased if the tube was cooled. Therefore, handling of the phototube was minimized, and applications were restricted to periods when the tube had cooled to temperatures less than 75 $^{\circ}$F. This procedure minimized the effects of thermionic emission on the low intensity measurements. In addition, no absorption measurements were performed for intensities where this contribution was a significant part of the output signal. This thermionic contribution was found to be of significant magnitude when amplification of a current corresponding to meter multiplier positions, which are discussed in the next paragraph, of .001 and .003 was attempted.

A wide range of intensity values were encountered in observations proceeding from the outer boundary to the jet centerline. In fact, differences of approximately two orders of magnitude were found to be common. The problem of data output under variations of this magnitude was handled by the insertion of precision resistors into the input circuit of the amplifier. This was accomplished by a meter multiplier switch which was an integral part of the Aminco Microphotometer. The multiplier switch was set in one of the following positions: 1, .3, .1, .03, .01, .003, or .001 positions which correspond to seven different resistor values. The relative intensity of the light incident upon the photomultiplier tube was the product of the meter multiplier reading and the photometer reading. Since relative intensity values were the desired output, the data was displayed on the oscillograph trace and the relative intensity values equated to the product of the meter multiplier reading and the output value produced on the oscillograph.

With an experimental arrangement of this type, and in view of the type of data scheme employed, the linearity of the output device when subjected to various intensity values was considered a very critical point in evaluating the validity of any results. Harrision, Lord, and Loofbourow (30) report the current output of the photoemissive cell to be linear over widely different intensities of illumination. Tests were conducted and the linear response of the photometer verified for various intensity levels over the entire spectral region of interest.

A constant ratio of photometer indication to galvanometer deflection was insured by the following factors. The output of the photocurrent amplifier varied linearly with intensity between zero and fifty millivolts for zero to full scale photometer indication regardless of the meter multiplier value. Thus for a fixed photometer indication, a known voltage was applied to the galvanometer circuit. Since the resistance of this circuit was fixed, and the deflection of the galvanometer was linear with input current for values lower than fifteen microamps, the ratio of photometer indication to galvanometer deflection was constant. The output trace on the light sensitive paper was linear with galvanometer current so long as the trace did not move more than approximately four inches from its equilibrium position. Since a DC signal was to be supplied to the galvanometer, and the maximum amount of resolution was desired within the linearity limits of the oscillograph, a central channel was selected for the intensity output galvanometer. The indicating beam was then manually deflected approximately three inches to a position near the lower edge of the trace paper. Values were then calculated and assigned to the circuit resistors subject to

three conditions. The prescribed conditions were: (1) the damping resistance seen by the galvanometer must be kept at approximately 350 ohms, (2) the input current to the galvanometer must be kept below fifteen microamps, and (3) full scale photometer indications should produce galvanometer deflections of approximately six inches for maximum intensity sensitivity. The resultant circuit was shown in Figure 20 of Chapter IV. The linearity of the entire detection system when exposed to incident radiation of varying intensity was checked for various intensity levels throughout the 3500 to 7000 Angstrom wavelength region by a mechanical chopper, and the system was found to respond linearily to intensity with an error of less than one per cent so long as the power requirements of the photometer were satisfied.

One set of data was rejected in an early phase of the program when large discrepanices were found to exist between data applicable to the same operating conditions. The problem was found to be due to a faulty power stabilizer which had been used to supply the photometer assembly. The power requirements for the photometer assembly were as follows: (1) 105-130 volts, (2) single-phase 60 cycle current, and (3) 17 watts available power. Designed into the assembly was a power regulator which furnished a fixed voltage to the amplifier so long as the supply voltage fell within the 105-130 volt limits. However, when the large air compressor which supplied air for the hydraulic-pneumatic scanning assembly started, voltages lower than 105 volts were observed at the supply terminals. A 1000 volt-ampere power regulator was added to the instrumentation circuit, and excellent data reproducibility was obtained.

Since large variations in intensity occurred in the plasma jet with a change in the vertical position of the detector, it was necessary to

require the phototube to move in the same horizontal plane from the initial to the final position of the scanning stroke. A horizontal movement was insured by the following procedure. (1) The entrance slit to the spectrograph was adjusted to a height of approximately .1 millimeter through the use of the V-slide. (2) The slit was illuminated by radiation which was distributed in a continuous spectrum over a wavelength region wider than the 420 Angstrom scan. (3) With the exit slit set at a height of approximately 0.1 millimeter, the detector was moved vertically, while in the retracted position, until a maximum signal was indicated on the photometer. (4) The detector was then extended to the end of the stroke and adjusted until the maximum signal was indicated on the photometer. The maximum signal occurred when the exit slit was coincident with the image of the entrance slit. (5) Adjustments were made to the hydraulic cylinder until the exit slit remained in the image of the entrance slit throughout the entire stroke. The deviation from horizontal between the beginning and end of the scanning stroke was then known to be less than the height of the larger of the two slits. Since both slits were approximately 0.1 millimeter in height, the deviation in vertical position of the detector between the initial and final horizontal positions was less than 0.1 millimeter.

Since only relative measurements at a fixed wavelength were involved in the determination of the absorption coefficients, the problems associated with the optical properties of the test section windows, lens, mirrors, etc. were not investigated. The effects of these materials, though unknown, were included by requiring that the radiation under consideration follow the same path length during each measurement, the only

difference in the optical paths being the presence of the argon column in one measurement. In this way, the method under consideration is superior to the "mirror" method which was discussed previously.

The absorption coefficients presented here were all obtained for an absorbing layer whose thickness was equal to the diameter of the plasma column. The point at which the secondary beam passed through the plasma column was made to coincide with the jet centerline by the following technique. At plasma temperatures less than approximately 15,000 $^{\circ}$K the maximum intensity of an emitted spectral line occurs at the jet centerline (31). Thus by measuring the spectral intensities at various vertical positions, the centerline of the jet was established, and the corresponding vertical position of the detector slit noted. The secondary source was then adjusted until a horizontal beam of light was imaged at the jet centerline and vertical adjustments were made in the source position until the image was located at the point previously identified as being on the centerline. Intensity versus wavelength readings were taken at various vertical positions, and the position of the image of the illuminated hole was found to agree with the point in the plasma column which exhibited the maximum emission.

In order to determine the state of the participating gas, the assumption was made that the emission characteristics of the jet were axisymmetric. Intensity measurements were taken at various vertical positions, and the results are shown in Figure 24. The intensity readings were slightly higher in the upper part of the plasma column. This result was attributed to small convective effects present in the test section. Measurements were taken in the lower half of the plasma column

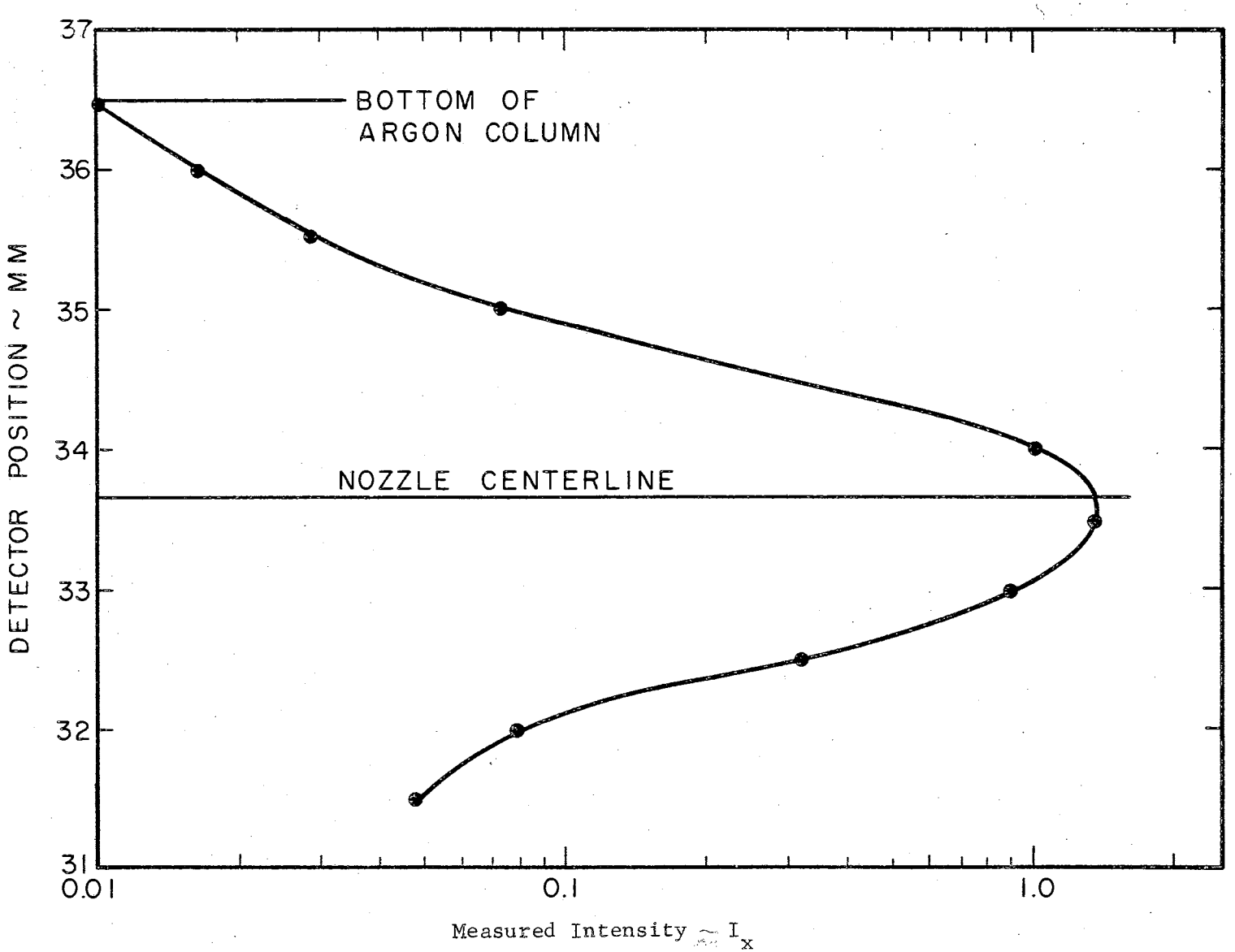

Figure 24. Intensity Variations Across the Plasma Column.

and these values were used to describe the state of the gas which was irradiated by the secondary beam.

One problem associated with the 1P21 phototube detection system concerns its spectral response characteristics. However, this problem would also have existed regardless of the detection device used since the response of any known detector is very highly dependent upon wavelength. Since the ratio of two intensity values at different wavelengths were required to determine the state of the participating gas, the intensity values need not be absolute, but the ratio of relative to absolute intensity must be constant for each of the wavelengths considered. This is not the case if spectral lines of widely different wavelengths are used in conjunction with the phototube. Two solutions to this problem of spectral response were considered here. A correction factor may be applied to the measured intensity values if spectral response curves similar to Figure 18 of Chapter IV are available. However, this response curve may not necessarily be representative of the response of a particular tube, and as such extreme care must be exercised in assigning correction factors to the measured intensity values.

In the absence of a spectral response curve for the particular phototube used in this study, the intensity values considered in state determination were restricted to spectral lines whose differences in wavelength were less than 100 Angstroms.

This additional separation requirement further restricted an already abbreviated list of spectral lines which might be used for state determination. A complete analysis of the state determination procedure is presented in Chapter VI.

The Argon Spectrum

Absorption coefficients which correspond to the wavelengths at which the plasma column emits were of primary concern during this study. However, absorption coefficients were also obtained at selected points in the continuous spectrum and the results included in Chapter VI. The wavelengths considered do not constitute the entire argon spectrum in the 3500 to 7000 Angstrom wavelength region, but the data do include those lines for which transition probabilities are known, and other lines whose intensity is quite high.

An investigation of the absorption data discloses the absence of an absorption coefficient for any transitions which involve the ground state of the argon atom. The longest wavelength in the atomic argon spectrum which is associated with a transition involving the ground state is approximately 1075 Angstroms. As this radiation is also readily absorbed by the windows of the test section, the spectrograph lens system, and oxygen and water vapor in the air; and many other problems occur when studies are conducted in this far ultraviolet region, only the transitions from one excited state to another were considered in this study.

Parameter Variations

Absorption coefficients were obtained for eleven different power input to mass flow rate ratios. The input parameters were selected to illustrate the effect of the mass flow rate and arc current level upon the absorption coefficients. These two parameters were easily controlled whereas the arc voltage was a function of generator geometry,

current level and chamber pressure. The mass flow rate was varied between 6.40 lb_m/hour and 15.9 lb_m/hour while the arc current was maintained at 400 amperes. Absorption coefficients were also obtained for varied arc currents between 250 and 450 amperes for a fixed mass flow rate of 10.0 lb_m/hour. In each instance the variable was incremented between the extremes of the operating envelope established for the OSU Plasma Facility. At mass flow rates of less than 6.40 lb_m/hour the jet became highly unstable. Instability also occurred when arc currents of less than 250 amperes were used to produce the plasma. The upper bound on the operating envelope was established by the maximum capacity of the gas supply system and power leads.

Each of the eleven operating points was investigated for the nine grating settings and corresponding wavelength regions listed in Table III. For the particular grating setting indicated on the spectrograph, the wavelength region covered by the scanning stroke is given in the table. Grating settings were selected to allow sufficient overlap in each wavelength region to prevent the omission of any spectral line from the study.

All of the absorption coefficients presented in this study were obtained for a disk-shaped plasma region located one-half inch downstream of the nozzle exit plane. The test section pressure was adjusted until the flow appeared to be free of shock waves, and until the flow neither converged nor diverged after leaving the nozzle. In this way, the one-half inch thickness for the absorbing layer was achieved. The properties of this region were then obtained and the corresponding absorption coefficients evaluated. The sequence of operations followed in obtaining these coefficients is presented in the following section.

TABLE III

EXPERIMENTAL BREAKDOWN OF THE VISIBLE SPECTRUM

Wavelength Interval	Grating Setting	Initial Wavelength	Final Wavelength
420 Å	5.06°	3550 Å	3970 Å
420	5.73	3945	4365
420	6.40	4340	4760
420	7.07	4735	5155
420	7.74	5130	5550
420	8.43	5525	5945
420	9.10	5920	6340
420	9.77	6315	6735
420 Å	10.44°	6710 Å	7130 Å

Operational Sequence

The general operating procedure used during the actual data collection phase of this study was as follows:

(1) At least 30 minutes before actual testing, apply power to motor-generator control system and photometer assembly and place meter multiplier switch in "zero adjust" position.

(2) Start motor generator set, and adjust photometer indicator needle to zero position.

(3) Close main contactor switch bringing power to main control console.

(4) Start cooling water to vacuum pump, heat exchanger, and main nozzle. Start cooling air over series grid resistor bank.

(5) Set grating indicator to position corresponding to desired wavelength region.

(6) Open main argon supply valve and throttle to 40 psig.

(7) Record barometric pressure reading and start temperature recorder.

(8) Place meter multiplier switch in .001 position and subtract "dark current," and then replace switch in "zero adjust" position and zero indicator needle.

(9) Start oscillograph, scan-assembly vacuum pump; throttle pneumatic supply pressure to 25 psig, and open slit to spectrograph.

(10) Adjust vertical position of detector to correspond with known jet centerline.

(11) Start vacuum pump, and apply 150 volts starting potential to plasma generator.

(12) Select argon mass flow rate and obtain desired flow-rate indication.

(13) Energize starter electrode and adjust arc current to desired value after jet starts.

(14) Scan the wavelength region at various meter multiplier settings until the galvanometer deflections corresponding to the most intense spectral lines in this region are approximately two inches.

(15) Extinguish the jet, and close argon flow valve.

(16) Apply power to secondary radiation source and adjust secondary source resistor until intensity level corresponds to a galvanometer deflection of approximately four inches maximum during the scan.

(17) Close iris diaphragm, and repeat steps 11 through 13.

(18) Using the bleed valve, adjust the plasma column until the jet neither converges nor diverges upon entering the test section.

(19) Move detector to vertical position corresponding to lower boundary of the plasma jet, and adjust the meter multiplier so that all intensities produce galvanometer deflections of less than five inches.

(20) Make final adjustments to input parameters and record all variables shown on data sheet.

(21) Start oscillograph and record spectral intensity versus wavelength.

(22) Raise detector position 0.5 millimeters and repeat step 21 adjusting meter multiplier to produce desired deflections. This step is to be repeated a total of five times with each vertical position being recorded.

(23) The final increment should place the detector at the known centerline position. At this position, two successive intensity versus

wavelength measurements are made to determine the jet emission characteristics.

(24) The iris diaphragm is opened and two successive intensity versus wavelength measurements made.

(25) The jet is extinguished, the mass flow stopped, but the low pressure value is maintained in the test section.

(26) Two successive intensity versus wavelength measurements were made to determine the emission characteristics of the secondary source.

(27) Select a new operating condition and repeat steps 11 through 26. This is done for the eleven operating points given in Table IV.

(28) After completion of step 27, a new grating position is selected which brings a different region of the argon spectrum under consideration, and steps 11 through 27 are repeated for each region of the spectrum.

The data obtained from this procedure are presented in Chapter VI.

CHAPTER VI

RESULTS AND DISCUSSION

Plasma State Evaluation

Intensity measurements at twenty-eight wavelength values in the 4000 to 6000 Angstrom region of the spectrum were made for various power and mass flow combinations shown in Table IV. The average enthalpy increase of the argon, Δh gas, was evaluated by performing an energy balance on the plasma, entering argon, cooling system, and power input.

Most of the spectral intensity distributions which were obtained were not used in establishing the temperature profile across the plasma column. The intensity distributions which were used in establishing T(r) were selected in pairs since the relative intensity-temperature method was being considered as a means of determining the state of the gas. The conditions which the two spectral lines, λ_1 and λ_2, were required to satisfy were as follows:

(1) both λ_1 and λ_2 must have known transition probabilities,

(2) λ_1 and λ_2 must be located sufficiently near one another in the spectrum to negate any effects due to the spectral response characteristics of the detector,

(3) the difference in energy values of the upper states corresponding to λ_1 and λ_2 should be as large as possible, and

(4) neither line should be significantly attenuated by the plasma itself.

TABLE IV

POWER-MASS FLOW RATE OPERATING VALUES

Current (Amperes)	Voltage (Volts)	Mass Flow Rate (lb_m/hour)	Δh_{gas} (BTU/lb_m)
250	22.1	10.0	1350
290	22.1	10.0	1614
330	22.5	10.0	1870
370	23.1	10.0	2142
410	23.1	10.0	2365
450	23.2	10.0	2560
400	21.1	6.4	3155
400	22.0	8.7	2485
400	24.0	11.2	2180
400	25.4	13.4	1910
400	26.7	15.9	1721

As mentioned previously, relatively few spectral lines have known transition probabilities, so that condition 1 severely limits the number of wavelengths which might be considered. Four intensity ratios were selected where both λ_1 and λ_2 satisfy the given condition. These four ratios are $I_{4259.4}/I_{4266.3}$, $I_{4259.4}/I_{4272.2}$, $I_{4259.4}/I_{4300.1}$, and $I_{5572.5}/I_{5558.7}$. The observed intensity measurements I_x at these six wavelengths were plotted for each of the mass flow rate-power combinations. Typical I_x data are presented in Figures 25 and 26 for two of the mass flow rate-power combinations and the remainder of the data is presented in Appendix B. Figure 25 presents the measured intensity variation for an arc current of 370 amperes and a mass flow rate of 10.0 lbm/hour, while Figure 26 shows the variation of I_x for a mass flow rate of 6.40 lbm/hour and a current of 400 amperes. In each figure the intensity value is based on a relative scale discussed in Chapter V. It may be seen from these figures that the intensity value varies by approximately two orders of magnitude from centerline to arc radius. The values which were obtained near the outer edges of the plasma column for many of the weaker intensity lines should be considered as approximate only since at this point the signal-to-noise ratio of the detector is low.

The observed intensity values shown in Figures 25 and 26 have been adjusted to account for the continuum spectrum which contributes to each measured intensity, but is not associated with the electronic transition. This continuum contribution was removed by measuring its value adjacent to the spectral line of interest and subtracting it from the total observed intensity of the spectral line.

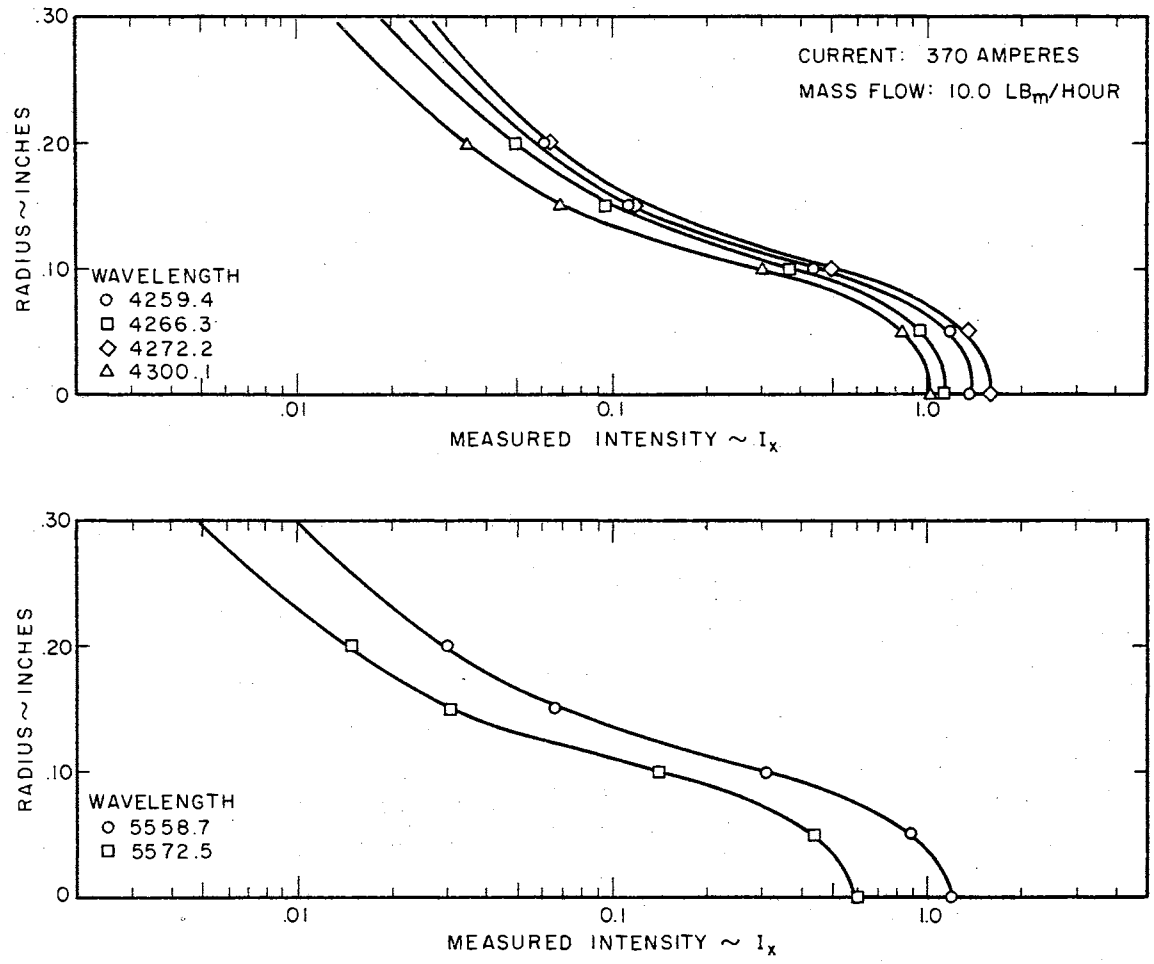

Figure 25. Measured Intensity Distributions for Selected Spectral Lines at i = 370 Amperes and $\dot{M}$ = 10.0 lb_m/hour.

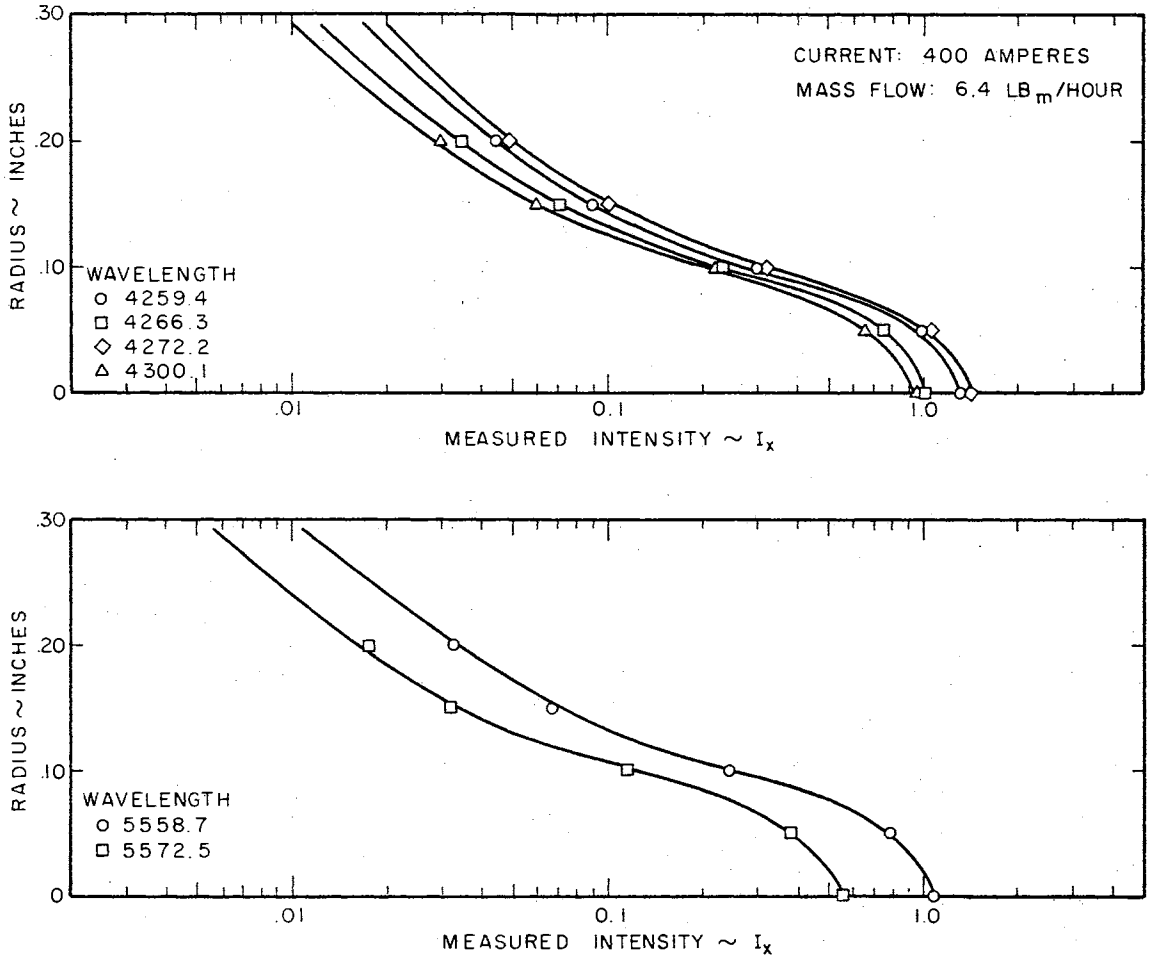

Figure 26. Measured Intensity Distributions for Selected Spectral Lines at i = 400 Amperes and $\dot{M}$ = 6.40 lb_m/hour.

After the measured intensities were plotted, each of the I_x profiles were "unfolded" by the method of Pearce to produce the I(r) values which were used in the intensity-temperature method. Fifteen I_x values for each of the mass flow-power combinations for each of the six selected lines were used in the unfolding process. The radial intensity values I(r) which were obtained from equation 2 of Chapter II are typified by those shown in Figures 27 and 28. These I(r) values correspond to the I_x values given in Figures 25 and 26. Having obtained the I(r) values, the T(r) values may be obtained from the expressions presented in Chapter II. The two-line relative intensity method related the temperature to the radial ratio through

$$\frac{I(r)_{\lambda_1}}{I(r)_{\lambda_2}} = \frac{(A^u_\ell \; gu \; \nu)_{\lambda_1}}{(A^u_\ell \; gu \; \nu)_{\lambda_2}} \exp \left[(E_{u_2} - E_{u_1})/kT \right] .$$

This expression is represented graphically in Figure 29. It may be seen that as many as three different temperatures may be obtained from one intensity ratio depending upon the A^u_ℓ values that are used. The values given by Olsen (7) are more current than those of Gericke (8), but Olsen presents only three values for neutral argon lines in the visible spectrum.

The effect of the variation in the ratio of transition probabilities is detected if one observes the predicted temperatures for $I_{4259.4}/I_{4266.3} = 1.50$. At this fixed intensity ratio the predicted temperatures range from 4,550 °K to 14,300 °K. Thus the problem of establishing the

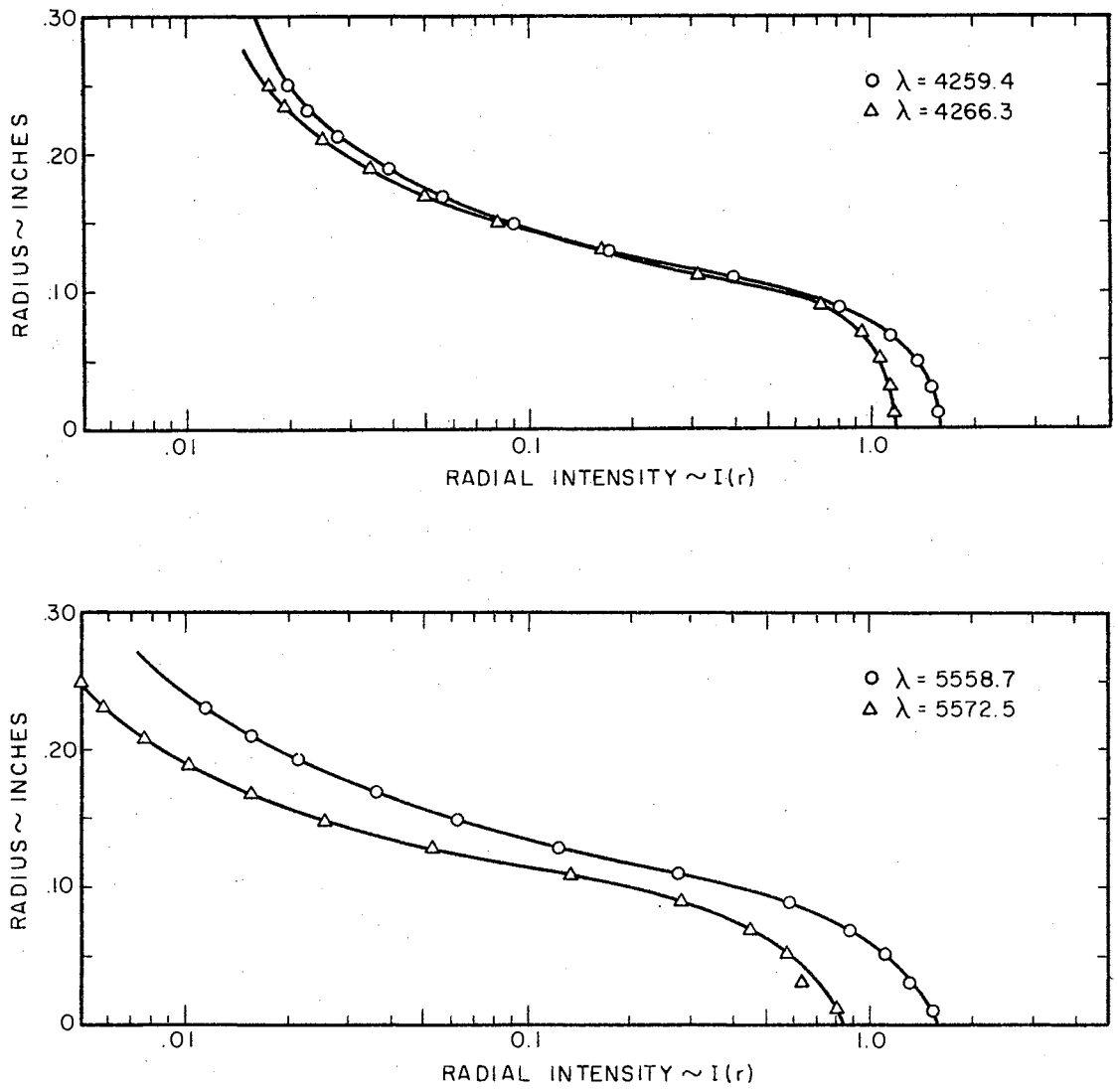

Figure 27. Radial Intensity Distributions for Selected Spectral Lines at i = 370 Amperes and $\dot{M}$ = 10.0 lb_m/hour.

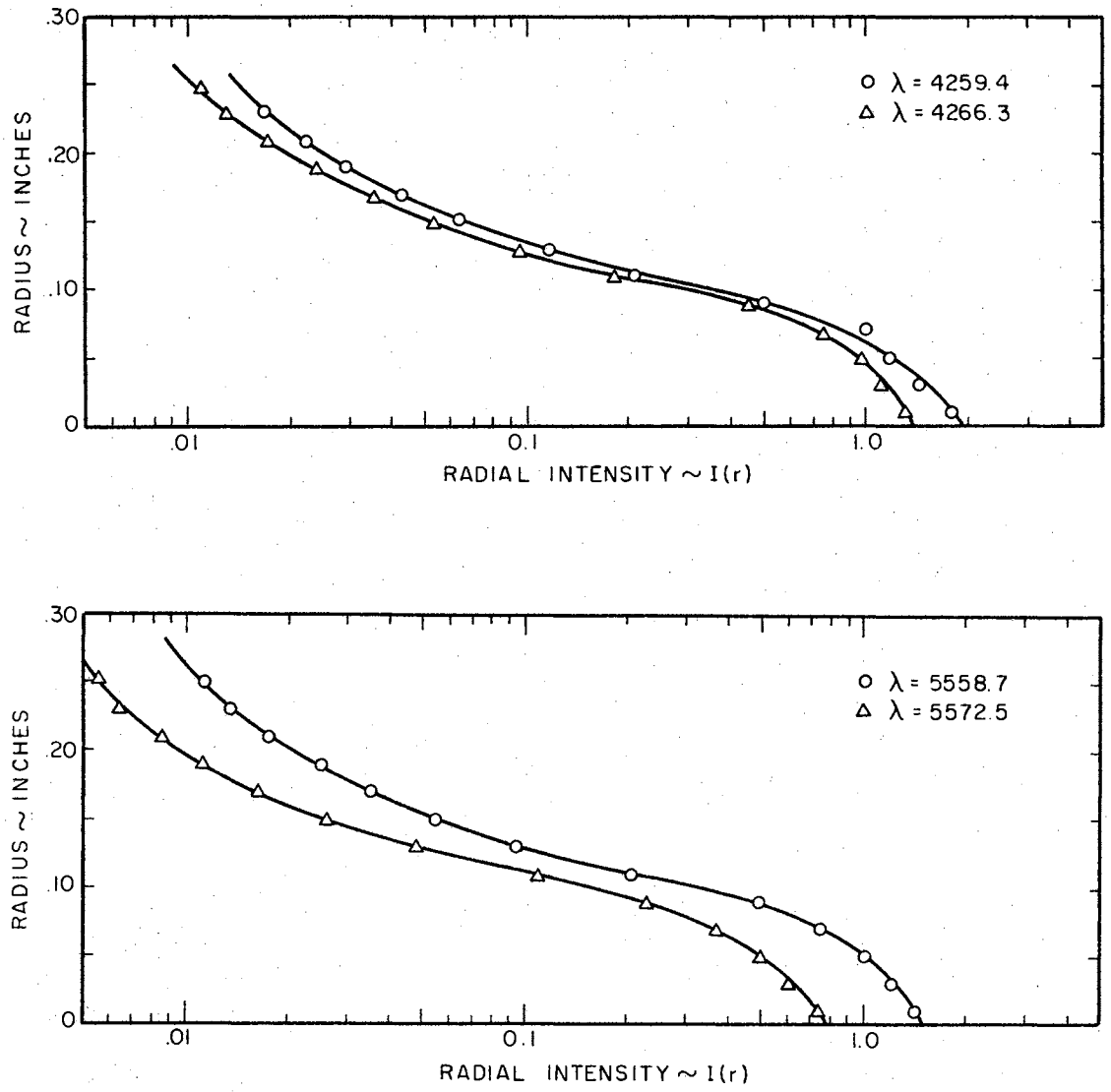

Figure 28. Radial Intensity Distributions for Selected Spectral Lines at i = 400 Amperes and $\dot{M}$ = 6.40 lb_m/hour.

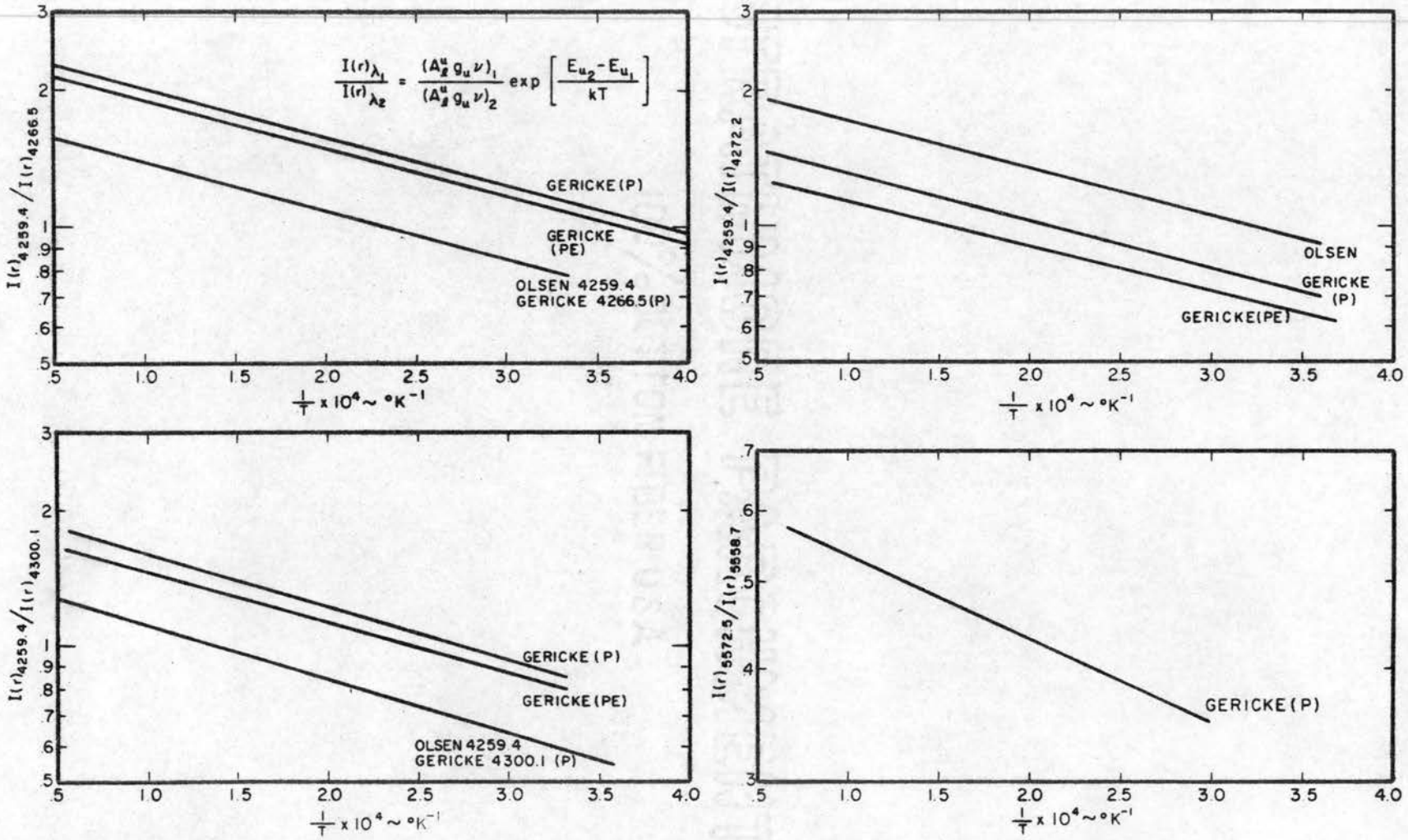

Figure 29. Temperature-Intensity Correlation for Selected Radial Intensity Ratios.

temperature of the plasma was based upon the selection of the correct combination of ${}^{1}A_{\ell}^{u}$ and ${}^{2}A_{\ell}^{u}$.

One of the operating points for this study has been selected to correspond to an operating condition given in reference 1. At a current setting of 400 amperes, a mass flow rate of 8.68 pounds per hour, and a power input to the gas of approximately 23,000 BTU per hour, reference 1 reported a centerline temperature of approximately 9000 °K. This value was obtained from a method completely independent of the intensity ratio technique, namely from the broadening of a hydrogen line. At the corresponding operating point the values predicted by the two-line relative intensity method were compared to the broadening results. The temperatures which differed radically from that given by the broadening technique were discounted. It was found that the values presented in Figure 30 produced results consistent with those produced by an independent measurement. Using the values presented in Figure 30, the intensity ratios obtained at the ten other operating conditions were shown to produce consistent results. Some variation, but on a much smaller scale, was still observed between the temperatures predicted by two different combinations of λ_1 and λ_2 from the I(r) ratios. For example, $I_{4259.4}/I_{4266.3}$ might predict a temperature of 9000 °K at some point in the plasma column while $I_{4259.4}/I_{4272.2}$ might predict a temperature of 8400 °K at the same point. It is felt that this variation is associated more with the uncertainty in the value of A_{ℓ}^{u} than with experimental error or deviation from local thermodynamic equilibrium.

Having selected the transition probability values to be used, the intensity ratios $I_{4259.4}/I_{4266.3}$, $I_{4259.4}/I_{4272.2}$, $I_{4259.4}/I_{4300.1}$, and

CURVE	λ_1	λ_2	${}^1A_\ell^u$	${}^2A_\ell^u$
A	4259.4	4266.3	24.6×10^{-5}	2.8×10^{-5}
B	4259.4	4272.2	29.0×10^{-5}	6.7×10^{-5}
C	4259.4	4300.1	36.0×10^{-5}	3.4×10^{-5}
D	5572.5	5558.7	3.9×10^{-5}	8.3×10^{-5}

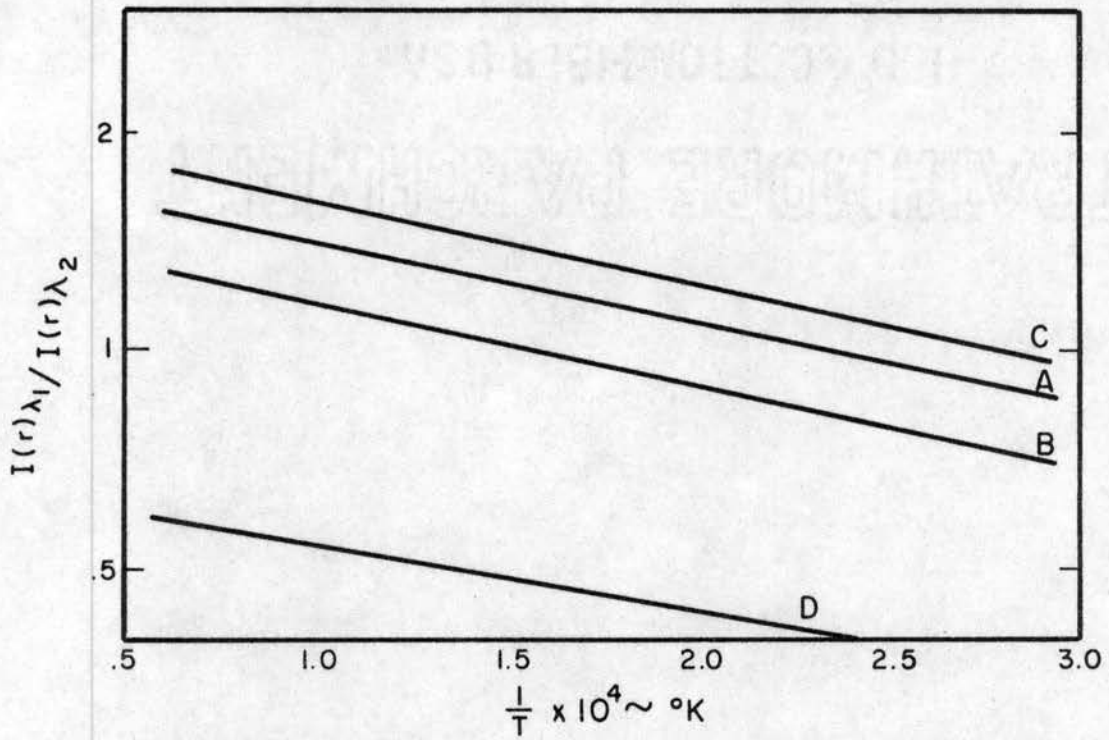

Figure 30. Intensity Ratios Used in Establishing Temperature.

$I_{5572.5}/I_{5558.7}$ were obtained at the centerline of the plasma column for each of the eleven operating conditions, and a corresponding temperature was obtained from Figure 30. These four temperature values (at each operating condition) were then averaged to arrive at the centerline temperature of the plasma column.

Once a temperature T^* is established at one point in the plasma column, a temperature distribution across the column may be obtained from

$$\frac{I(r)}{I(r^*)} = \frac{n_o(T)Z(T^*)}{n_o(T^*)Z(T)} \exp\left[\frac{E_u}{k}\left(\frac{1}{T^*} - \frac{1}{T}\right)\right] . \qquad (12)$$

In the temperature range encountered in this study the partition function Z varies from 1.00 to approximately 1.008, so that $Z(T^*)/Z(T)$ may be considered constant. The number density of neutral particles n_o is a function of temperature only for a fixed pressure. Figure 31 shows the variation of n_o with temperature at the test section pressure of 20 mm of mercury. Figure 32 was generated to eliminate the necessity of using an iteration technique to obtain a solution to equation 12. Once the temperature T^* is known at some radius r^* where the radial intensity has a value $I(r^*)$, then the remaining quantities in equation 12 are either known or functions only of T for a fixed pressure. The I(r) values were nondimensionalized with respect to $I(r^*)$ and plotted as a function of T for the fixed T^*. Curves similar to those shown in Figure 27 may be generated for any spectral line of interest, and then T at any radius r may be determined if T^*, $I(r^*)$, and I(r) are known.

The temperature distribution T(r) for each of the mass flow-power combinations is presented in Figures 33 through 43. These distributions

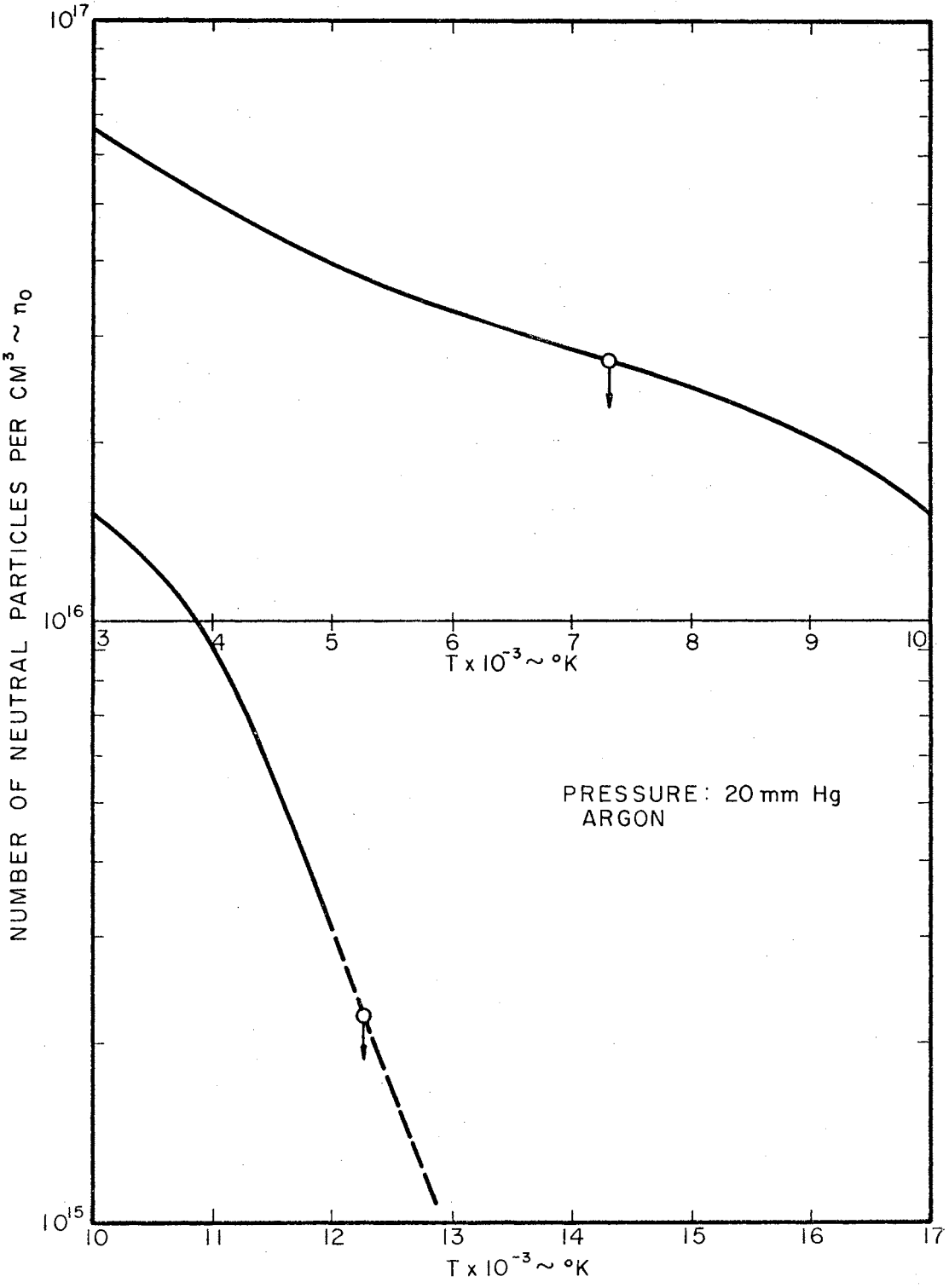

Figure 31. Number Density of Neutral Particles as a Function of Temperature at a Pressure of 20 mm Hg.

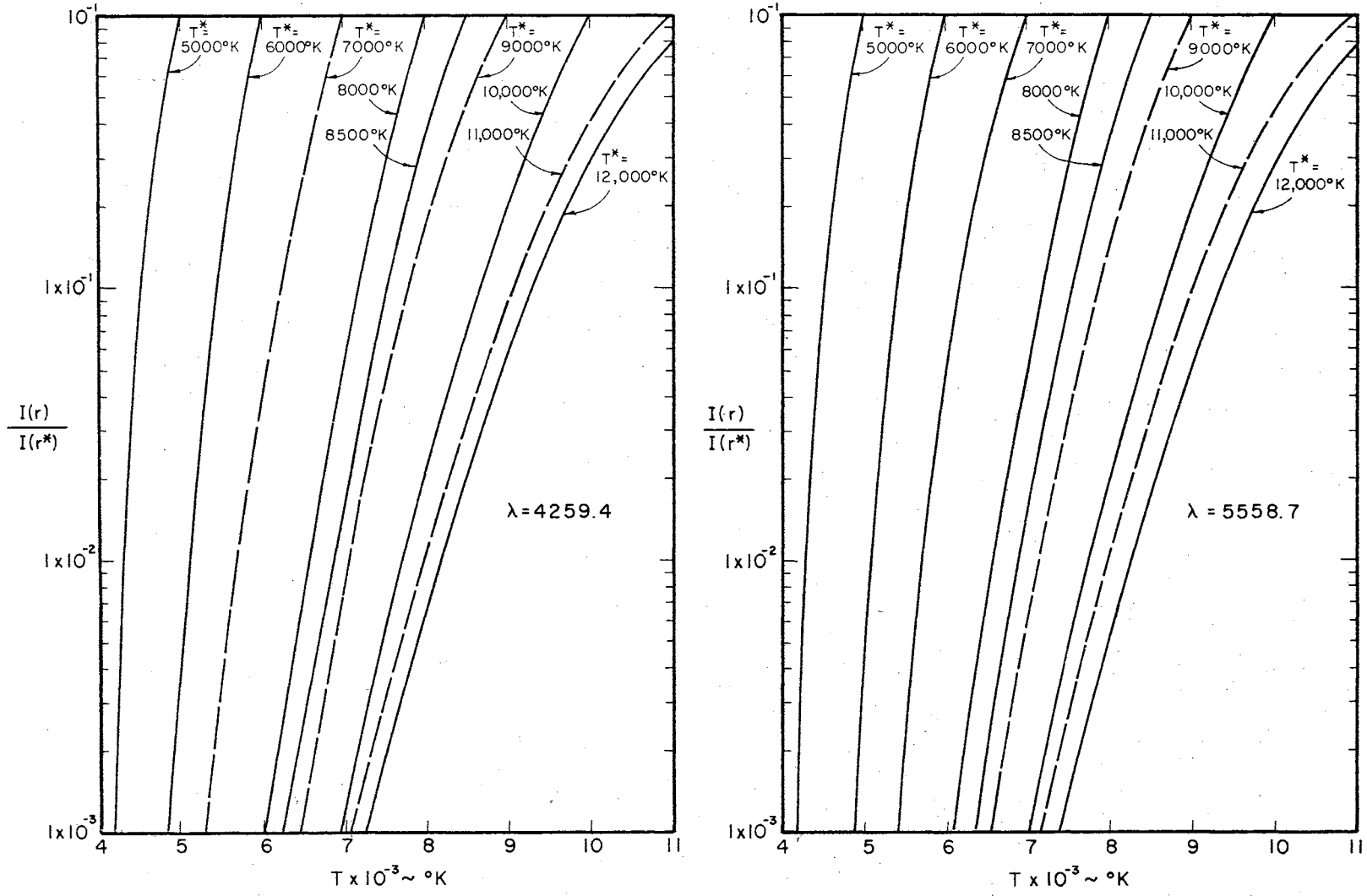

Figure 32. Temperature as a Function of I(r)/I(r*) for Various T* Values at λ = 4259.4 and λ = 5558.7 Angstroms.

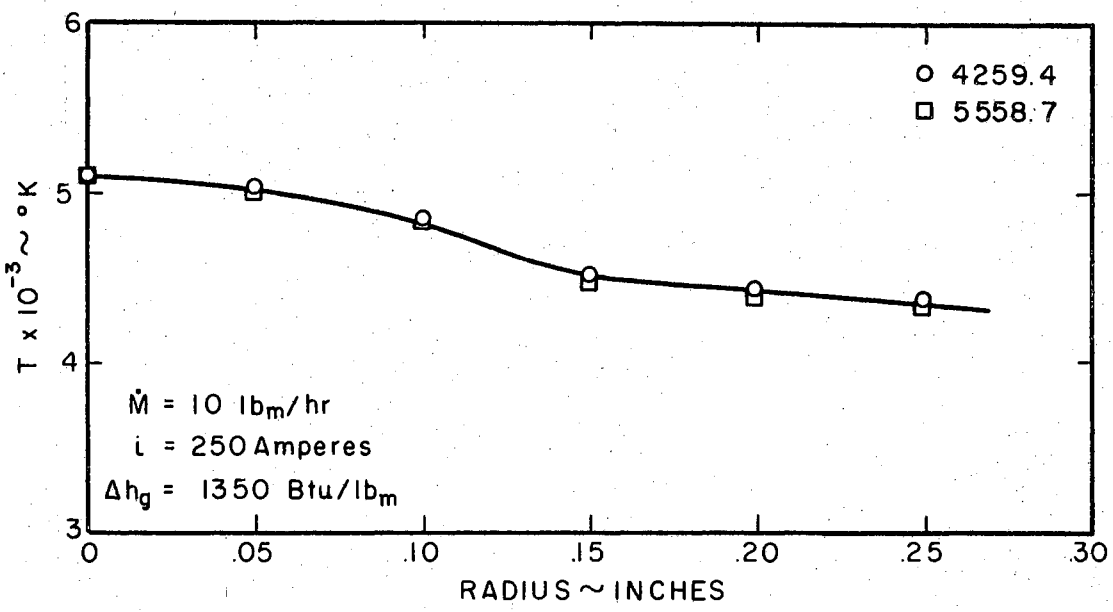

Figure 33. Temperature Profile for i = 250 Amperes and $\dot{M}$ = 10.0 lb_m/hour.

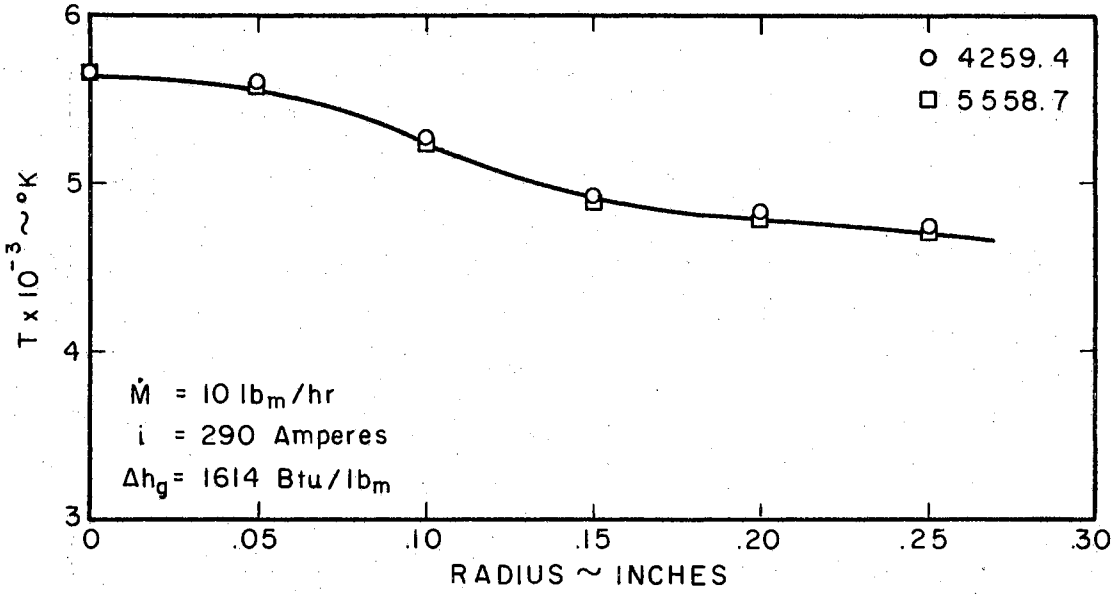

Figure 34. Temperature Profile for i = 290 Amperes and $\dot{M}$ = 10.0 lb_m/hour.

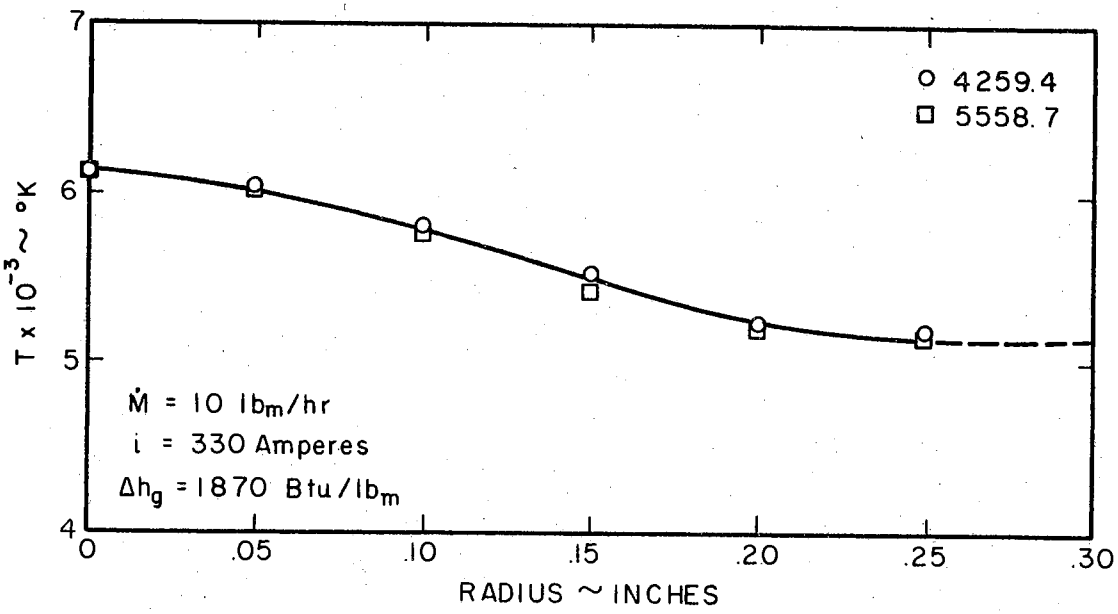

Figure 35. Temperature Profile for i = 330 Amperes and $\dot{M}$ = 10.0 lb_m/hour.

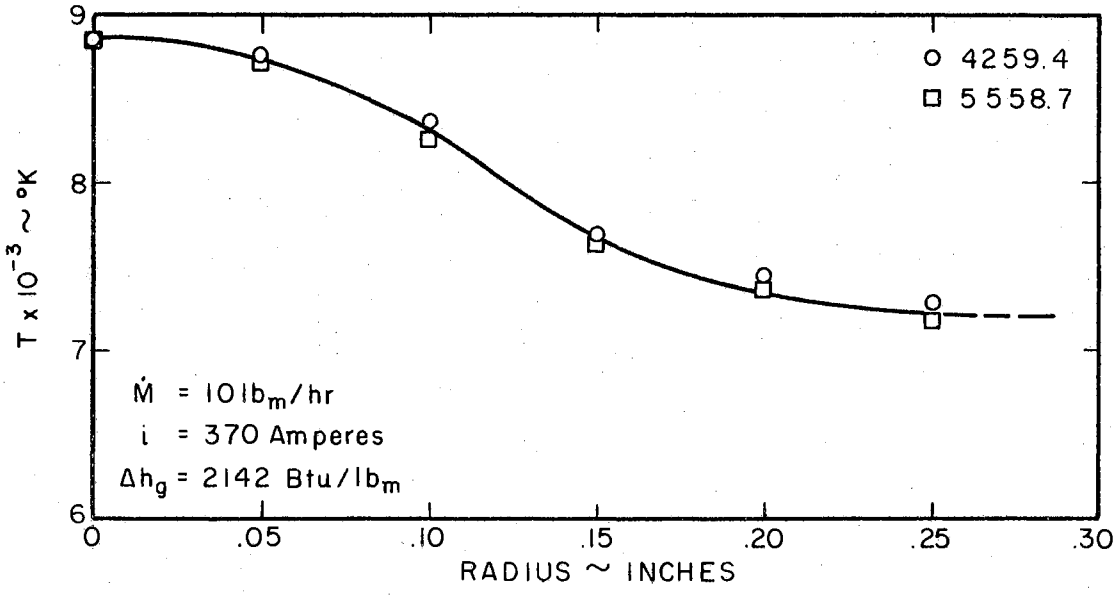

Figure 36. Temperature Profile for i = 370 Amperes and $\dot{M}$ = 10.0 lb_m/hour.

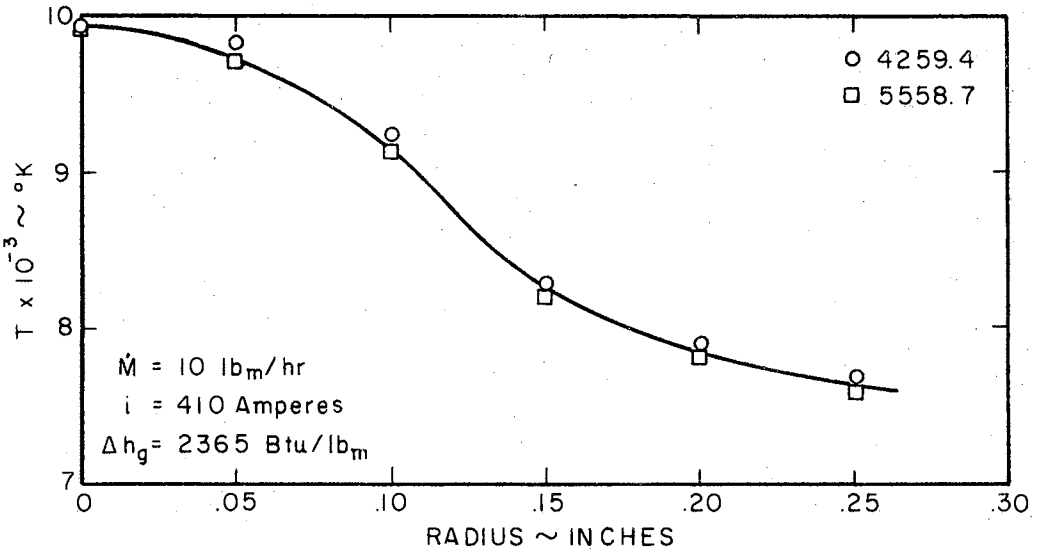

Figure 37. Temperature Profile for i = 410 Amperes and $\dot{M}$ = 10.0 lb_m/hour.

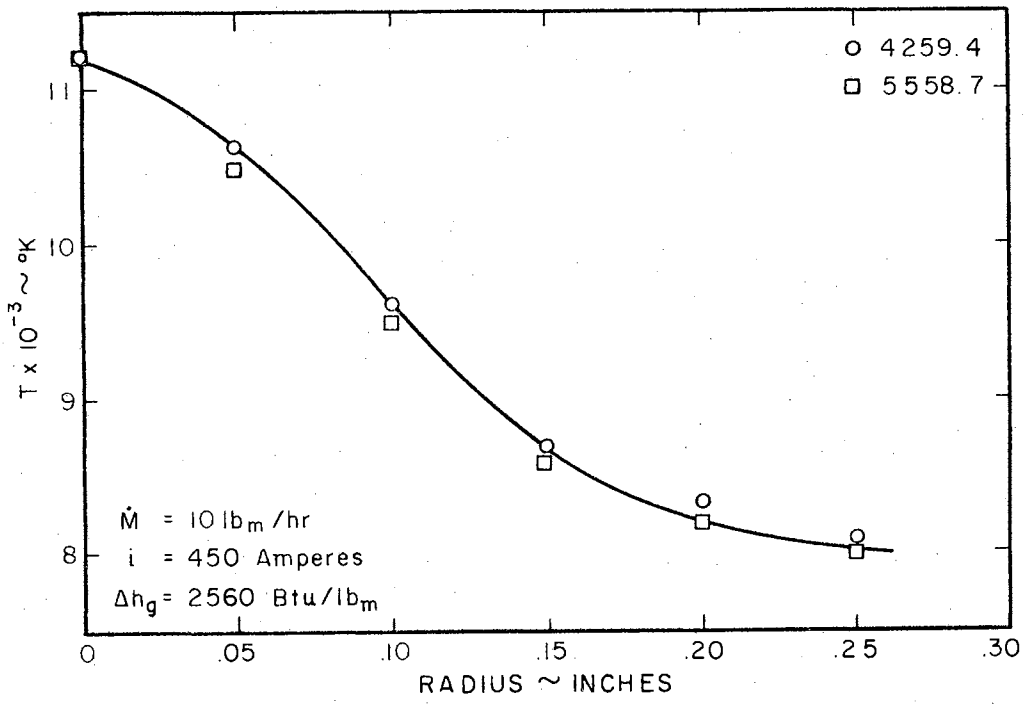

Figure 38. Temperature Profile for i = 450 Amperes and $\dot{M}$ = 10.0 lb_m/hour.

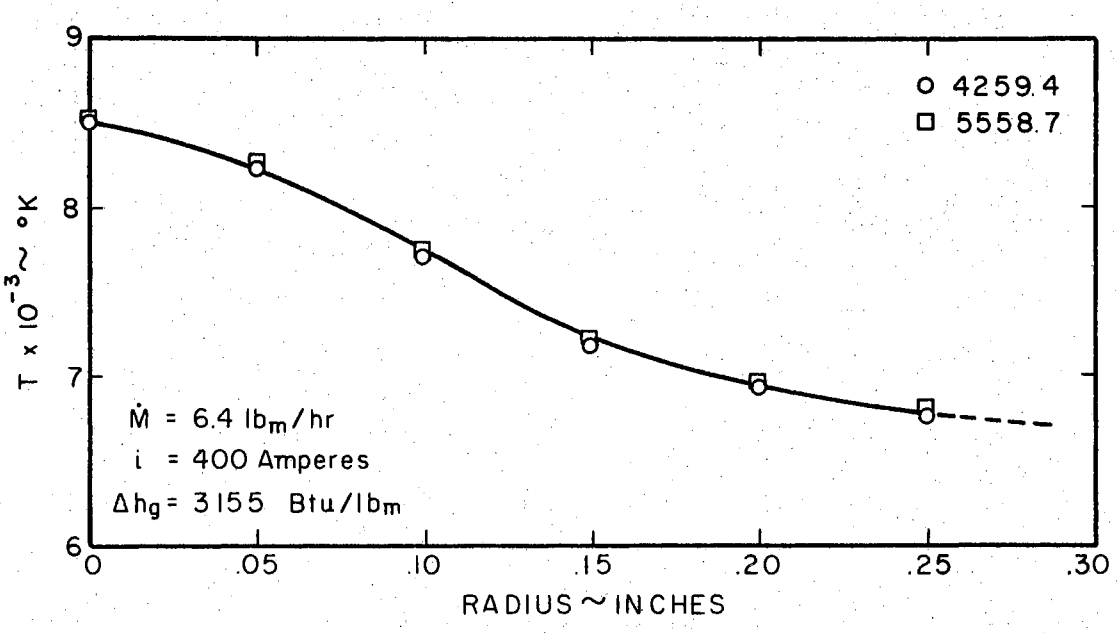

Figure 39. Temperature Profile for i = 400 Amperes and $\dot{M}$ = 6.40 lb_m/hour.

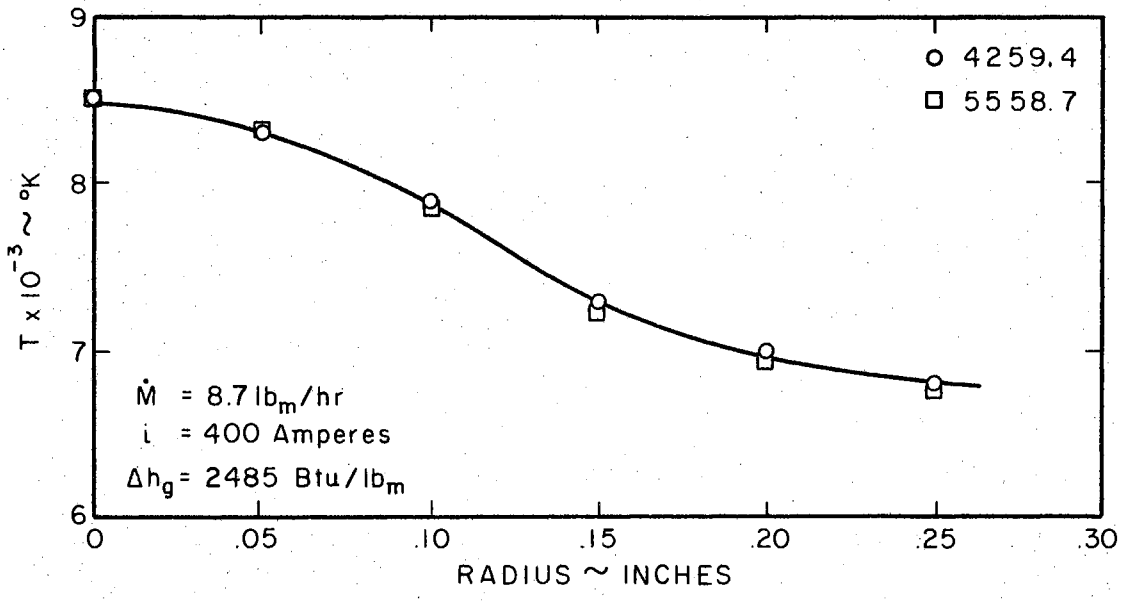

Figure 40. Temperature Profile for i = 400 Amperes and $\dot{M}$ = 8.7 lb_m/hour.

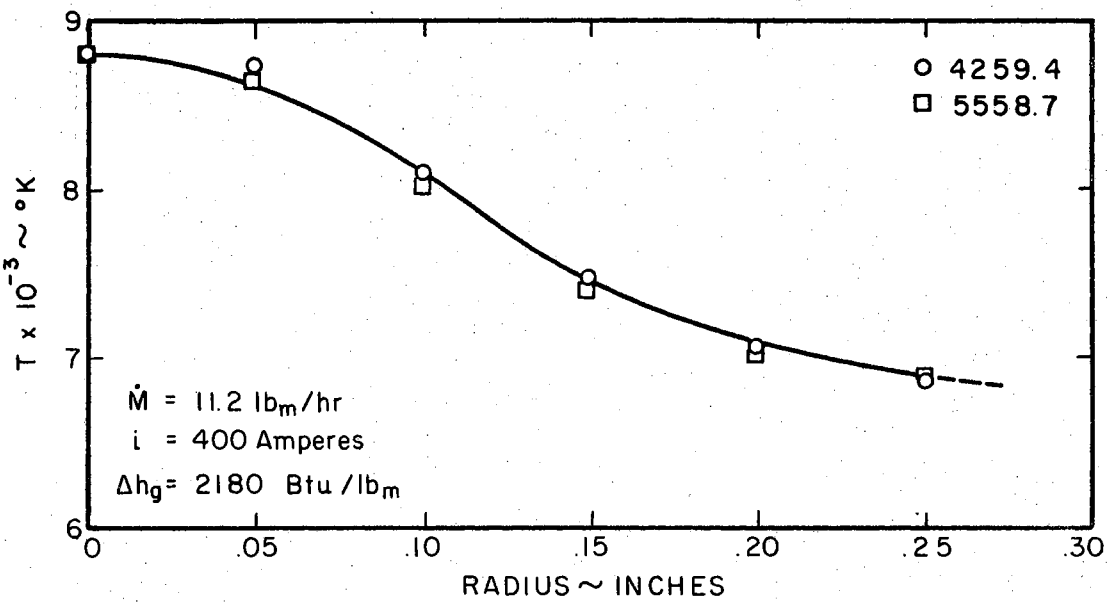

Figure 41. Temperature Profile for i = 400 Amperes and $\dot{M}$ = 11.2 lb_m/hour.

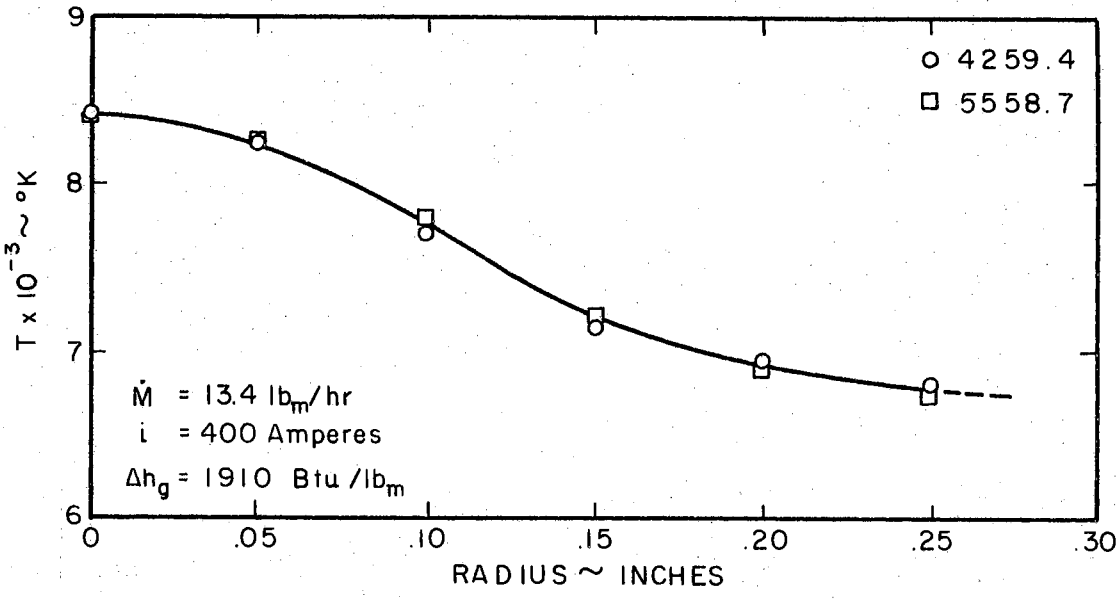

Figure 42. Temperature Profile for i = 400 Amperes and $\dot{M}$ = 13.4 lb_m/hour.

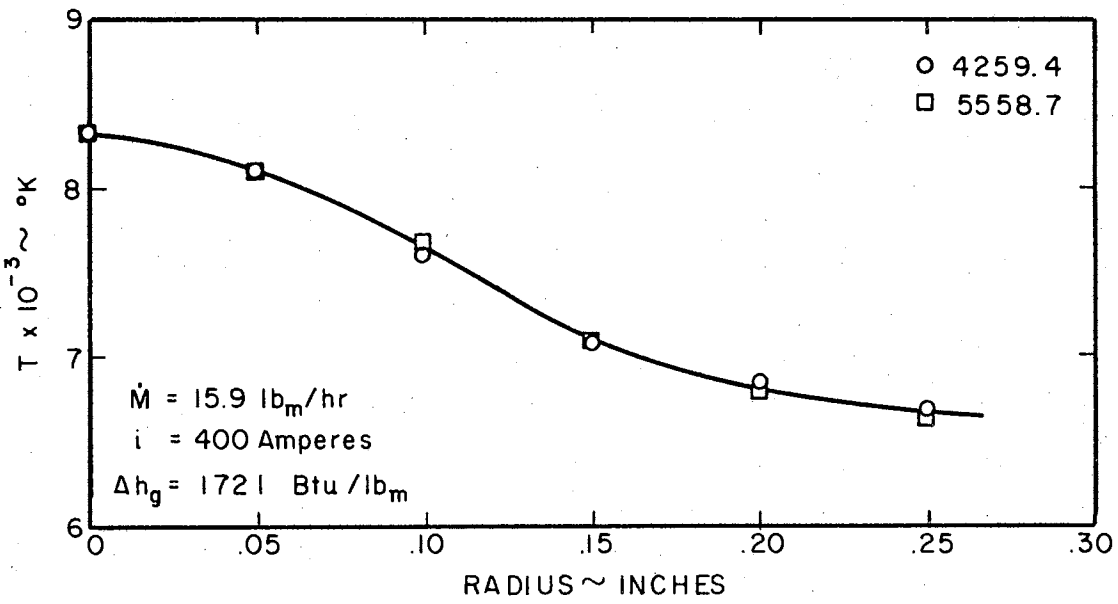

Figure 43. Temperature Profile for i = 400 Amperes and $\dot{M}$ = 15.9 lb_m/hour.

represent the temperature profile across the luminous plasma column. It is known that a region of cooler, non-luminous gas exists around the luminous column, but the determination of the state of this non-luminous zone is not possible by the methods presented here.

It may be seen that excellent agreement in temperature profiles is obtained by applying equation 11 to the 4259.4 Å and 5558.7 Å spectral lines. This agreement would appear to substantiate the argument that the differences in temperature predicted by various intensity ratio values was due to uncertainties in the transition probabilities and not to experimental errors.

From these temperature distributions, it appears that the arc current is the determining factor in establishing the temperature profile of the plasma column. For a fixed mass flow rate, an increase in current brought about a corresponding increase in T(r). This increase may be observed in Figures 33 through 38. However, a variation in mass flow rate from 6.40 to 15.9 lb_m/hour did not appreciably alter the temperature profile which was produced at a constant current value of 400 amperes (Figures 39 through 43). It appears that a fixed quantity of gas passes through the arc regardless of the flow rate, and that increases in mass flow rate result in temperature changes of the non-luminous region only.

It would appear that the uncertainties in the evaluation of the transition probability would negate the usefulness of the relative intensity method as a temperature determining technique. However, having been through the problems associated with this technique, the author feels that a better approach to the problem might have significantly

reduced its complexities. One point which becomes obvious upon examining Figure 29 is that the two-line relative intensity method predicts very large temperature changes with very small intensity ratio changes. For example, in the region of interest (approximately 6,000 to 10,000 $^{\circ}K$) a ten per cent change in intensity ratio results in approximately a thirty per cent change in temperature. Changes in A_{ℓ}^{u} have the same effect as changes in intensity ratio; so that the effects of variations of ten to twenty per cent in A_{ℓ}^{u} are reduced if the absolute values of the slope in Figure 29 is increased. It was an awareness of this fact that brought about condition three in the wavelength selection criteria since the slope is directly proportional to the difference in upper energy levels of the two spectral lines. One means of increasing the slope and reducing the effects of uncertainties in A_{ℓ}^{u} is to use spectral lines which originate from different types of particles, i.e., one spectral line from an ion transition and one spectral line from a neutral transition. However, in order to obtain reliable ion intensity values, power levels are required which are in excess of those available in many facilities. If an exact spectral response curve similar to Figure 18 is available for the detector used in making the intensity measurements, then condition two of the selection criteria may be removed. This then allows the selection of wavelengths λ_1 and λ_2 which have much greater differences in upper energy levels and therefore the absolute value of the slope of the intensity ratio versus temperature curve is greatly increased. By the simple spectral calibration of the radiation detector, wavelengths may be selected such that the slope is increased by a factor of four or more over that presented in Figure 29, and the effects of uncertainties in A_{ℓ}^{u} are significantly reduced.

Absorption Evaluation

Absorption measurements were performed at thirty different wavelengths in the visible spectrum for each of the eleven different mass flow-power combinations.

The absorption values typified by Figures 44 and 45 were obtained from the three measurements discussed in Chapter V. The remainder of the absorption data are presented in Appendix C. The absorption measurements were conducted on neutral argon lines and at continuum wavelengths only since relatively few ionized particles exist at the temperatures encountered in this study.

The absorption coefficient $\bar{\mu}(\lambda)$ was evaluated from equation 11 of Chapter V using an absorbing thickness of 0.50 inches. This thickness was established by the techniques described in Chapter V. To establish this thickness, the pressure in the test section was adjusted until the plasma column neither diverged nor converged upon exiting from the nozzle. Intensity data were taken approximately one-half inch downstream of the nozzle exit plane. The resultant absorption coefficients are presented in Figures 46 through 50. The data are plotted versus an average temperature of the absorbing layer. The T_{AVG} was obtained by applying a simple averaging process to data presented in Figures 33 through 43.

Discussion of Results

In the development of the temperature distribution across the plasma column a requirement was imposed upon the selected wavelengths that there be no significant attenuation of the energy whose wavelength

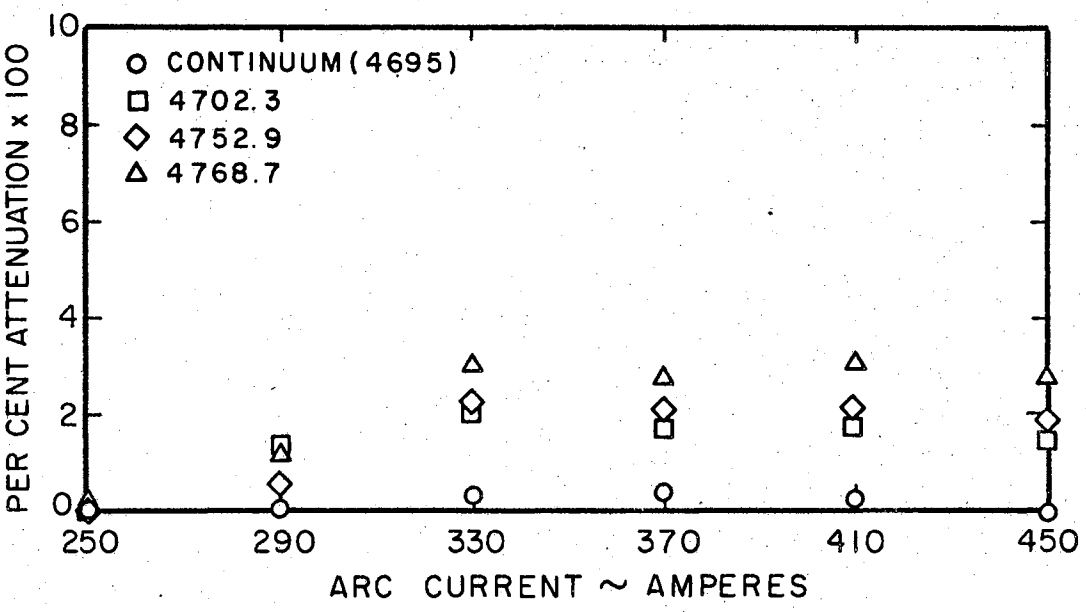

Figure 44. Absorption Data as a Function of Arc Current for Fixed Mass Flow Rate.

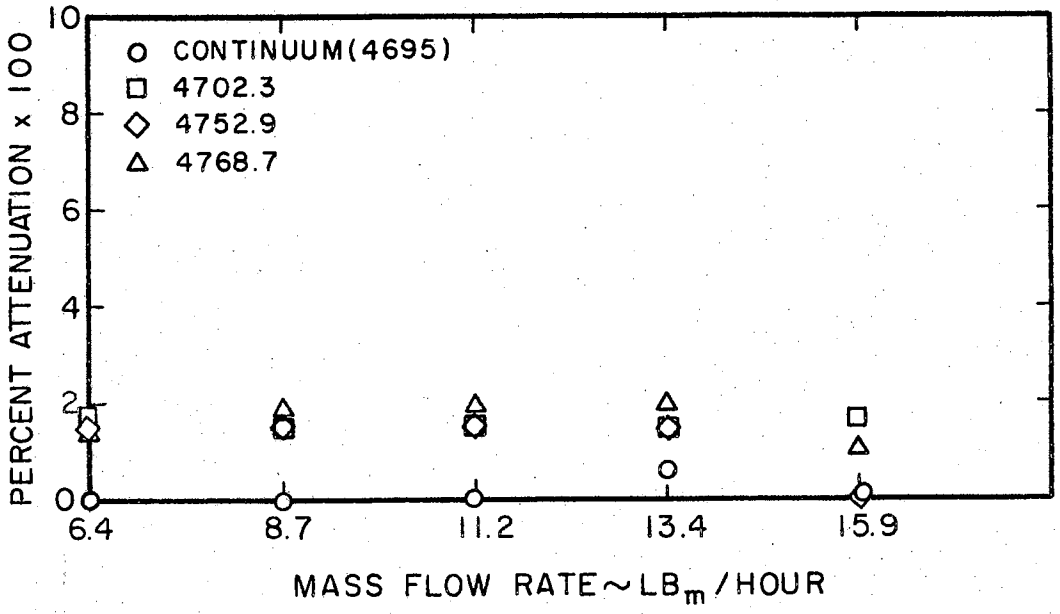

Figure 45. Absorption Data as a Function of Mass Flow Rate for a Fixed Current.

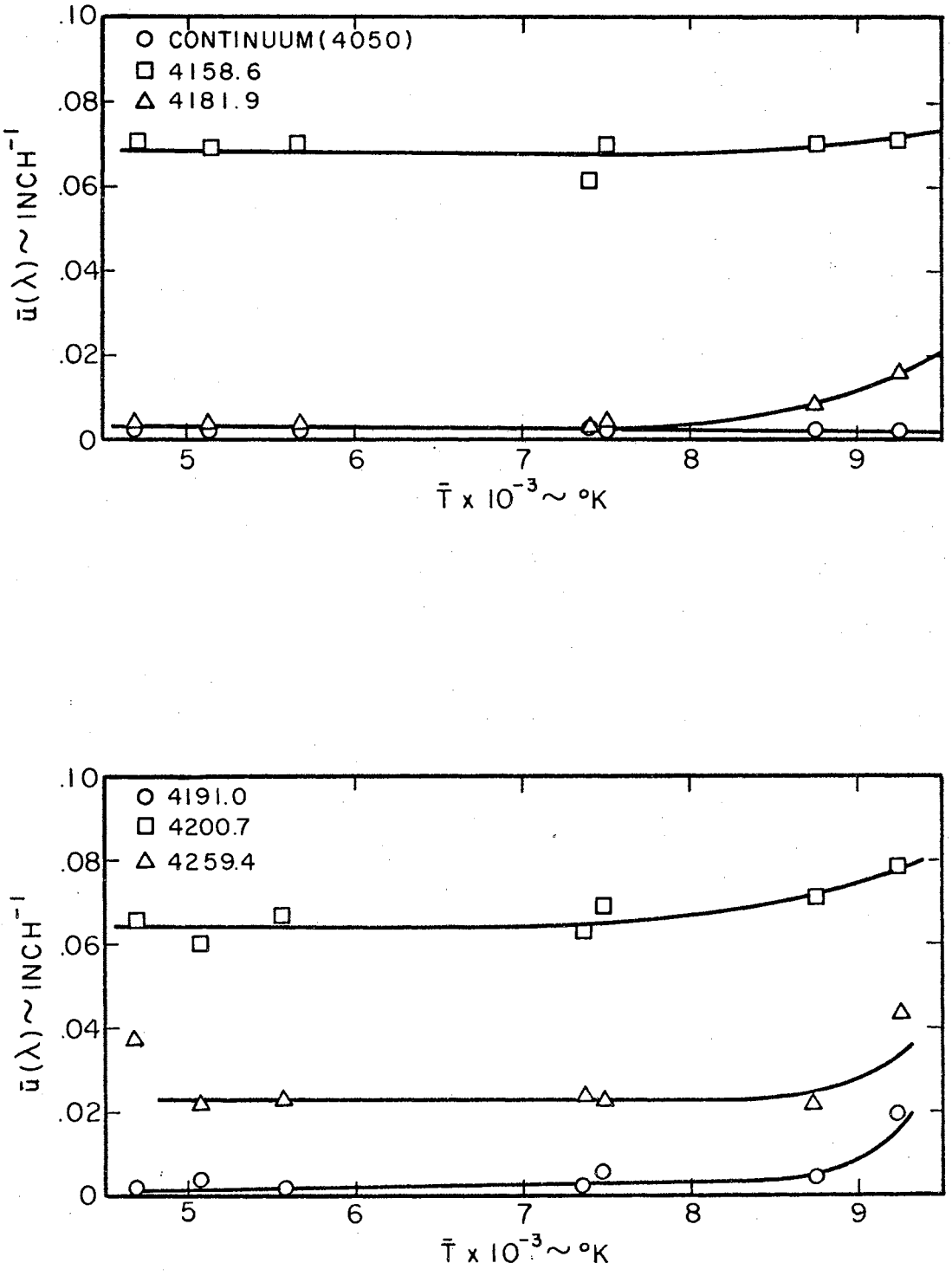

Figure 46. Absorption Coefficient $\bar{\mu}(\lambda)$ Versus Average Temperature for Selected Wavelengths.

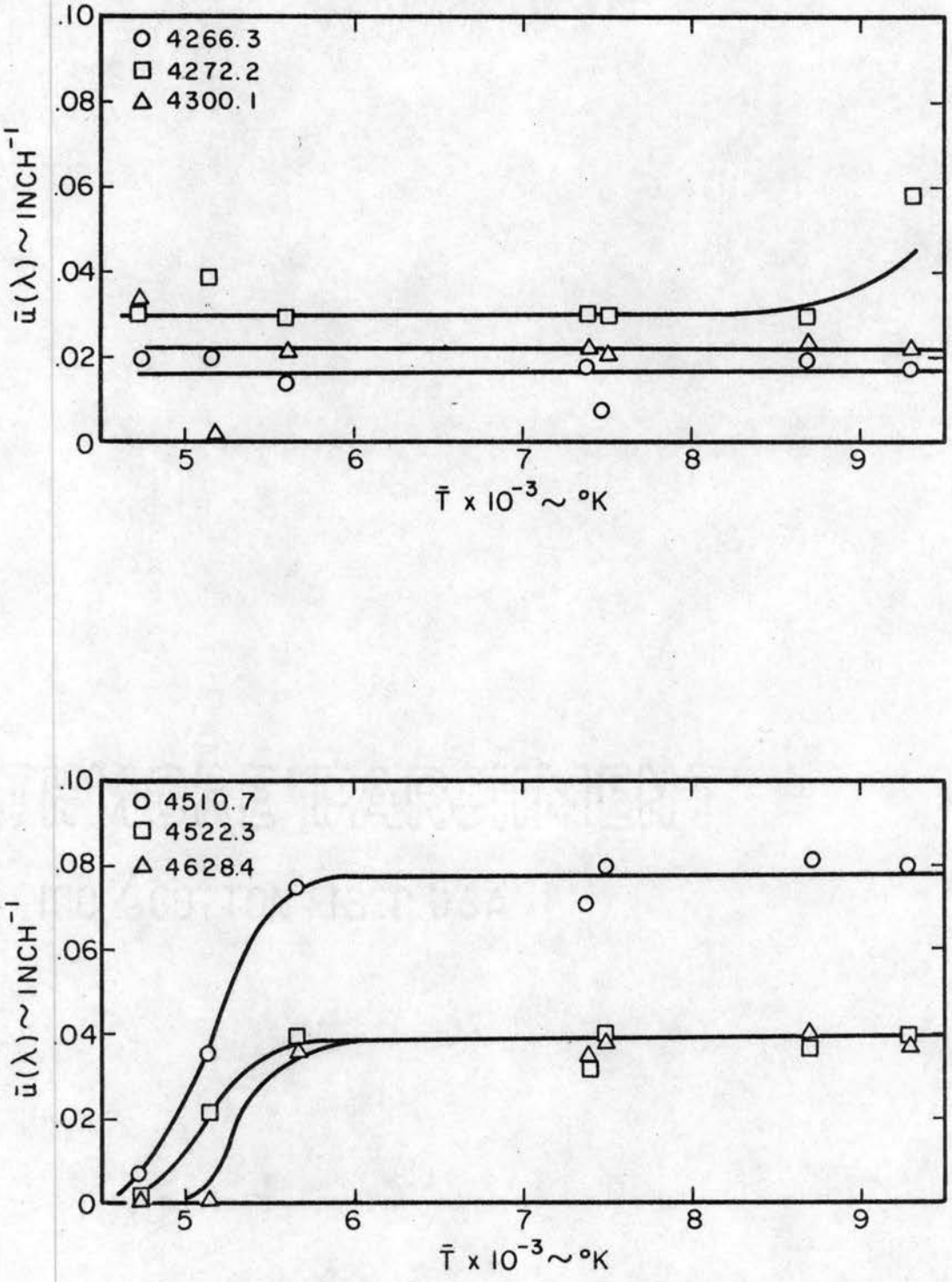

Figure 47. Absorption Coefficients $\bar{\mu}(\lambda)$ Versus Average Temperature for Selected Wavelengths.

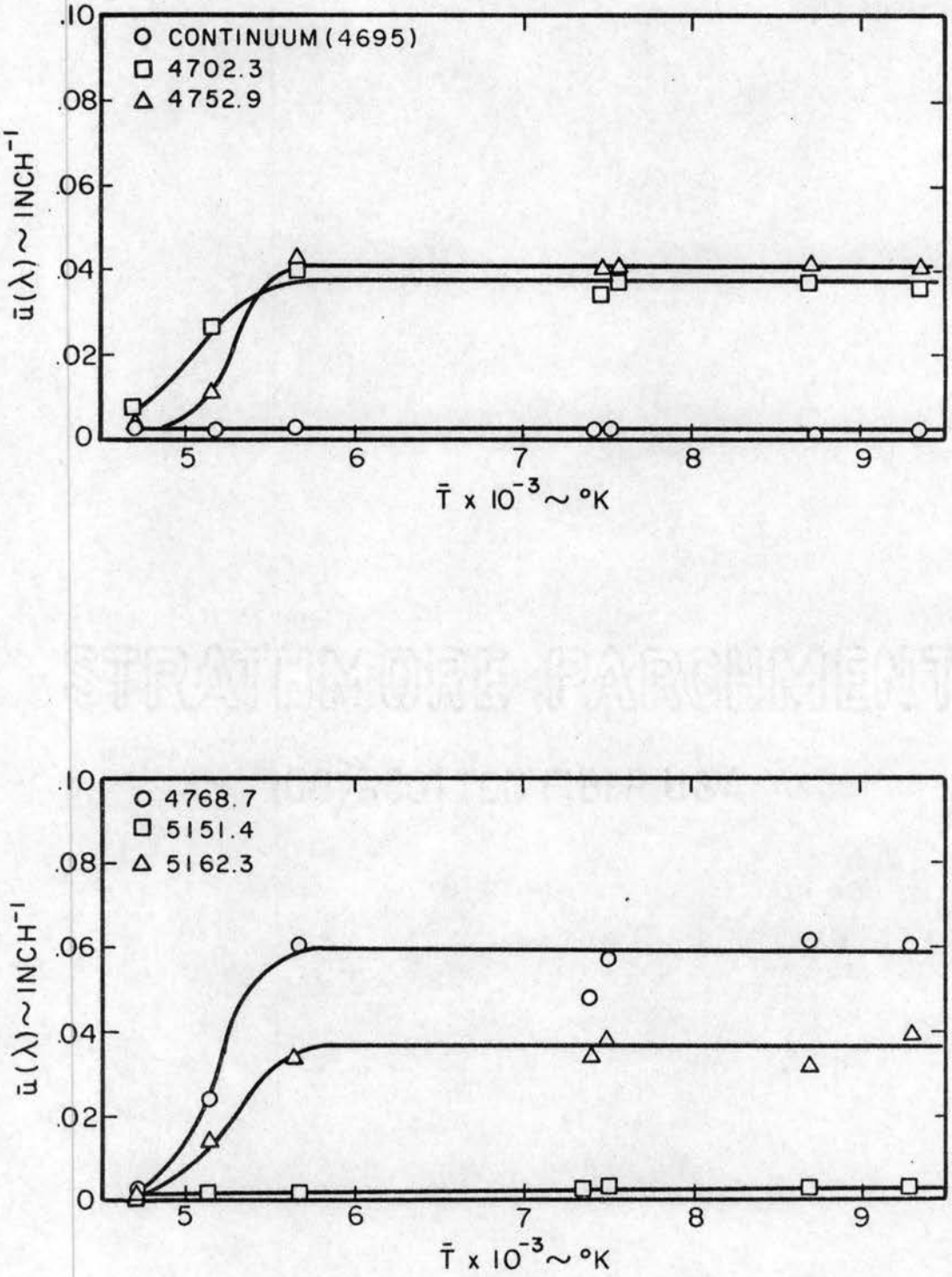

Figure 48. Absorption Coefficient $\bar{\mu}(\lambda)$ Versus Average Temperature for Selected Wavelengths.

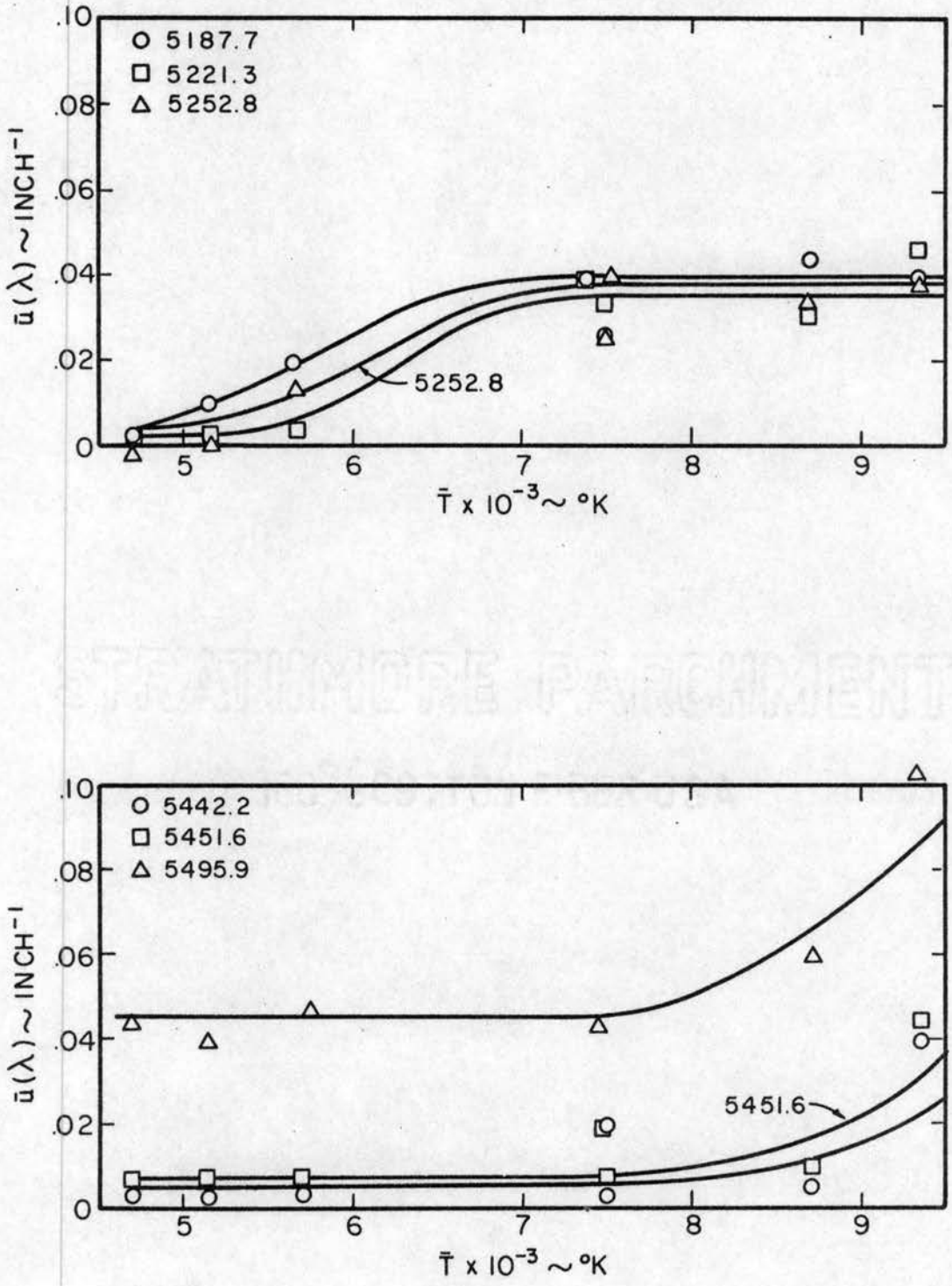

Figure 49. Absorption Coefficient $\bar{\mu}(\lambda)$ Versus Average Temperature for Selected Wavelengths.

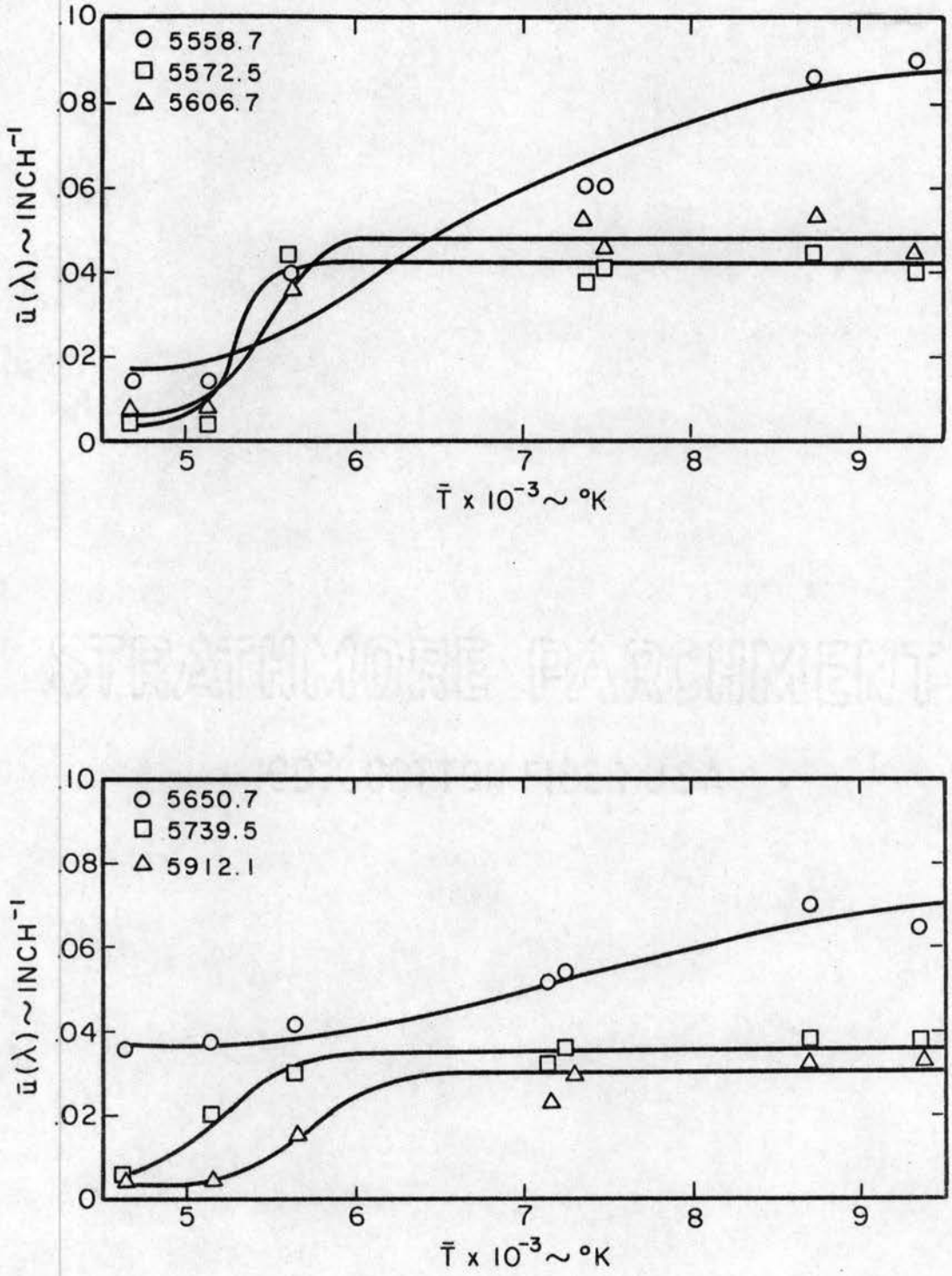

Figure 50. Absorption Coefficient $\bar{\mu}(\lambda)$ Versus Average Temperature for Selected Wavelengths.

is λ by the plasma column. This condition is verified for the operating conditions of this study by the data presented in Figures 44 and 45. The amount of self-absorption experienced by one of the argon spectral lines may be evaluated from

$$\frac{I_{(OBSERVED)}}{I_{(EMITTED)}} = e^{-\bar{\mu}(\lambda)x} \qquad (13)$$

where $\bar{\mu}(\lambda)$ is presented in Figures 46 through 50 and x is the thickness of the absorbing layer. The energy emitted from the region near the plasma center should experience the maximum amount of self-absorption since it must travel through more mass than that emitted at some radius $r > 0$. The $\bar{\mu}(\lambda)$ is obtained from Figures 46 through 50 if the average temperature of the absorbing media is known. However, the T(r) values and resultant T_{AVG} values were obtained from lines for which $I_{(OBSERVED)}/I_{(EMITTED)} = 1.0$. In most cases, one knows an approximate temperature of the plasma column and therefore the following iterative technique may be used in determining T(r) and T_{AVG}.

(1) Establish an approximate value of T_{AVG}.

(2) Select λ_1 and λ_2 subject to conditions

a) A_{ℓ}^{u} is known for both λ_1 and λ_2, and

b) $E_{u_1} - E_{u_2}$ is as large as possible.

(3) Establish $\bar{\mu}(\lambda_1)$ and $\bar{\mu}(\lambda_2)$ from Figures 46 through 50.

(4) Evaluate $I_{(OBSERVED)}/I_{(EMITTED)}$ from equation 13 for λ_1 and λ_2 where x is the radius of the plasma column.

(5) If the results of step 4 indicate a value of approximately .92

or less for λ_1 or λ_2, delete the wavelength whose intensity was attenuated from consideration.

(6) If both λ_1 and λ_2 satisfy step 5, i.e., indicate no significant self-absorption, then obtain T(r) from either equation 7 or from equation 5 after one point has been established in the column.

(7) After obtaining T(r), evaluate T_{AVG} from $T_{AVG} = \frac{1}{n}\sum_{i=1}^{n} T_i$ where T_i values are temperatures at various radial positions.

(8) From this T_{AVG} check the validity of the original value of $\bar{\mu}(\lambda)$. If the values vary significantly, reselect λ_1 and λ_2 and repeat the process.

For a small diameter plasma column, the process is an academic one since all wavelengths satisfy the selection criteria. For the flow conditions experienced in this study, the maximum absorption occurred at $\lambda = 5558$ Å, but was not of significant magnitude since the plasma column had a radius of only .25 inches. Therefore

$$\left[\frac{I_{(OBSERVED)}}{I_{(EMITTED)}}\right]_{minimum} = \left[e^{-(.09)\,(.25)} = 0.977\right]_{\lambda = 5558\ \text{Å}}.$$

Thus the fourth condition of the wavelength selection criteria was satisfied for all lines considered in this study.

However, the self-absorption effects are increased significantly when the diameter of the plasma column is increased. Facilities with much higher power capabilities and much larger plasma columns than those available for this study are capable of producing plasma conditions for which self-absorption may result in significant attenuation of the

energy emitted from the center core. A survey of various arc facilities indicates that a three inch diameter column is not uncommon (32). If the average temperature and density of the column are comparable to those existing in this study, then some spectral lines may be absorbed by as much as thirteen per cent. For those facilities capable of producing even larger, more dense columns, the self-absorption effects should not be neglected.

The applicability of the absorption coefficients presented in Figures 46 through 50 is restricted to plasma densities comparable to those existing in this study. The attempts to evaluate the effects of increased density upon the absorption characteristics by increasing the mass flow rate failed to produce any significant changes in the attenuation data. This invariance in absorption data was attributed to the fact that the temperature profile within the luminous core did not significantly change with variations in mass flow rate from 6.40 to 15.9 lb_m/hour. Thus within the density range considered, the temperature of the plasma column appears to be the controlling factor in the determination of the absorption coefficient.

A few of the neutral argon spectral lines which might be of interest are not included in this study. The original intent was to cover the spectral range from 3600 to approximately 8000 Å, but the band was narrowed to 4000 to 6000 Å for the following reasons. First, the 3606.5 Å line was too low in intensity due to attenuation by the test section windows, lenses, etc. to be considered. Other lines in the spectrum were not included in the study if they were too low in intensity or formed a part of an unresolvable pair. The study was terminated

at λ = 6000 Å since the intensity of lines between 6000 and 8000 Å was too low to be of interest. The spectral lines at λ = 8103.7 and 8115.3 were of great interest since other experimental data were available for comparison at these wavelengths, but the spectral response of the detector was not sufficient to measure the intensities at these long wavelengths, and as such, they were omitted from the study.

Data Agreement and Accurary

The data which are presented in Figures 46 through 50 are subject to a considerable amount of scatter, but this is to be expected when one considers the nature of the phenomena being considered and the magnitude of the attenuation experienced by the energy in passing through such a thin absorbing layer. It is anticipated that the faired curves through the data are often in error by twenty-five per cent or more. However, one of the purposes of this study was to provide a tool in selecting λ_1 and λ_2 for determining the state of a plasma column and the results of Figures 46 through 50 provide a selection criteria for various flow conditions which were previously not available. For example, λ = 5572.5 would appear to be superior to λ = 5558.7 as one of the wavelengths to be considered in a technique to determine the state of a large plasma column.

Though no theoretical expressions are available to predict $\bar{\mu}(\lambda)$ accurately, the data presented here are in agreement with the trend predicted by the theoretical expressions of Chapter III. In all cases the absorption increases with increasing temperature. Since the visible radiation considered in these studies are associated with transitions

which occur in the outer electron shells, one would expect the absorption to increase as the number of particles having electrons in these outer shells increases. Since the number of particles having electrons in the outer shell increases with temperature, the data trend is as anticipated. The fact that some of the spectral lines appear to be unaffected by the presence of the plasma column may be due to a low number density of particles in the lower energy level or a low transition probability value.

CHAPTER VII

CONCLUSIONS AND RECOMMENDATIONS

The objectives of the work reported in this thesis were to determine the absorption characteristics of an argon plasma for radiation in the visible spectrum and to provide information concerning the selection of spectral lines to be used in the determination of the state of the plasma.

The absorption coefficients for most of the neutral argon lines in the visible spectrum were obtained and were presented as a function of the average temperature of the gas. The results indicate that the self-absorption effects are insignificant for the plasma produced by the OSU Plasma Facility, but that self-absorption may cause a significant decrease in the observed intensities if the radius of the plasma column is larger than one inch.

The maximum power input to the facility resulted in an average temperature of the luminous core of approximately 9500 $^{\circ}$K. Many facilities operate at power levels much in excess of those available for this study and these facilities may produce flow conditions where absorption effects are of considerable significance. Additional studies are needed to establish the absorption characteristics at these higher temperature levels.

It was found that the relative intensity-temperature technique for establishing the state of the plasma was unacceptable unless wavelengths

were selected which were widely separated in the visible spectrum. If spectral lines were selected such that changes in the spectral response of some detector were insignificant, then uncertainties in the values of the transition probabilities and small experimental uncertainties created prohibitive uncertainties in the evaluation of the temperature. It is suggested that applications of the relative intensity-temperature technique be restricted to wavelengths λ_1 and λ_2 where both λ_1 and λ_2 do not originate from the same type of basic particle (one from a neutral atom and one from an ion) or to wavelength values which differ by at least 1000 Å and preferably more. Since intensity values associated with ion transitions are often too low to be considered, the use of widely separated spectral lines is suggested. This method requires that the experimenter either calibrate the radiation detector for a known input intensity at the wavelengths of interest, or use multiple detectors. If detectors are positioned so as to observe intensities at wavelengths λ_1 and λ_2 it is still necessary to compensate for the response changes as a function of wavelength, but this method offers the advantage of obtaining I_{λ_1} and I_{λ_2} simultaneously. By using this method and establishing the effects of self-absorption from the procedure given in Chapter VI, it is felt that the relative intensity-temperature technique establishes a reasonable means of determining the temperature of a plasma column.

In conclusion, suggestions for future plasma research are given in the following lines.

Further investigations into the evaluation of transition probabilities are needed. Not only are values needed for additional spectral

lines, but further improvements in currently available values are also needed.

Since absorption processes of the type considered in this thesis occur in all plasmas, studies of this type should be conducted for all gases commonly used in plasma production. The absorption coefficients should be obtained for a variety of densities and power levels for each of the spectral lines which might be used in determining the temperature of the plasma.

Additional techniques are needed to establish the velocity and density gradients which are known to exist in most plasma generators. Until these techniques are developed, the usefulness of the plasma arc as a high temperature gas dynamics facility is greatly diminished. A complete understanding of the thermodynamic processes which take place when a model is placed in a plasma stream may not be accomplished until better information on velocity profiles become available. The problems associated with the determination of velocity and density variations are essentially the same as those associated with determining the temperature profile. Due to the extreme temperatures encountered and the disturbing effects of large water-cooled probes, the existing conventional methods of handling this problem are not adequate.

BIBLIOGRAPHY

1. Haworth, D. R. "Development of a Plasma Facility and Spectroscopic Determination of Plasma Temperatures." (unpub. Ph.D. Dissertation, Oklahoma State University, 1961).

2. Pearce, W. J. "Plasma Jet Temperature Study." WADC Tech. Report, 59-346, 1960.

3. Cambel, A. B. Plasma Physics and Magnetofluidmechanics. McGraw-Hill, New York, N.Y. (1963).

4. Sherman, M. P., P. F. Jacobs, and J. Grey. "Electron-Heavy-Particle Nonequilibrium In An Argon Arcjet." ARL 64-210, 1964.

5. Fowler, R. H. and E. A. Milne. "Dissociation Equilibria by the Method of Partitions." Phil. Mag. 45; 1, 1923.

6. Larenz, R. W. "Concerning a Method for the Measurement of Very High Temperatures in Nearly Transparent Arc Columns." NASA Technical Translation F-54, 1960.

7. Olsen, H. H. "The Electric Arc as a Light Source for Quantitative Spectroscopy." J. Quant. Spectrosc. Radiat. Transfer. Vol. 3 (1963) pp. 305-333.

8. Gericke, W. E. "Messung Der Ubergangswahrscheinlichkeit Von AI-Linien." Z. Astrophys. Vol. 53 (1961) p. 68.

9. Griem, H. R. Plasma Spectroscopy. McGraw-Hill, New York, N.Y. (1964).

10. Longmire, M. S., S. H. Sternick, and S. B. Herskovitz. "The Determination of Plasma Properties by Radiation Techniques: A Survey." AFCRL 348, 1961.

11. Cremers, C. J. and E. Pfender. "Thermal Characteristics of a High and Low Mass Flux Argon Plasma Jet." ARL 64-191, 1964.

12. Marlotte, G. L. and M. L. Dalton. "Basic Research on Gas Flows Through Electric Arcs." ARL 64-208, 1964.

13. Hill, W. W., Jr., and P. E. Stanley. "Instrumentation Studies for Plasma Jet and Hypersonic Wind Tunnel." Purdue University Rept. A-59-12, 1959.

14. Nagler, R. G. "Application of Spectroscopic Temperature Measuring Methods to Definition of a Plasma Arc Flame." JPL Rept. 32-66, 1961.

15. Jahn, R. E. "Spectroscopic Measurements of the Temperature of Plasma Jets." Ionization Phenomenon in Gases. Vol. 1. (1959) p. 955.

16. Touryan, K. J. "Lectures on Plasma Physics and Magnetogasdynamics." Sandia Corporation Rept. SCTM 93-63(71), 1963.

17. Shipley, K. L. "Spectrographic Analysis of Plasmajets--Progress Report II." Sandia Corporation Rept. SC-4776(RR).

18. Cowan, R. D. and G. H. Dieke. "Self-Absorption of Spectrum Lines." Rev. of Mod. Physics. Vol. 20, No. 2. (1948) p. 418.

19. Weissler, G. L. "A Survey of Radiation Processes in Gases." Ionization Phenomenon in Gases. Vol. 2. (1961) p. 195.

20. Herzberg, G. Atomic Spectra and Atomic Structure. Dover, New York, N.Y. (1944).

21. Kuhn, H. G. Atomic Spectra. Academic Press, New York, N.Y. (1962).

22. Penner, S. S. Quantitative Molecular Spectroscopy and Gas Emissivities. Addison-Wesley, Reading, Mass. (1959).

23. Smith, H. L. "A Constant Linear Velocity Photomultiplier Scanning Assembly for a Plane Grating Spectrograph." (unpub. M. S. Rept., Oklahoma State University, 1965).

24. Olsen, H. N. "Measuremement of Argon Transition Probabilities Using the Thermal Arc Plasma as a Radiation Source." J. Quant. Spectrosc. Radiat. Transfer. Vol. 3. (1963) pp. 59-76.

25. Knopp, C. F. "A Spectroscopic Technique for the Measurement of Temperature in Transparent Plasmas." (unpub. M. S. thesis, Northwestern University, 1961).

26. Tourin, R. H., P. M. Henny, E. T. Liang, M. L. Hecht, and S. Dolin. "Measurement of Temperatures in Ionized Gases by Means of Infrared Radiation." ARL 26-314, 1962.

27. Ryan, L. R., H. J. Babrov, and R. H. Tourin. "Infrared Spectra and Temperatures of Plasmajets." ARL 62-35, 1963.

28. Hamberger, S. M. "Measurement of Neutral Atom Density in a Highly Ionized Plasma by Absorption of Line Radiation." Ionization Phenomenon in Gases. Vol. 2. (1961) p. 1919.

29. Smith, M. W., M. Cobb, and J. Day. "Testing of a Constant Linear Velocity Hydraulic Ram." (unpub. rept., Oklahoma State University, 1965).

30. Harrison, G. R., R. C. Lord, and J. R. Loofbourow. Practical Spectroscopy. Prentice-Hall, New York, N.Y. (1948).

31. Jahn, R. G. and W. Jaskowsky. "Spectroscopic Investigation of the Plasma State." Plasmadyne Corp. Rept. PLR-88, 1960.

32. Tillian, D. J. "Plasma Arc Facilities in the United States." LTV Research Center Rept. 0-71000/3R-22, 1963.

APPENDIX A

DEVELOPMENT OF THE MEASURED INTENSITY DISTRIBUTION AS A FUNCTION OF THE RADIAL INTENSITY DISTRIBUTION

Electromagnetic radiation is emitted from a plasma column when electrons undergo transitions from one energy level to another of lower value.

The spectrograph receives radiation which is emitted from a cross section of the plasma jet which is perpendicular to the direction of flow (Figure 51). Only that radiation which is emitted parallel to the y-direction from a disc shaped plasma region is received. This region which is bounded by two planes at z and $z + \Delta z$, and has a radius r_o, may be selected arbitrarily be merely focusing different sections of the plasma jet on the entrance slit of the spectrograph.

It is convenient to subdivide the emitting disc into a number of horizontal sections of height Δx (Figure 52). From each of these horizontal columns the spectrograph receives radiation which produces a number of spectral lines of intensity I_x, where the intensity varies with wavelength λ. For any spectral line the observed intensity I_x is proportional to the radiation emitted by the plasma subdivision. If one further divides these horizontal columns into smaller volume elements by passing planes parallel to the x-axis, a volume bounded by the planes x, $x + \Delta x$; y, $y + \Delta y$; z, and $z + \Delta z$ is formed. In any of these elemental volumes there exists a radiation density u_r which is defined

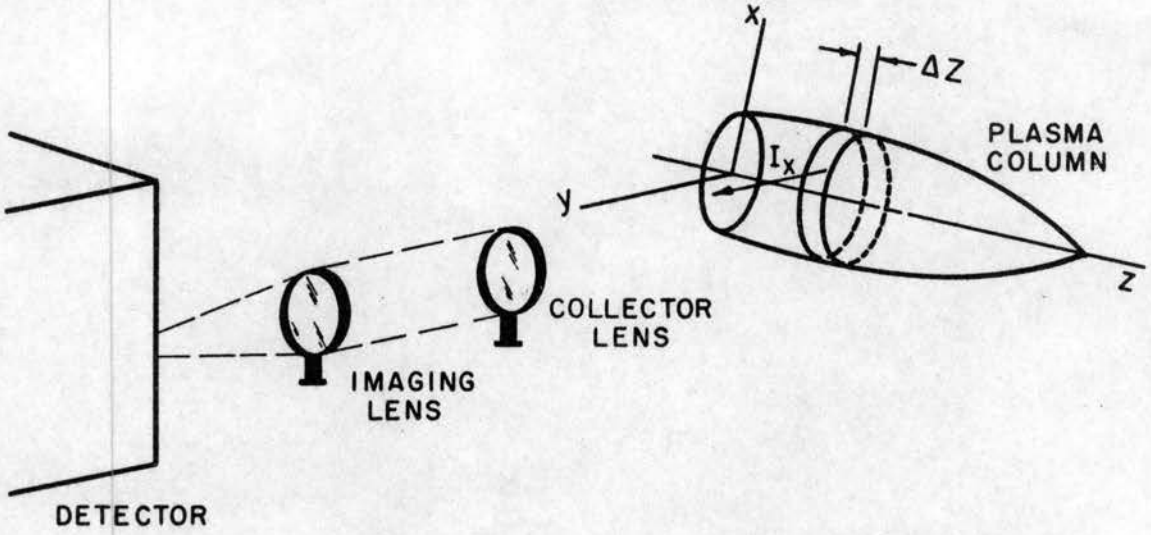

Figure 51. Diagram of Data Collection System.

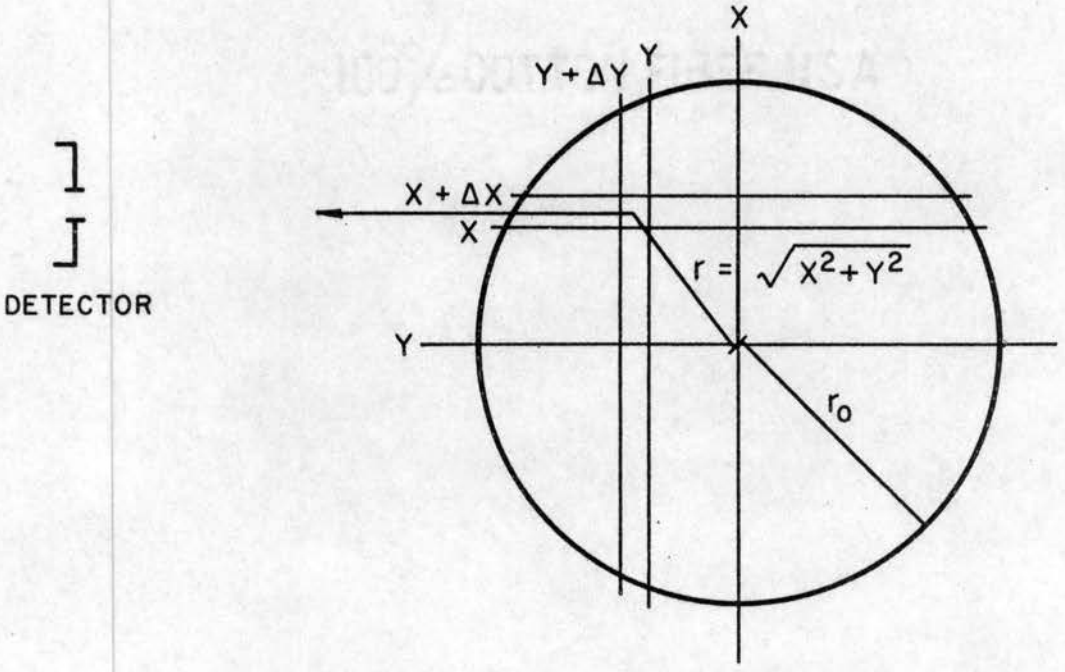

Figure 52. Subdivision of Emitting Plasma Disc.

as the radiant energy per unit volume. Then a fraction ΔI_x of the observed intensity I_x for a given spectral line is due to this elemental volume and is proportional to

$$\frac{u_r \cdot \Delta v}{(\text{Projected Area})} \quad .$$

Since $\Delta v = \Delta x \cdot \Delta y \cdot \Delta z$ and the projected area is $\Delta x \cdot \Delta z$, one obtains

$$\Delta I_x = k \cdot u_r \cdot \Delta y$$

where k is the constant of proportionality.

For a fixed vertical position the observed intensity I_x is the sum of the elemental contributions, i.e.,

$$I_x = \sum_i \Delta I_{x_i} = \sum_i k_i \cdot u_r \cdot \Delta y$$

if the absorption of radiation from an interior point by the intermediate regions is neglected.

When the element size is decreased, approaching zero in the limit, the following equation is obtained,

$$I_x = \int_{y=-y_o}^{y=y_o} k \cdot u_r \cdot dy \quad .$$

Using the expression $r = \sqrt{x^2 + y^2}$ and considering the plasma column to be axisymmetric, one obtains

$$I_x = 2\int_{y=0}^{y=\sqrt{r_o^2 - x^2}} k \cdot u_r \cdot dy \quad .$$

There exists a correlation between the radiation density u_r and the energy I(r) which is emitted in the y-direction, in unit time, in unit solid angle, per unit area of the radiating surface. This correlation is given by

$$I(r) = \frac{c}{4\pi} u_r,$$

where c is the speed of light.

If one incorporates this expression into the equation for I_x, the following equation is obtained,

$$I_x = k''\int_{y=0}^{y=\sqrt{r_o^2 - x^2}} I(r)\, dy \quad .$$

If one substitutes $y = \sqrt{r^2 - x^2}$ and $dy = \frac{rdr}{\sqrt{r^2 - x^2}}$ for x = constant, into the preceding equation and performs a change in variables, then one obtains

$$I_x = k''\int_{r=x}^{r=r_o} \frac{r \cdot I(r)\, dr}{\sqrt{r^2 - x^2}} \quad .$$

Since relative intensity measurements are of primary concern, the modified proportionality constant k'' will no longer be considered and the preceding equation is reduced to a particular form of Abel's integral equation,

$$I_x = \int_{r=x}^{r=r_o} \frac{r \cdot I(r)\, dr}{\sqrt{r^2 - x^2}} \quad .$$

APPENDIX B

MEASURED INTENSITY DATA

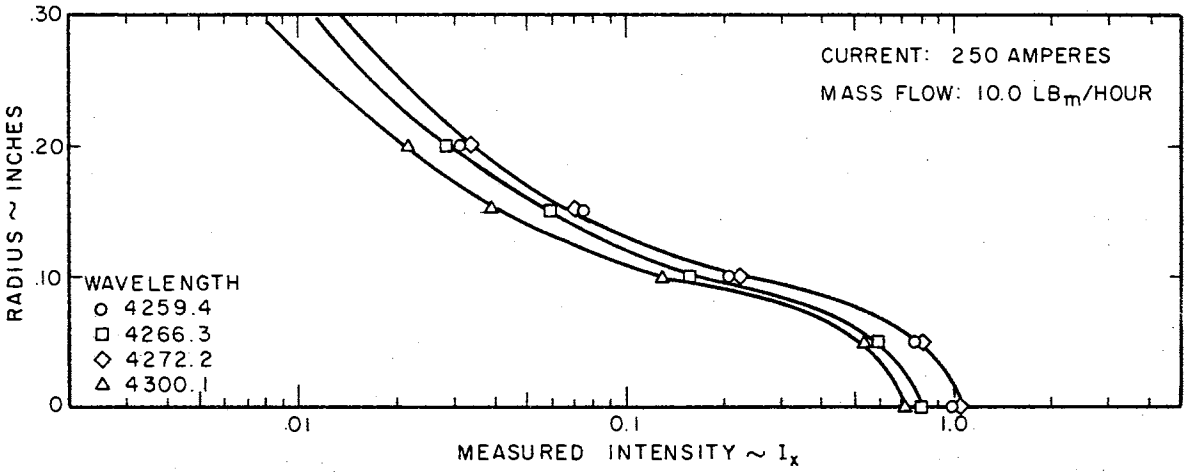
.30
.20
.10
0
RADIUS ~ INCHES
CURRENT: 250 AMPERES
MASS FLOW: 10.0 LBm/HOUR
WAVELENGTH
o 4259.4
□ 4266.3
◇ 4272.2
△ 4300.1
.01
0.1
1.0
MEASURED INTENSITY ~ Ix

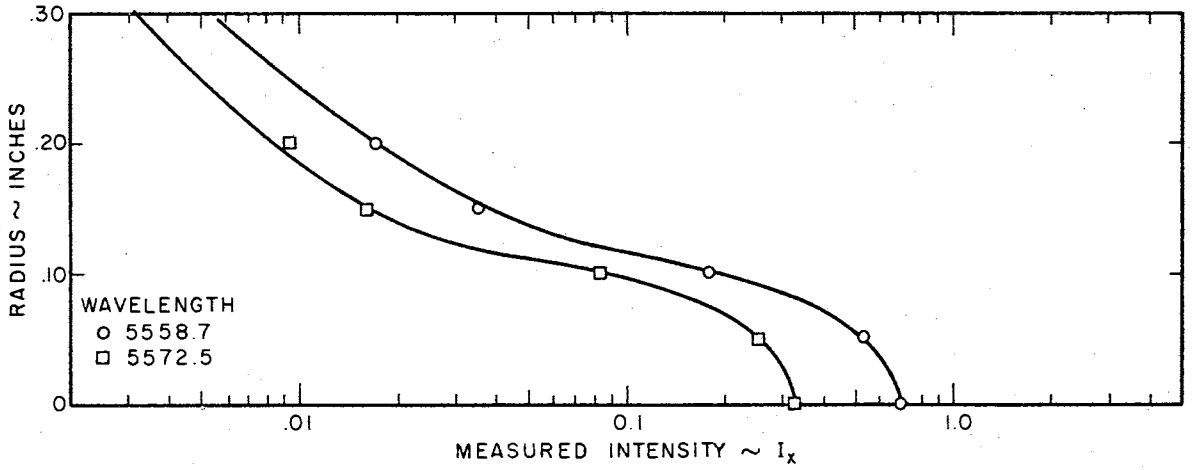
.30
.20
.10
0
RADIUS ~ INCHES
WAVELENGTH
o 5558.7
□ 5572.5
.01
0.1
1.0
MEASURED INTENSITY ~ Ix

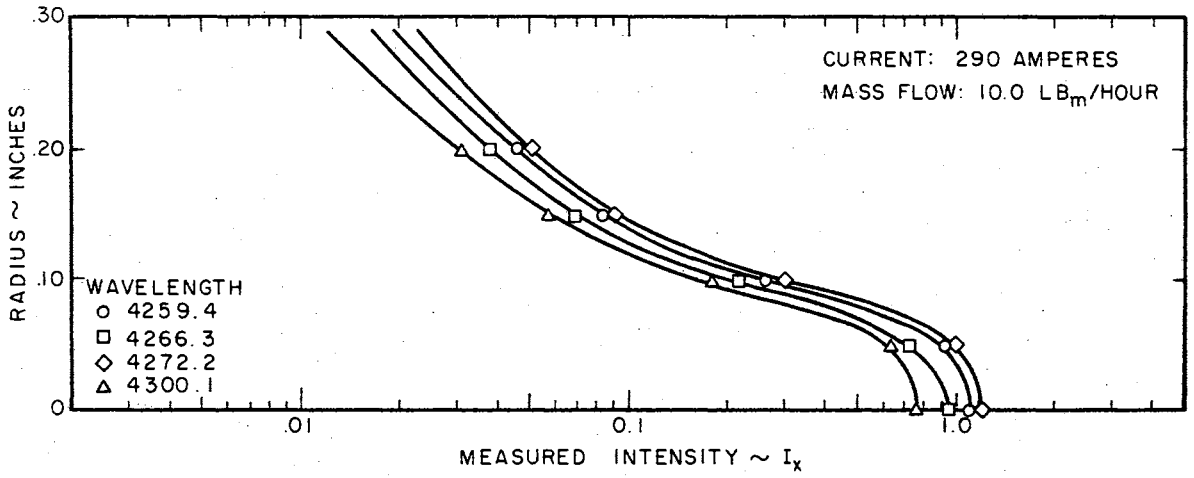
.30
.20
.10
0
RADIUS ~ INCHES
CURRENT: 290 AMPERES
MASS FLOW: 10.0 LB$_m$/HOUR
WAVELENGTH
o 4259.4
□ 4266.3
◇ 4272.2
△ 4300.1
.01
0.1
1.0
MEASURED INTENSITY ~ I_x

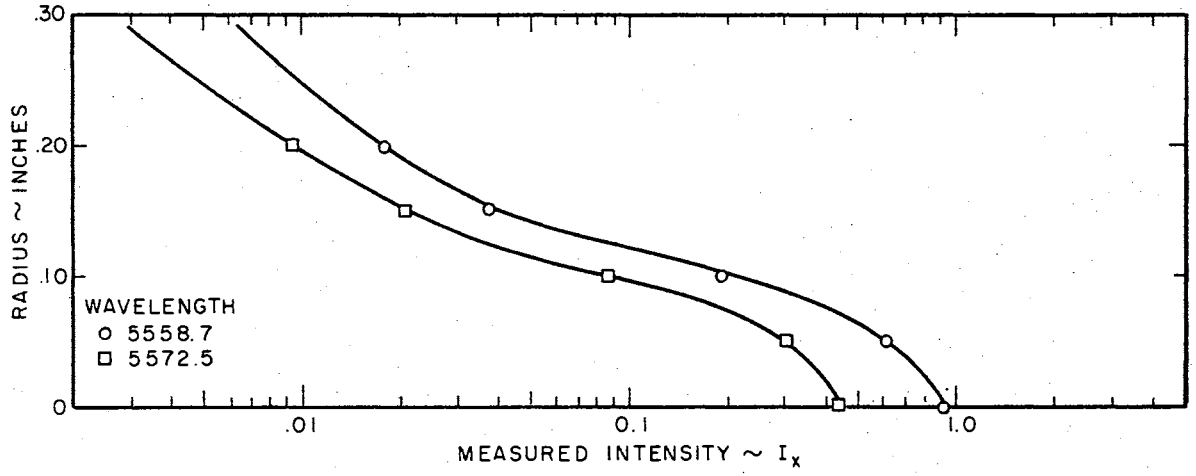
.30
.20
.10
0
RADIUS ~ INCHES
WAVELENGTH
o 5558.7
□ 5572.5
.01
0.1
1.0
MEASURED INTENSITY ~ I_x

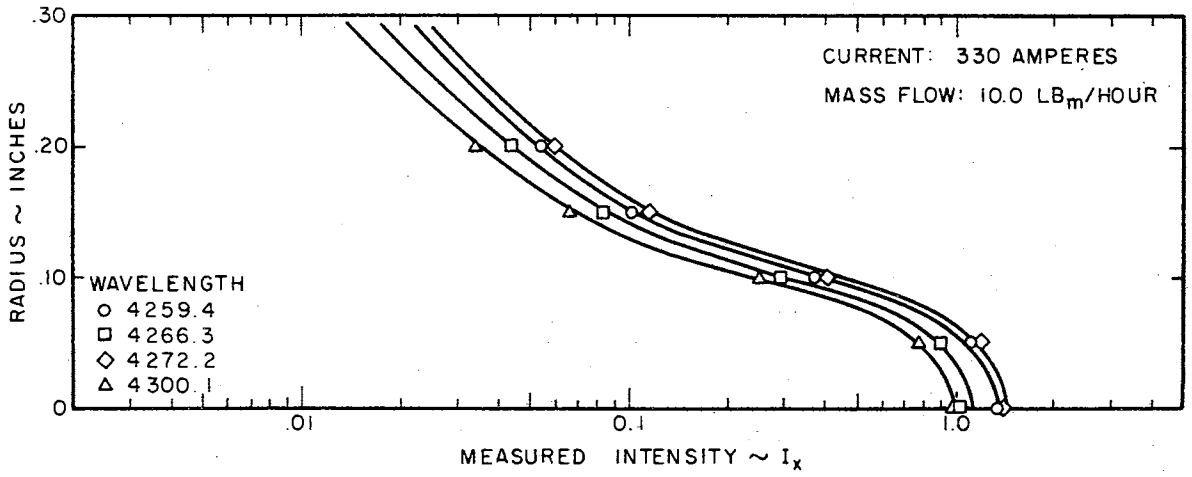
.30
.20
.10
0
RADIUS ~ INCHES
CURRENT: 330 AMPERES
MASS FLOW: 10.0 LB$_m$/HOUR
WAVELENGTH
○ 4259.4
□ 4266.3
◇ 4272.2
△ 4300.1
.01
0.1
1.0
MEASURED INTENSITY ~ I_x

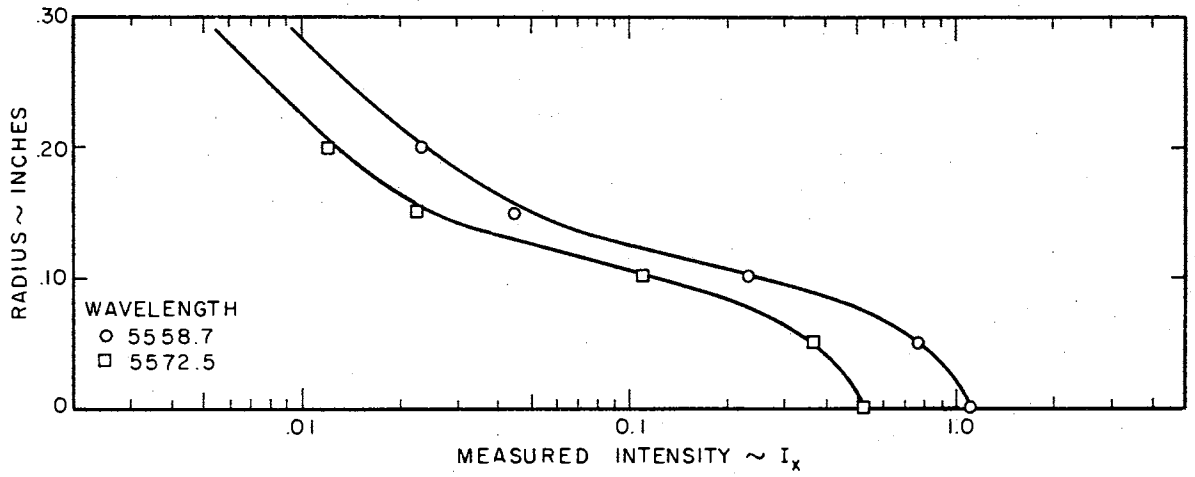
.30
.20
.10
0
RADIUS ~ INCHES
WAVELENGTH
○ 5558.7
□ 5572.5
.01
0.1
1.0
MEASURED INTENSITY ~ I_x

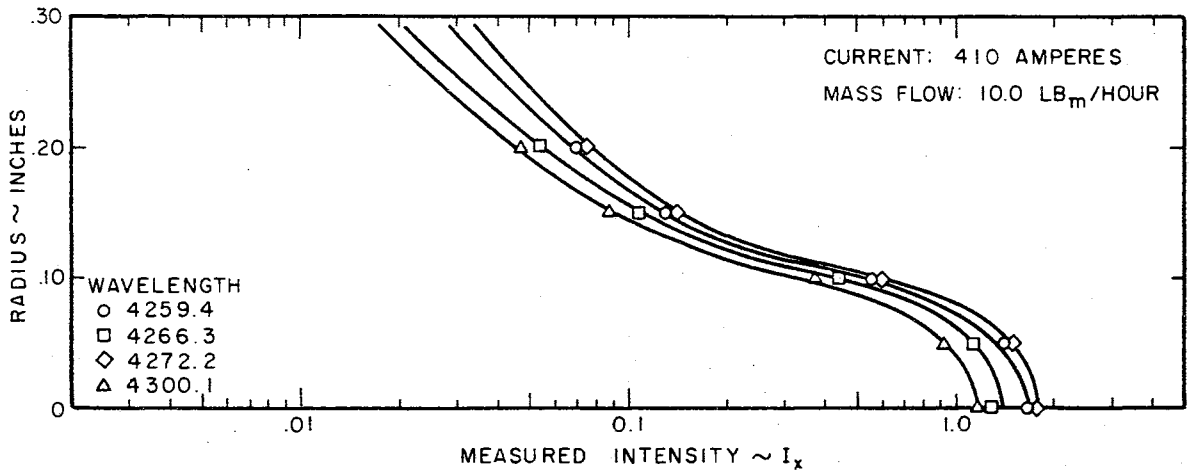
.30
.20
.10
0
RADIUS ~ INCHES
CURRENT: 410 AMPERES
MASS FLOW: 10.0 LB$_m$/HOUR
WAVELENGTH
○ 4259.4
□ 4266.3
◇ 4272.2
△ 4300.1
.01
0.1
1.0
MEASURED INTENSITY ~ I_x

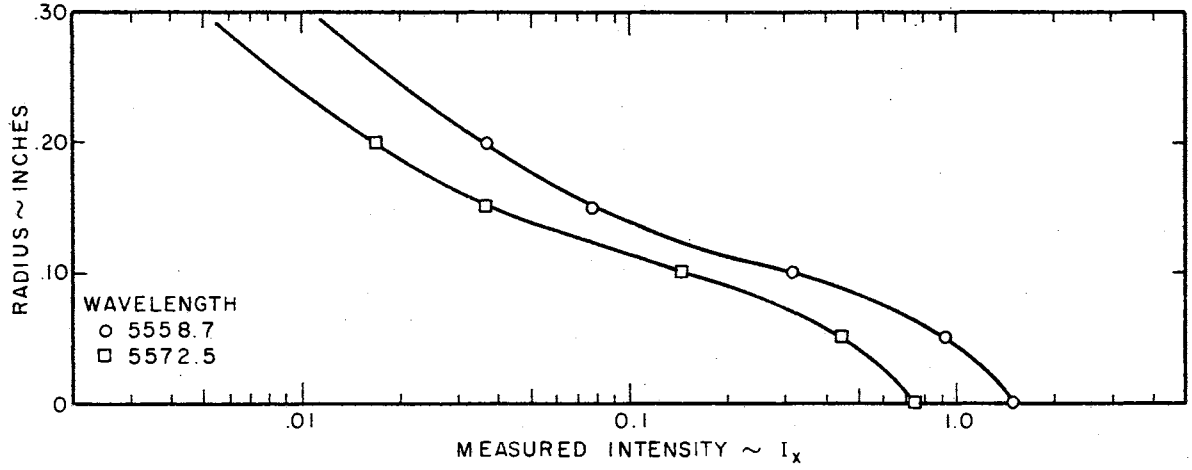
.30
.20
.10
0
RADIUS ~ INCHES
WAVELENGTH
○ 5558.7
□ 5572.5
.01
0.1
1.0
MEASURED INTENSITY ~ I_x

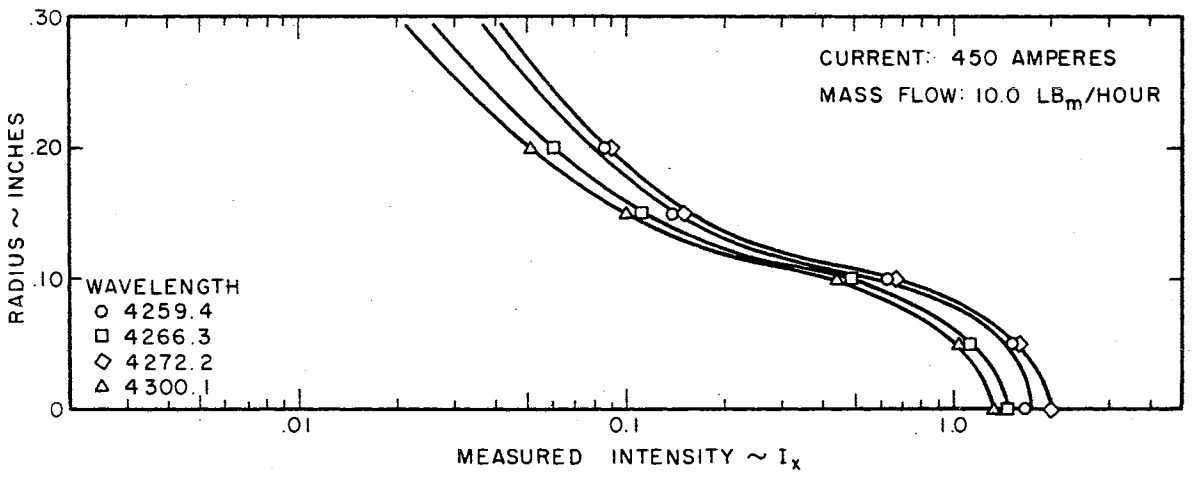
.30
.20
.10
0
RADIUS ~ INCHES
CURRENT: 450 AMPERES
MASS FLOW: 10.0 LB$_m$/HOUR
WAVELENGTH
o 4259.4
□ 4266.3
◇ 4272.2
△ 4300.1
.01
0.1
1.0
MEASURED INTENSITY ~ I_x

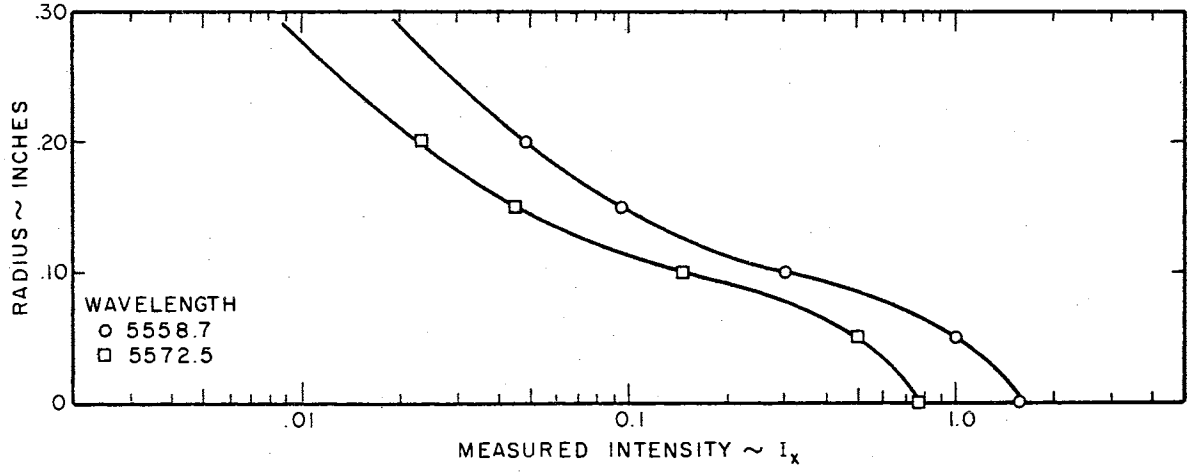
.30
.20
.10
0
RADIUS ~ INCHES
WAVELENGTH
o 5558.7
□ 5572.5
.01
0.1
1.0
MEASURED INTENSITY ~ I_x

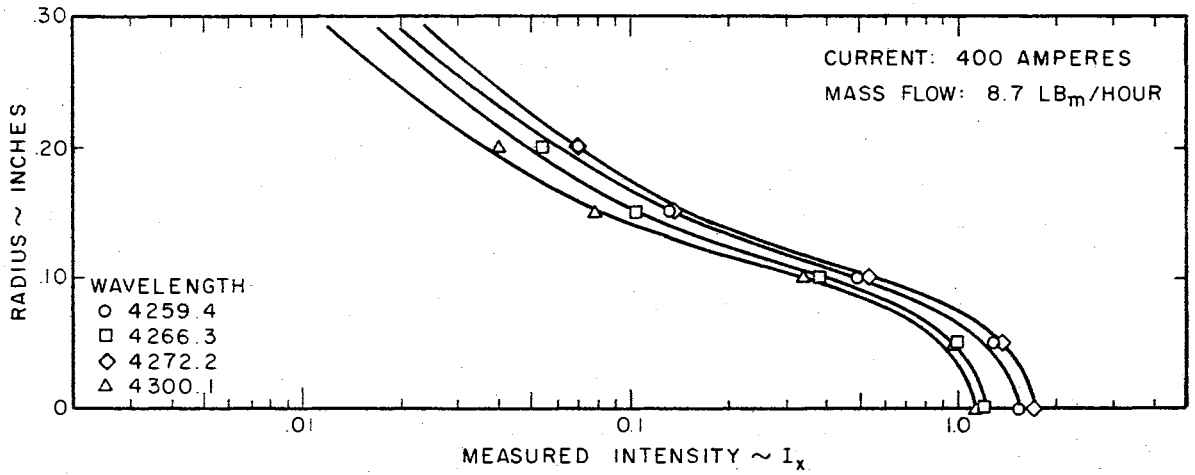
CURRENT: 400 AMPERES
MASS FLOW: 8.7 LBm/HOUR
WAVELENGTH
○ 4259.4
□ 4266.3
◇ 4272.2
△ 4300.1
RADIUS ~ INCHES
.30
.20
.10
0
.01
0.1
1.0
MEASURED INTENSITY ~ Ix

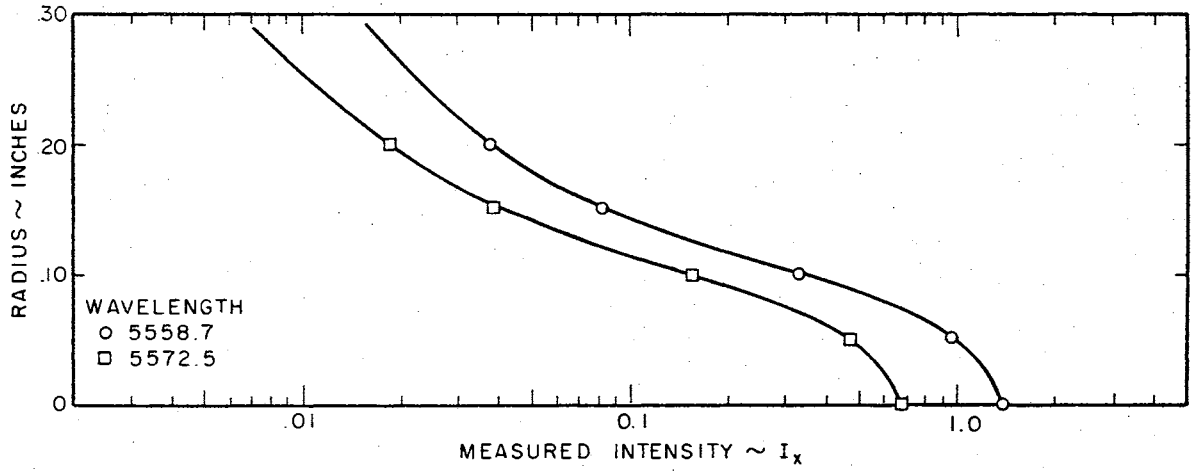
WAVELENGTH
○ 5558.7
□ 5572.5
RADIUS ~ INCHES
.30
.20
.10
0
.01
0.1
1.0
MEASURED INTENSITY ~ Ix

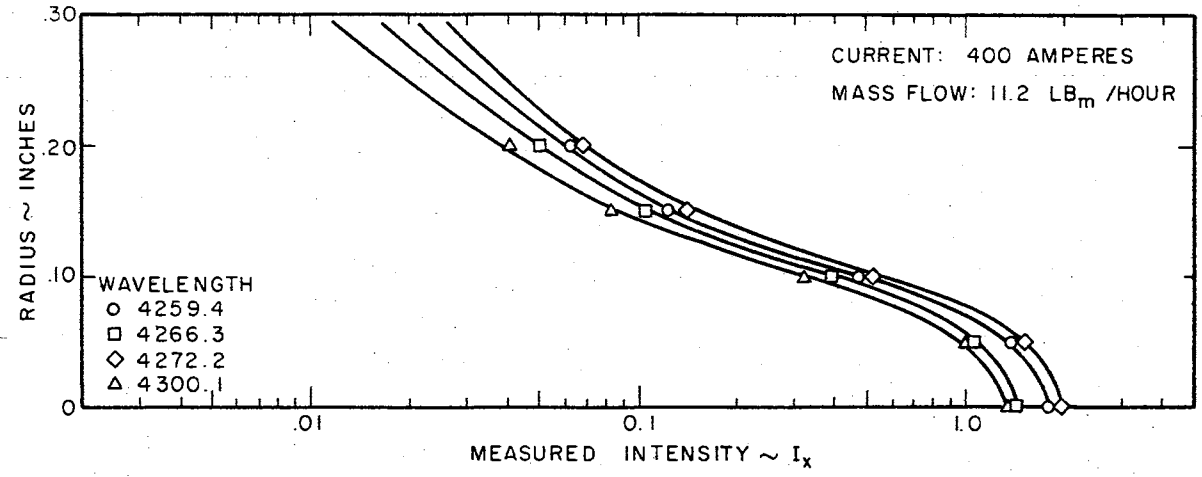
.30
.20
.10
0
RADIUS ~ INCHES
CURRENT: 400 AMPERES
MASS FLOW: 11.2 LBm /HOUR
WAVELENGTH
○ 4259.4
□ 4266.3
◇ 4272.2
△ 4300.1
.01
0.1
1.0
MEASURED INTENSITY ~ Ix

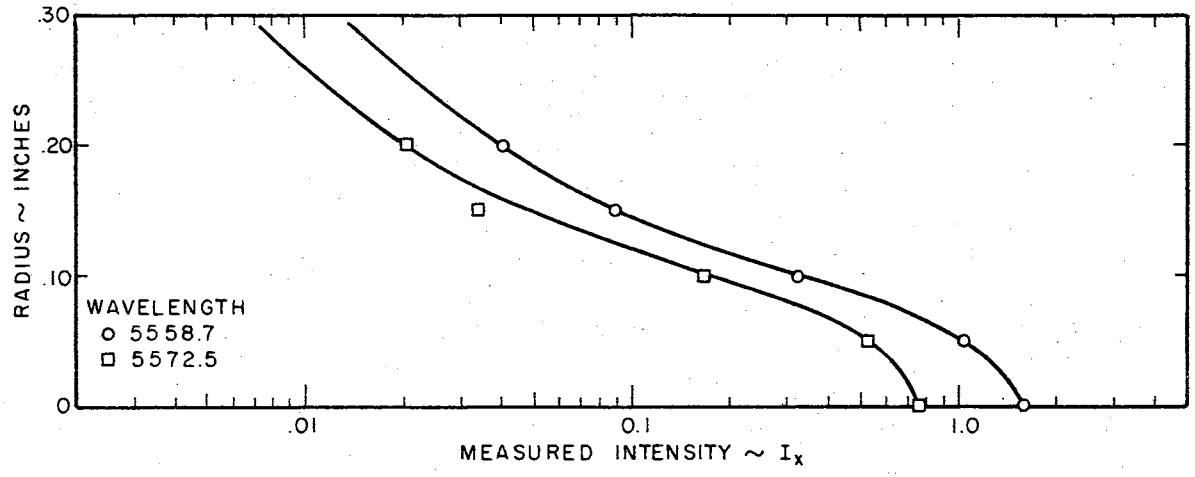
.30
.20
.10
0
RADIUS ~ INCHES
WAVELENGTH
○ 5558.7
□ 5572.5
.01
0.1
1.0
MEASURED INTENSITY ~ Ix

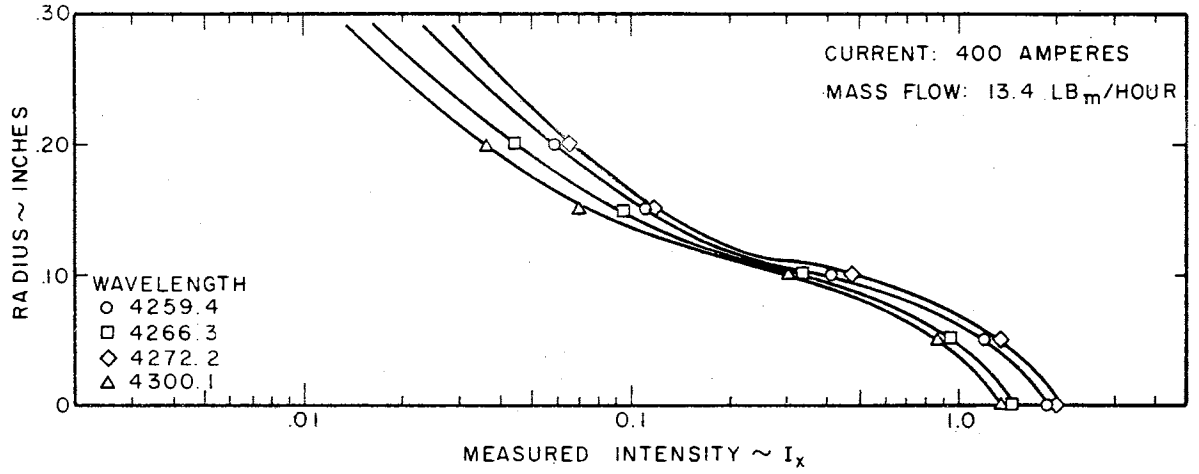
CURRENT: 400 AMPERES
MASS FLOW: 13.4 LB$_m$/HOUR
WAVELENGTH
○ 4259.4
□ 4266.3
◇ 4272.2
△ 4300.1
RADIUS ~ INCHES
.30
.20
.10
0
.01
0.1
1.0
MEASURED INTENSITY ~ I_x

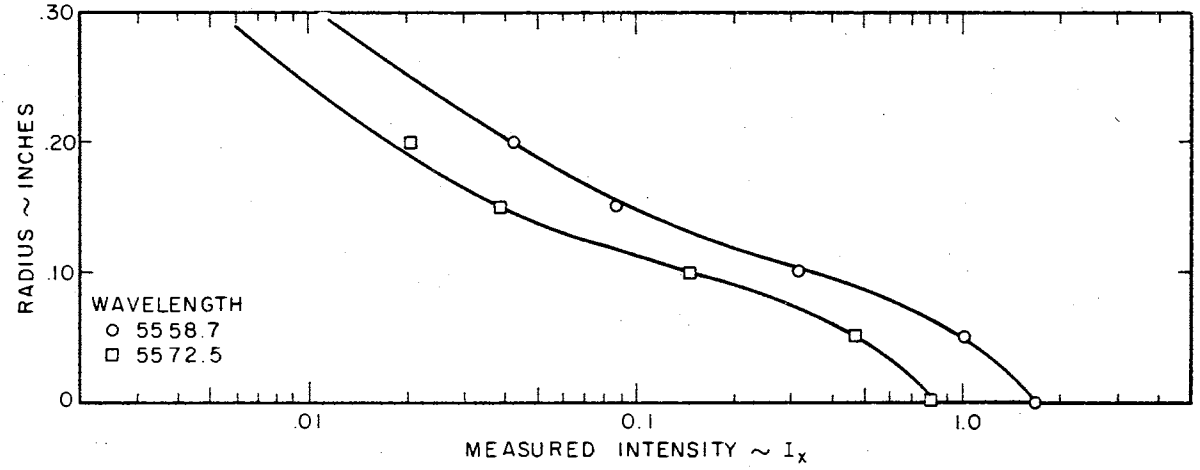
WAVELENGTH
○ 5558.7
□ 5572.5
RADIUS ~ INCHES
.30
.20
.10
0
.01
0.1
1.0
MEASURED INTENSITY ~ I_x

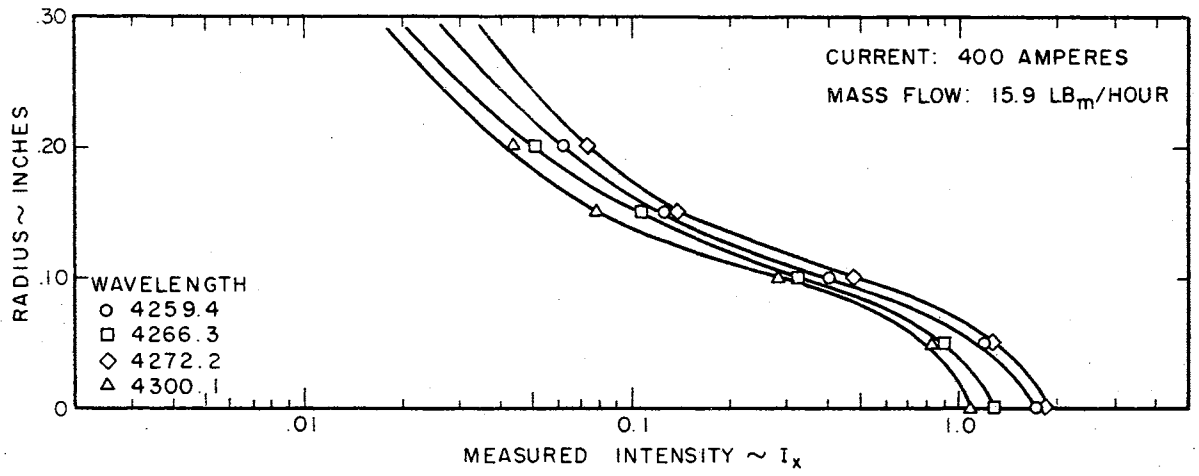
.30
.20
.10
0
RADIUS ~ INCHES
CURRENT: 400 AMPERES
MASS FLOW: 15.9 LB$_m$/HOUR
WAVELENGTH
o 4259.4
□ 4266.3
◇ 4272.2
△ 4300.1
.01
0.1
1.0
MEASURED INTENSITY ~ I_x

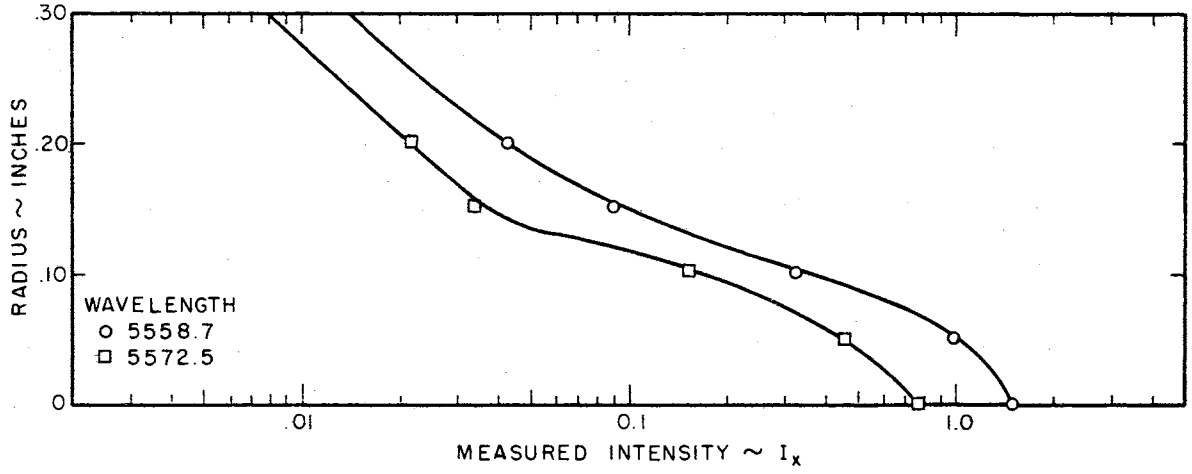
.30
.20
.10
0
RADIUS ~ INCHES
WAVELENGTH
o 5558.7
□ 5572.5
.01
0.1
1.0
MEASURED INTENSITY ~ I_x

APPENDIX C

ABSORPTION DATA

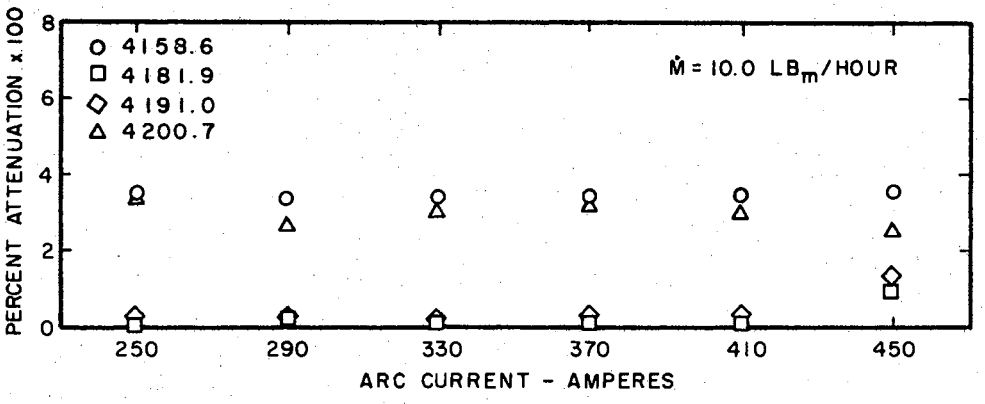
PERCENT ATTENUATION x 100
8
6
4
2
0
○ 4158.6
□ 4181.9
◇ 4191.0
△ 4200.7
Ṁ = 10.0 LBm/HOUR
250
290
330
370
410
450
ARC CURRENT - AMPERES

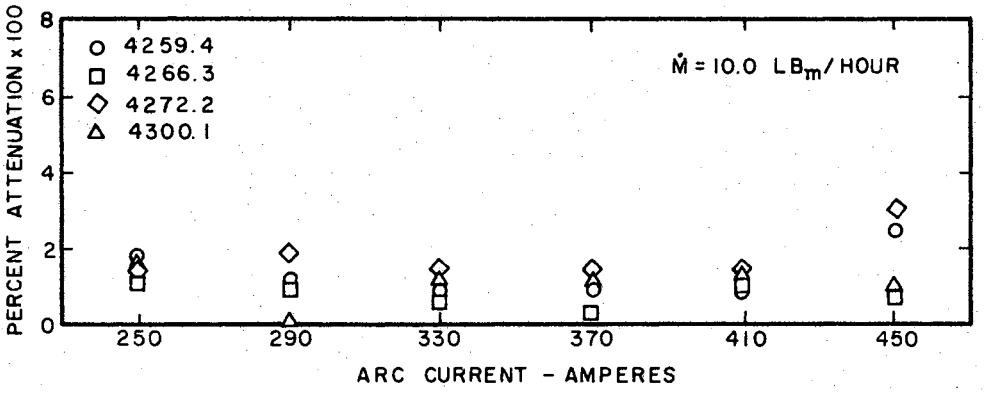
PERCENT ATTENUATION x 100
8
6
4
2
0
○ 4259.4
□ 4266.3
◇ 4272.2
△ 4300.1
Ṁ = 10.0 LBm/HOUR
250
290
330
370
410
450
ARC CURRENT - AMPERES

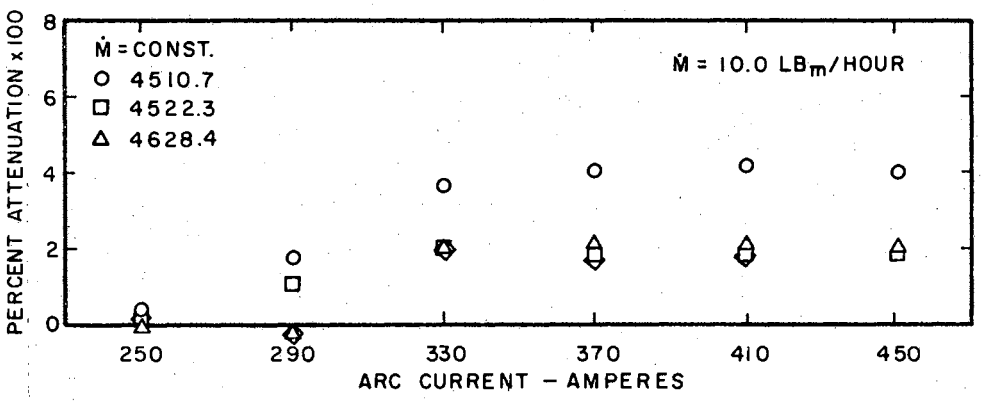
PERCENT ATTENUATION x 100
8
6
4
2
0
Ṁ = CONST.
○ 4510.7
□ 4522.3
△ 4628.4
Ṁ = 10.0 LBm/HOUR
250
290
330
370
410
450
ARC CURRENT - AMPERES

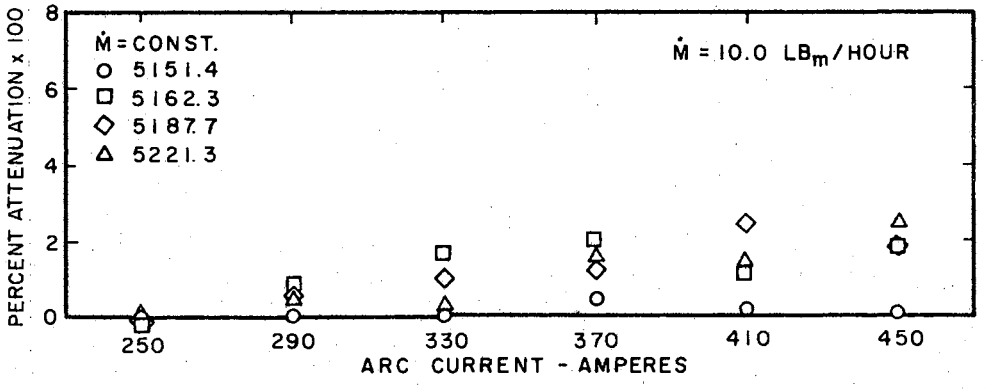
PERCENT ATTENUATION x 100
8
6
4
2
0
Ṁ = CONST.
○ 5151.4
□ 5162.3
◇ 5187.7
△ 5221.3
Ṁ = 10.0 LBm/HOUR
250
290
330
370
410
450
ARC CURRENT - AMPERES

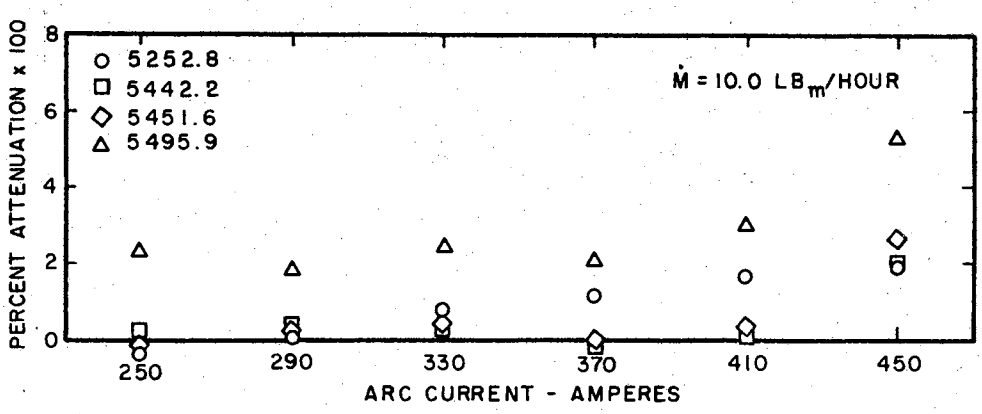
PERCENT ATTENUATION x 100
8
6
4
2
0
5252.8
5442.2
5451.6
5495.9
$\dot{M}$ = 10.0 LB_m/HOUR
250
290
330
370
410
450
ARC CURRENT - AMPERES

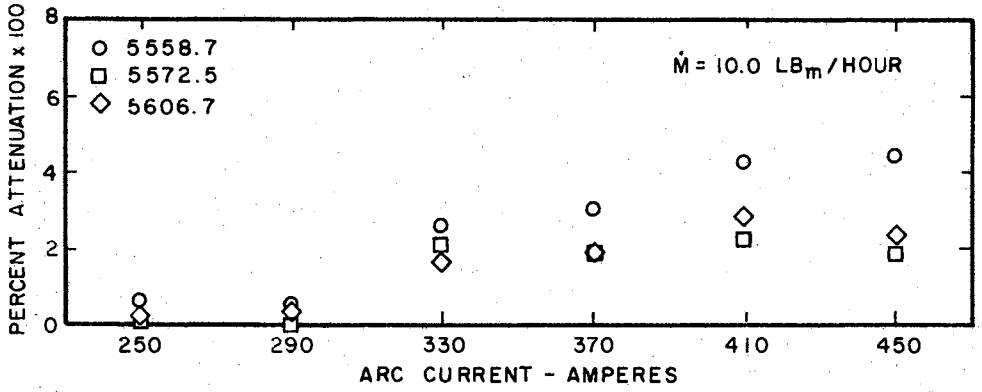
PERCENT ATTENUATION x 100
8
6
4
2
0
5558.7
5572.5
5606.7
$\dot{M}$ = 10.0 LB_m/HOUR
250
290
330
370
410
450
ARC CURRENT - AMPERES

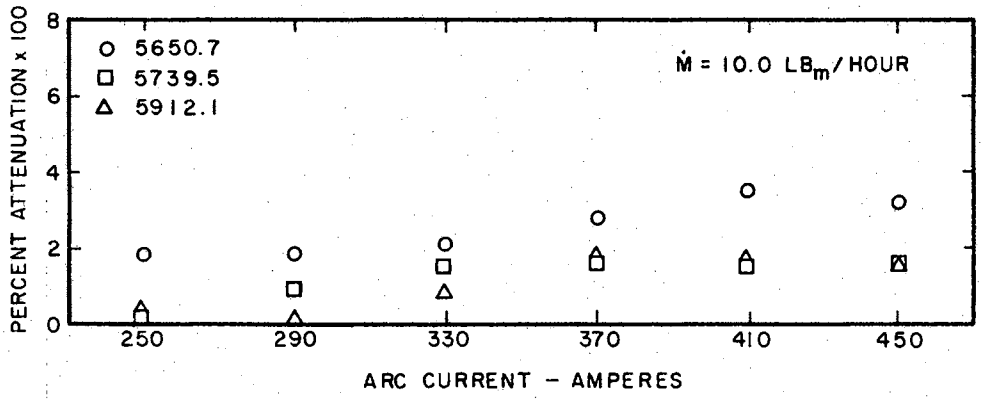
PERCENT ATTENUATION x 100
8
6
4
2
0
5650.7
5739.5
5912.1
$\dot{M}$ = 10.0 LB_m/HOUR
250
290
330
370
410
450
ARC CURRENT - AMPERES

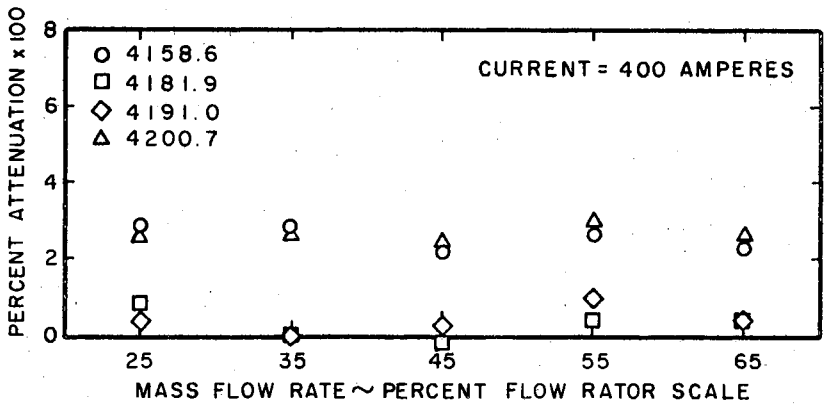
PERCENT ATTENUATION x 100
0
2
4
6
8
4158.6
4181.9
4191.0
4200.7
CURRENT = 400 AMPERES
25
35
45
55
65
MASS FLOW RATE ~ PERCENT FLOW RATOR SCALE

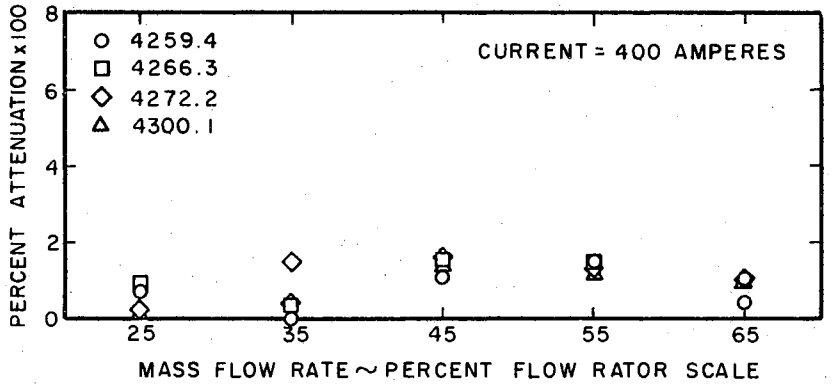
PERCENT ATTENUATION x 100
0
2
4
6
8
4259.4
4266.3
4272.2
4300.1
CURRENT = 400 AMPERES
25
35
45
55
65
MASS FLOW RATE ~ PERCENT FLOW RATOR SCALE

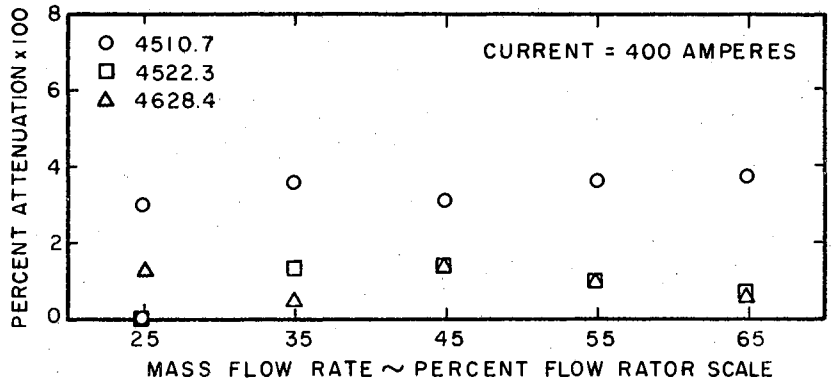
PERCENT ATTENUATION x 100
0
2
4
6
8
4510.7
4522.3
4628.4
CURRENT = 400 AMPERES
25
35
45
55
65
MASS FLOW RATE ~ PERCENT FLOW RATOR SCALE

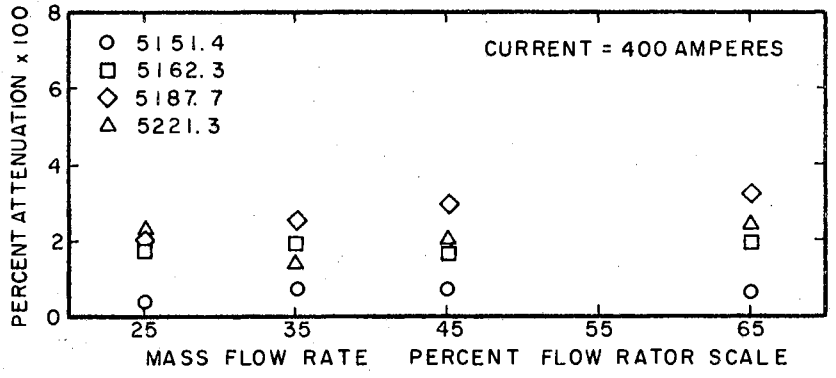
PERCENT ATTENUATION x 100
0
2
4
6
8
5151.4
5162.3
5187.7
5221.3
CURRENT = 400 AMPERES
25
35
45
55
65
MASS FLOW RATE PERCENT FLOW RATOR SCALE

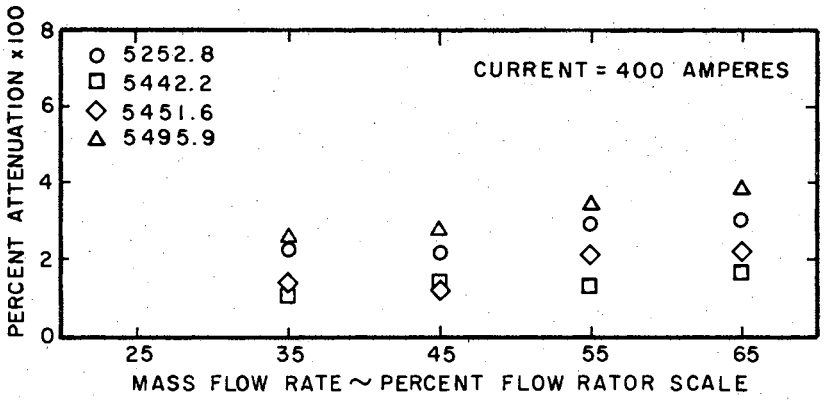
PERCENT ATTENUATION x 100
0
2
4
6
8
5252.8
5442.2
5451.6
5495.9
CURRENT = 400 AMPERES
25
35
45
55
65
MASS FLOW RATE ~ PERCENT FLOW RATOR SCALE

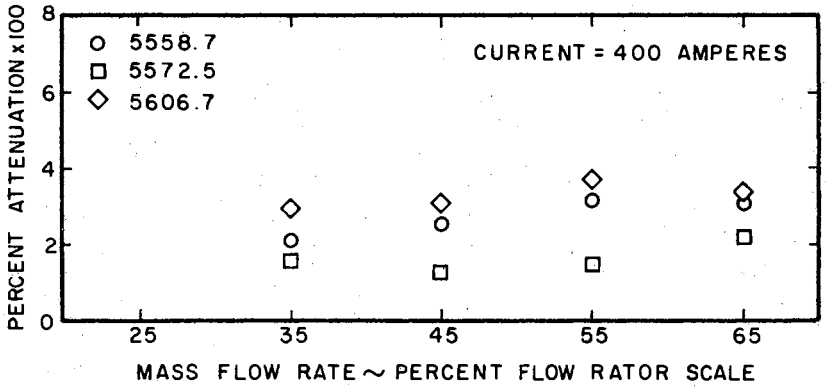
PERCENT ATTENUATION x 100
0
2
4
6
8
5558.7
5572.5
5606.7
CURRENT = 400 AMPERES
25
35
45
55
65
MASS FLOW RATE ~ PERCENT FLOW RATOR SCALE

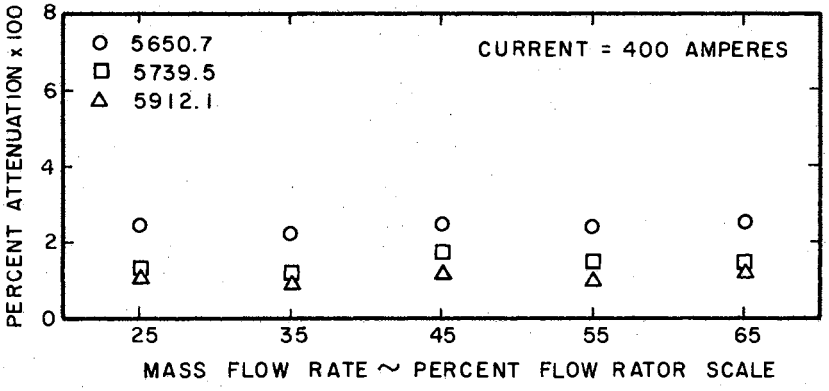
PERCENT ATTENUATION x 100
0
2
4
6
8
5650.7
5739.5
5912.1
CURRENT = 400 AMPERES
25
35
45
55
65
MASS FLOW RATE ~ PERCENT FLOW RATOR SCALE

APPENDIX D

FORTRAN PROGRAM FOR DIRECT CALCULATION OF TEMPERATURE FROM MEASURED INTENSITIES

```
     MON$$      JOB  252740044       JC HESTER    7550
     MON$$      ASGN MJB,A2
     MON$$      ASGN MGO,A3
     MON$$      MODE GO,TEST
     MON$$      EXEC FORTRAN
      DIMENSION WL(30),A(30),G(30),COEF(15,15),EM(30),
     1EXPI(15,30),RADI(15,30)
1001  FORMAT (10X,5E12.6)
2001  FORMAT (10X,5E14.8)
3001  FORMAT (1X,5E20.6)
      READ (1,1001)WL,A,G
      READ (1,2001)EM
      DO 5 I=1,15
    5 READ (1,2001)(COEF(I,J),J=1,15)
      DO 6 I=1,15
    6 READ (1,1001)(EXPI(I,J),J=1,30)
      DO 7 I=1,15
      DO 7 J=1,30
      RADI(I,J)=0.0
      DO 7 K=1,15
    7 RADI(I,J)=RADI(I,J)+COEF(I,K)*EXPI(K,J)
      DO 8 J=1,30,2
      PRODN=WL(J)*G(J+1)*A(J+1)
      PRODD =A(J)*G(J)*WL(J+1)
      ANUM=(-1.43868)*(EM(J)-EM(J+1))
      DO 8 I=1,15
      RATIR=RADI(I,J)/RADI(I,J+1)
      DENM=RATIR*(PRODN/PRODD)
      DENOM=ALOG(DENM)
      RADT=ANUM/DENOM
    8 WRITE (3,3001)WL(J),WL(J+1),RADI(I,J),RADI(I,J+1),RADT
      END
```

APPENDIX E

COEFFICIENTS OF I_x TO OBTAIN I(r) VALUES

ID INVERSE MATRIX 15 RADIAL OBSERVATIONS

	1	2	3	4	5	6	7	8	9
1	63661828+00+	58450955-00+	85254369+01-	68530431-01-	21474020-02-	14839217-01-	61298899-02-	12673290-01-	12506624+02-
2	CCCCCCCC-CC+	4C704348+00+	35428323-00+	52033841+01-	45319909-01-	29507793-02-	10876884-01-	50678953-02-	48827159-02-
3	CCCCCCCC-CC+	CCCCCCCC-CC+	32284309+00+	27623838-00+	42151932+01-	36229820-01-	24312427-02-	89405290-02-	42775147-02-
4	CCCCCCCC-CC+	CCCCCCCC-CC+	00000000-00+	27574873+00+	23397892-00+	36706935+01-	31001276-01-	19949046-02-	77231161-02-
5	CCCCCCCC-CC+	CCCCCCCC-CC+	00000000-00+	00000000-00+	24464652+00+	20656500-00+	33048330+01-	27506664-01-	16737821-02-
6	CCCCCCCC-CC+	CCCCCCCC-CC+	00000000-00+	00000000-00+	00000000-00+	22214521+00+	18695569-00+	30345580+01-	24964946-01-
7	CCCCCCCC-CC+	CCCCCCCC-CC+	00000000-00+	CCCCCCCC-CC+	00000000-00+	00000000-00+	20489410+00+	17203979-00+	28232240+01-
8	CCCCCCCC-CC+	CCCCCCCC-CC+	00000000-00+	00000000-00+	00000000-00+	00000000-00+	00000000-00+	19112456+00+	16020199-00+
9	CCCCCCCC-CC+	CCCCCCCC-CC+	00000000-00+	00000000-00+	00000000-00+	00000000-00+	00000000-00+	00000000-00+	17980373+00+
10	CCCCCCCC-CC+	CCCCCCCC-CC+	00000000-00+	00000000-00+	00000000-00+	00000000-00+	00000000-00+	00000000-00+	00000000-00+
11	CCCCCCCC-CC+	CCCCCCCC-CC+	00000000-00+	00000000-00+	00000000-00+	00000000-00+	00000000-00+	00000000-00+	00000000-00+
12	CCCCCCCC-CC+	CCCCCCCC-CC+	00000000-00+	00000000-00+	00000000-00+	CCCCCCCC-CC+	00000000-00+	00000000-00+	00000000-00+
13	CCCCCCCC-CC+	CCCCCCCC-CC+	00000000-00+	CCCCCCCC-CC+	00000000-00+	00000000-00+	00000000-00+	00000000-00+	00000000-00+
14	CCCCCCCC-CC+	CCCCCCCC-CC+	00000000-00+	00000000-00+	00000000-00+	00000000-00+	00000000-00+	00000000-00+	00000000-00+
15	CCCCCCCC+CC+	00000000+00+	00000000+00+	00000000+00+	00000000+00+	00000000+00+	00000000+00+	00000000+00+	00000000+00+

ID INVERSE MATRIX 15 RADIAL OBSERVATIONS

	10	11	12	13	14	15
1	44826588-02-	21324634-02-	23722203-02-	18509678-02-	16593183-02-	14246891-02-
2	35512234-02-	29973572-02-	24512609-02-	20799286-02-	17737996-02-	15362308-02-
3	41432878-02-	30604839-02-	26044811-02-	21508051-02-	18391781-02-	15794940-02-
4	37215602-02-	36340285-02-	27050661-02-	23171710-02-	19257175-02-	16554764-02-
5	68712511-02-	33134022-02-	32585381-02-	24376237-02-	20973715-02-	17510522-02-
6	14365723-02-	62395535-02-	30003733-02-	29638219-02-	22274190-02-	19232747-02-
7	23011464-01-	12530910-02-	57447076-02-	27566276-02-	27400496-02-	20589007-02-
8	26516289+01-	21450797-01-	11158967-02-	53440940-02-	25572673-02-	25521542-02-
9	15051232-00+	25085260+01-	20167738-01-	10036237-02-	50158978-02-	23918673-02-
10	17028262+00+	14239121-00+	23866611+01-	19088622-01-	91257942-03-	47389860-02-
11	CCCCCCCC-CC+	16212974+00+	13545631-00+	22911900+01-	18165271-01-	83727504-03-
12	CCCCCCCC-CC+	CCCCCCCC-CC+	15504573+00+	12944497-00+	21887303+01-	17363257-01-
13	CCCCCCCC-CC+	CCCCCCCC-CC+	00000000-00+	14881617+00+	12416867-00+	21067396+01-
14	CCCCCCCC-CC+	CCCCCCCC-CC+	00000000-00+	00000000-00+	14328187+00+	11948889-00+
15	CCCCCCCC+CC+	CCCCCCCC+CC+	00000000+00+	CCCCCCCC+CC+	00000000-00+	13832215+00+

VITA

Jarrett Charles Hester

Candidate for the Degree of

Doctor of Philosophy

Thesis: THE ABSORPTION CHARACTERISTICS OF RADIATION IN THE VISIBLE SPECTRUM BY AN ARGON PLASMA

Major Field: Mechanical Engineering

Biographical:

Personal Data: Born in Mount Vernon, Texas, December 14, 1938, the son of Jarrett and Edith Hester.

Education: Received the Bachelor of Science degree from Arlington State College, Arlington, Texas, with a major in Mechanical Engineering, in August, 1962; received the Master of Science degree from Oklahoma State University, Stillwater, Oklahoma, with a major in Mechanical Engineering, in January, 1964; completed requirements for the Doctor of Philosophy degree in May, 1966.

Professional experience: Alternated work and study sessions between Ling-Temco-Vought Aerospace Corporation, Arlington State College, and Oklahoma State University from June, 1957, to August, 1965; Engineering Specialist LTV Corporation, Dallas, Texas, from August, 1965, to February, 1966.

Professional organizations: The author is a member of the following honorary, educational, and professional organizations: Pi Tau Sigma, Phi Kappa Theta, American Society of Mechanical Engineers, and American Institute of Aeronautics and Astronautics.